(1)

REPORT DOCUMENTATION PAGE

READ INSTRUCTIONS BEFORE COMPLETING FORM

1. REPORT NUMBER: AFIT/CI/NR 88- 5	2. GOVT ACCESSION NO.
3. RECIPIENT'S CATALOG NUMBER	
4. TITLE (and Subtitle): MESOSCALE STRUCTURE AND CLIMATOLOGY OF RAIN-SNOW LINES OVER NORTH CAROLINA	5. TYPE OF REPORT & PERIOD COVERED: MS THESIS
	6. PERFORMING ORG. REPORT NUMBER
7. AUTHOR(s): KENNETH FLETCHER CAREY	8. CONTRACT OR GRANT NUMBER(s)
9. PERFORMING ORGANIZATION NAME AND ADDRESS: AFIT STUDENT AT:	10. PROGRAM ELEMENT, PROJECT, TASK AREA & WORK UNIT NUMBERS
11. CONTROLLING OFFICE NAME AND ADDRESS	12. REPORT DATE: 1988
	13. NUMBER OF PAGES: 95
14. MONITORING AGENCY NAME & ADDRESS (if different from Controlling Office): AFIT/NR, Wright-Patterson AFB OH 45433-6583	15. SECURITY CLASS. (of this report): UNCLASSIFIED
	15a. DECLASSIFICATION/DOWNGRADING SCHEDULE

16. DISTRIBUTION STATEMENT (of this Report)

DISTRIBUTED UNLIMITED: APPROVED FOR PUBLIC RELEASE

17. DISTRIBUTION STATEMENT (of the abstract entered in Block 20, if different from Report)

SAME AS REPORT

18. SUPPLEMENTARY NOTES

Approved for Public Release: IAW AFR 190-1
LYNN E. WOLAVER Lynn Wolaver 12 July 88
Dean for Research and Professional Development
Air Force Institute of Technology
Wright-Patterson AFB OH 45433-6583

19. KEY WORDS (Continue on reverse side if necessary and identify by block number)

20. ABSTRACT (Continue on reverse side if necessary and identify by block number)

ATTACHED

DD FORM 1 JAN 73 1473 EDITION OF 1 NOV 65 IS OBSOLETE

Abstract

CAREY, KENNETH F. Mesoscale Structure and Climatology of Rain-Snow Lines Over North Carolina. (Under the direction of Steven Businger and Gerald Watson.)

An investigation of the mesoscale structure and climatology associated with rain-snow lines across North Carolina was undertaken. A case study focused on a rain-snow line occurrence on 14-15 February 1986 during the GALE field project. The GALE enhanced-resolution surface and upper-air data network was used to describe the kinematic and thermodynamic processes in the vicinity of the rain-snow line. The Barnes objective analysis scheme was used to interpolate data to grid point values.

An attempt was made to document mesoscale circulations associated with the rain-snow line. Evidence for the existence of a mesoscale circulation was found from surface analyses of operational and GALE data, satellite imagery signatures, and time-averaged divergence fields.

Analyses of the 285°K isentropic surface during this rain-snow line event were presented. Strong ascent was indicated over the eastern Carolinas during most of the period. A comparison of our isentropic analysis, which included the special GALE rawinsonde sites, with that of Homan and Uccellini (1987), found that a more detiled vertical motion pattern emerged, with some vertical velocities more than twice that found by these authors.

The three-dimensional atmospheric structure in the vicinity of the rain-snow line was further explored by means of Barnes-generated fields of divergence. Divergence was obtained on constant pressure levels and kinematic vertical velocity calculated. The pattern of vertical velocity at 950 and 850 mb seem to be consistent with that based on isentropic-surface analyses and the precipitation patterns based on radar reflectivity.

The First Law of Thermodynamics, in a coordinate system following the 0°C isotherm (chosen to represent the rain-snow line), was employed. The results indicate that cooling due to melting and/or sublimation was occurring at the rain-snow line. After the rain-snow line passage, warm air advection then increased the low-level temperatures.

A 22-year (1966-87) climatology of rain-snow lines in North Carolina was compiled. The relationship between rain-snow line location and that of the parent surface cyclone showed a limited correlation. Rain-snow lines first occur anywhere from the mountains to the coast. Secondly, a correlation between surface variables and

precipitation type was documented. The freezing temperature (0°C ± 2°) was the dominant surface dry-bulb, wet-bulb, and dew-point temperature range for frozen (ice pellets (sleet)), freezing (freezing rain/drizzle), and mixed (combination of snow and/or ice pellets (sleet) and rain or drizzle) precipitation types. All precipitation of these types occurred most frequently with winds from the NNE through ENE (020-070°).

Mesoscale Structure and Climatology of Rain-Snow Lines over North Carolina

by

Kenneth Fletcher Carey

A thesis submitted to the Graduate Faculty of
North Carolina State University
in partial fulfillment of the
requirements for the Degree of
Master of Science

Department of Marine, Earth, and Atmospheric Sciences

Raleigh
1988

Approved By:

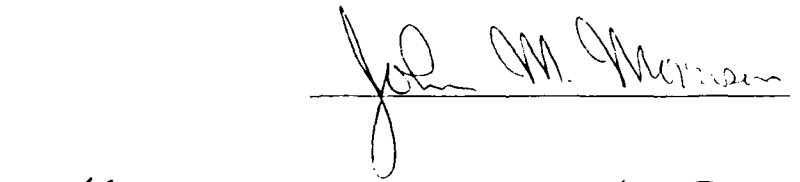

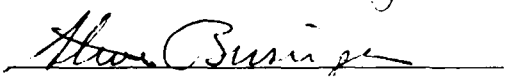

Co-Chairman of Advisory Committee

Co-Chairman of Advisory Committee

Acknowledgements

The author would like to sincerely thank Dr. Steven Businger and Dr. Gerald Watson for their guidance, expertise, and patience during the preparation of this thesis.

Particular thanks goes to Mary McVicker for superlative work on the drafting of figures for this thesis, Jeff Medlin for his enormous help in the plotting of surface data for the climatology section, Mr. Kermit Keeter for his providing literature and constructure thoughts on operational forecasts of precipitation type, Andy Wachob for his assistance with slide preparation for my oral defense, fellow MEAS graduate students for their camaraderie and fellowship, and to the United States Air Force for this degree opportunity and financial support.

Finally, the author wishes to express his utmost appreciation to his wife, Chin Sun, for her patience, personal and moral support during my course of study.

Table of Contents

List of Figures

1. ATMOSPHERIC STRUCTURE ASSOCIATED WITH RAIN-SNOW LINES

1.1 Introduction

Midlatitude cyclones produce a spectrum of precipitation types across the southeastern United States during the winter season. Generally, as a cyclone tracks northeastward across this region snow falls in the Appalachian mountains, while rain prevails across the coastal areas. In the region between, a mixture of precipitation types, including sleet and freezing rain, often occurs. The potential impact of these precipitation types on local communities can be significant. Transportation can be severely disrupted in the snow region, whereas water runoff and flooding can be a major hazard in the rain area. In the region of transition precipitation, the formation of an icy glaze on roads, vehicles, and electrical transmission and communication lines can literally paralyze communities, making transportation nearly impossible, toppling trees, and endangering livestock, crops, and wildlife.

The meteorological conditions necessary to produce a mixture of precipitation types are determined by the vertical profile of temperature (or wet-bulb temperature in the case of evaporative cooling; Penn, 1957). In the case of freezing precipitation, precipitation either forms in or falls through a warm (above-freezing) layer aloft, falls through a surface-based cold (sub-freezing) layer, becomes supercooled, and freezes upon impact with the ground. Bocchieri (1980) found that the average depth of the warm layer was about 1700 m, while Young (1978) found that the cold layer usually extended 300-1200 m above the surface. Very deep warm layers may prevent supercooling in the subfreezing layer. Subfreezing layers which are very deep, or warm layers which are not warm enough or deep enough to completely melt snowflakes falling through them, result in the formation of sleet (ice pellets). Figure 1.1 shows typical vertical temperature profiles associated with the different precipitation types.

Despite excellent knowledge of the vertical temperature and moisture profiles which are conducive for a mixture of precipitation types and rain-snow (R-S) lines, forecasting the location of the various types of precipitation is difficult. The R-S boundary is mesoscale in extent, frequently occurring along a narrow swath. Stewart and King (1987) found, after examining R-S boundaries over southern Ontario, that the width of the R-S boundary varied from 11 to 64 km. A literature review by Forbes et al. (1987) revealed that areas of icing range from 35 to 160 km. In addition, in many cases the time scale of the precipitation event is significantly smaller than the interval between

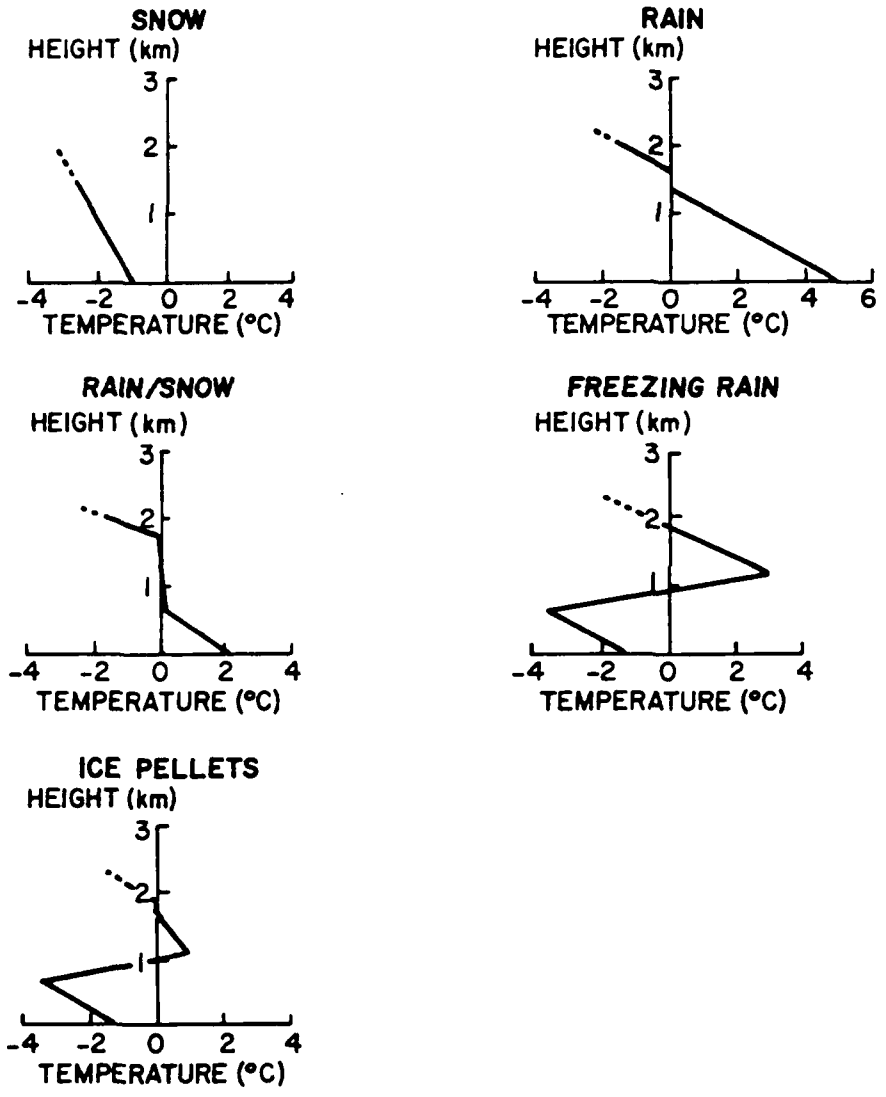

Figure 1.1. Schematic diagrams showing temperature profiles which can be associated with different precipitation types (from Stewart, 1985).

successive upper-air observations. Furthermore, only minor variations of temperature in relatively shallow layers are required to radically alter the type of precipitation that can fall. For the purposes of this study, the R-S line is defined as the leading edge of snow, provided that liquid and/or freezing precipitation is also being reported.

Traditionally, forecasters have relied upon predicted critical thickness values to forecast the precipitation type. Lamb (1955) used the 1000-500 mb thickness value; Koolwine (1975) found the 1000-850 mb 1314 m thickness line to be associated with the R-S line boundary, whereas Hanks et al. (1967) concluded, after studying snowstorms of the central United States, that the 1000-700 mb thickness contour of 2840 m was the most effective single decision tool for separating rain from snow. However, this method only identifies potential areas of frozen and unfrozen precipitation and must be used in conjunction with other subjective and objective methods for a timely identification of the R-S line.

The diabatic process of melting also seems to play a large role in the formation and maintenance of R-S lines. The atmospheric conditions in the vicinity of the R-S line must be such that snow entirely melts on the rain side, partial melting occurs to produce a mixture of rain and snow, and no melting occurs on the snow side. Lumb (1961) showed that a few hundred meters are required for snow to melt in temperatures up to 3°C. Findeisen (1940) first showed that the process of melting commonly produces 0°C layers in the atmosphere. Stewart (1984) showed that some 0°C layers can exceed 1 km in depth. As pointed out by Wexler et al. (1954), cooling of the air by melting can also cause snow to fall in regions where initially only rain fell. Lin and Stewart (1986), using a numerical model, found that a mesoscale circulation was induced by an elevated horizontal gradient of melting snow (Fig. 1.2). Stewart and King (1987) concluded that a mesoscale circulation driven by melting snow was consistent with observed radar, satellite, and surface observations. Szeto et al. (1988) employed a non-linear two-dimensional model and found that melting can induce horizontal wind perturbations of several meters per second and vertical motions of tens of centimeters per second.

When surface high pressure areas approach the New England coast from Canada, a northeasterly flow of very stable cold air develops along the Atlantic coast. The westward component of this flow is blocked by the eastern slopes of the Appalachian mountains. This "damming" results in the formation of a low-level (≈ 850 mb) northerly jet east of the mountains and a wedge of cold air between the mountains and the Atlantic Ocean that often persists for several days (Forbes et al., 1987). The boundary between the shallow northerly flow of cold, dry air in the cold wedge and the southeasterly flow of air that has

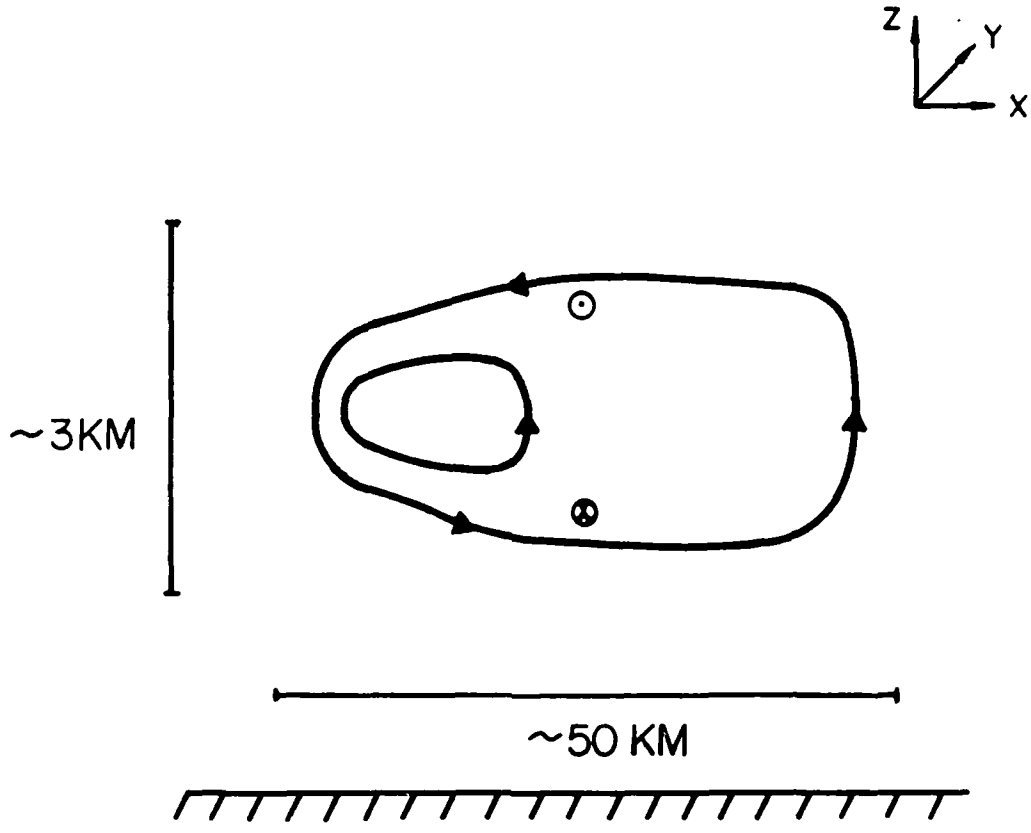

Figure 1.2. Schematic streamline sketch of a mesoscale thermal circulation in the meridional xz plane (from Lin and Stewart, 1986).

been modified over the warm waters of the Gulf Stream can result in an intense baroclinic zone called the coastal front. Studies by Bosart (1981) and Richwein (1980) show that coastal fronts are often the dividing line between frozen and non-frozen precipitation. Present numerical weather prediction models have difficulty in forecasting the position of the coastal front in that they inadequately depict and prematurely eliminate the cold wedge trapped between the mountains and the ocean. These deficiencies may be the result of poor representations of the topography, poor or nonexistent parameterization of oceanic and moisture heat fluxes (Bosart, 1981), and/or insufficient representation of the boundary layer in the models (e.g., Forbes et al., 1987; Homan and Uccellini, 1987).

Harrold (1973) developed the concept of "conveyor belts" using relative-flow isentropic analysis that approximates air motions within a cyclone. The conveyor belt concept is based upon two airflows: the "warm" conveyor belt and "cold" conveyor belt. The warm conveyor belt flows northward and ascends over the surface warm front, transporting large quantities of heat, moisture, and momentum poleward (Browning, 1986). The cold conveyor belt flows westward ahead of the surface warm front and below the warm conveyor belt. It has been suggested that the interaction between the warm and cold conveyor belts influence the orientation and location of the various bands of precipitation that are typically produced during a winter storm system (Browning and Pardoe, 1973). Blevins (1985) renamed Carlson's (1980) warm and cold conveyor belts the "Atlantic" and "Gulf" conveyor belts and found that the Atlantic conveyor belt experienced much stronger lift due to the presence of the cold wedge east of the Appalachians. Blevins concluded that the vertical coincidence of the Atlantic and Gulf conveyor belts over the cold air results in the development of an area of mixed precipitation.

A large amount of research has been performed by the Techniques Developmental Laboratory of the National Weather Service (NWS) regarding the forecast of precipitation associated with R-S lines. Their statistical studies on precipitation type resulted in a conditional probability of frozen precipitation system (Glahn and Bocchieri, 1975; Bocchieri and Glahn, 1976) which was developed and implemented operationally within the NWS in 1972, a system for forecasting the conditional probability of precipitation type (PoPT) (Bocchieri, 1979) implemented in 1978, and an improved PoPT system in 1982 (Bocchieri and Maglaras, 1983). Table 1.1 lists the most important predictors as determined by the screening procedure used by Bocchieri and Maglaras.

Recently, many forecasters have become better able to recognize, diagnose, and predict frozen, freezing, and unfrozen precipitation events through the combined use of

centralized facsimile products, numerical guidance, satellite imagery, radar, and local forecast schemes. In addition, forecasters are beginning to be provided with enhanced display systems, with facilities for image replay and superposition. In spite of these new diagnostic tools, a primary obstacle to improved precipitation type forecasts is the limited resolution of the data currently available, and lack of the understanding of how dynamical and mesoscale processes affect R-S line evolution and maintenance.

TABLE 1.1. The 10 most important predictors as determined by the Regression Estimate of Event Probabilities (REEP) screening procedure (after Bocchieri and Maglaras, 1983). Ranking is based both on the order and frequency of selection.

- 850 mb temperature and boundary-layer potential temperature for snow or ice pellets
- Observed surface temperature
- 1000-500 mb thickness and boundary-layer potential temperature for freezing rain or drizzle
- 850-500 mb thickness and 1000-850 mb thickness for snow or ice pellets
- Climatic frequency of freezing rain or drizzle
- Observed surface dewpoint temperature
- 850 mb temperature and boundary-layer potential temperature for freezing rain or drizzle
- 1000-850 mb thickness
- 850-500 thickness and 1000-850 thickness for freezing rain or drizzle
- 850 mb wet-bulb temperature

1.2 Research Goals/Objectives

The goals of the present research are to employ the enhanced-resolution data set collected during the Genesis of Atlantic Lows Experiment (GALE) to:

i) investigate the thermodynamic and kinematic processes that influence the

evolution, location, and orientation of the R-S line

ii) document surface features associated with the R-S line

iii) document possible mesoscale circulations associated with the gradient of melting or sublimation in the vicinity of the R-S line.

1.3 GALE Project

The field phase of the GALE project was conducted from 15 January to 15 March 1986. The objectives of GALE were to study mesoscale precipitation and air-sea interaction processes in East Coast winter storms, with their particular contributions to cyclogenesis (Dirks et al., 1988). To accomplish these objectives, the research described in this thesis deals primarily with a case study of the evolution of a R-S line occurrence during the period of 14 to 15 February 1986 [Intensive Observing Period (IOP) 6]. This period was chosen because it presented a unique opportunity to study the synoptic and mesoscale features associated with the development of the R-S line.

The GALE observing systems consisted of soundings, surface measurements, ships, aircraft and radar operations, and satellite systems. They are described in the next section.

2. CASE STUDY DATA AND METHODOLOGY

2.1 Data

The data for this research were a combination of standard observations with special observations at NWS and military stations and special sites operated specifically for the GALE field program.

There were two data-gathering areas of particular significance to the present research:

a) Inner GALE Area

In this area the meso-α processes of frontogenesis and R-S line development can be examined. The time and space scale for R-S lines and fronts are on the order of 2-24 h and 200-2000 km (Dirks et al., 1988). The Inner GALE Area was approximately 500-km wide, centered on the coast, and extended 1000 km from Georgia to Virginia (Fig. 2.1). Portable-Automated-Mesonet (PAM) II, Doppler radars, ships, buoys, most aircraft flights and the Cross-chain Loran Atmospheric Sounding System (CLASS) rawinsonde sites were in this area.

b) Regional GALE Area

The Regional GALE Area was 1,000-km wide (from the ridge of the Appalachians to 500-km offshore), and 1,500-km long (from Florida to New Jersey; see Fig. 2.1).

A brief description of the observing facilites used in this research is provided here.

a) Sounding operations

The GALE sounding operations were designed to provide three-dimensional fields with time resolution adequate to resolve the structure and evolution of mesoscale weather systems in the GALE observational network. GALE dropwindsonde flights off the Carolina coast sought to complement the dense land-based network (Fig. 2.1).

b) Surface measurements

The surface measurements were designed to provide surface data fields of standard meteorological parameters within the Inner GALE Area with mesoscale resolution and to provide a complement to the data gathered through sounding operations. Standard measurements included air temperature, dewpoint temperature, barometric pressure, wind speed, and wind direction. In addition, land-based stations measured precipitation, and sea-based stations measured sea temperature.

The fifty-station PAM-II network (Fig. 2.2) provided 5-minute meteorological surface observations over the eastern half of North Carolina and South Carolina and southeastern Virginia. A line of four stations extended northwestward to support a sounding cross-section for cold-wedge studies.

Deployment of the eight special GALE buoys, six North Carolina State University buoys and two NOAA-E buoys (Fig. 2.2), supported studies of the development of the coastal front and augmented observations in the data-sparse oceanic region in the Inner GALE Area.

c) Ships

The oceanographic research vessel (R/V) Cape Hatteras (RVC) was available during IOP 6 and operated off the southeast coast of North Carolina.

d) Aircraft operations

Generic flight tracks for each of the research airplanes were developed for a variety of

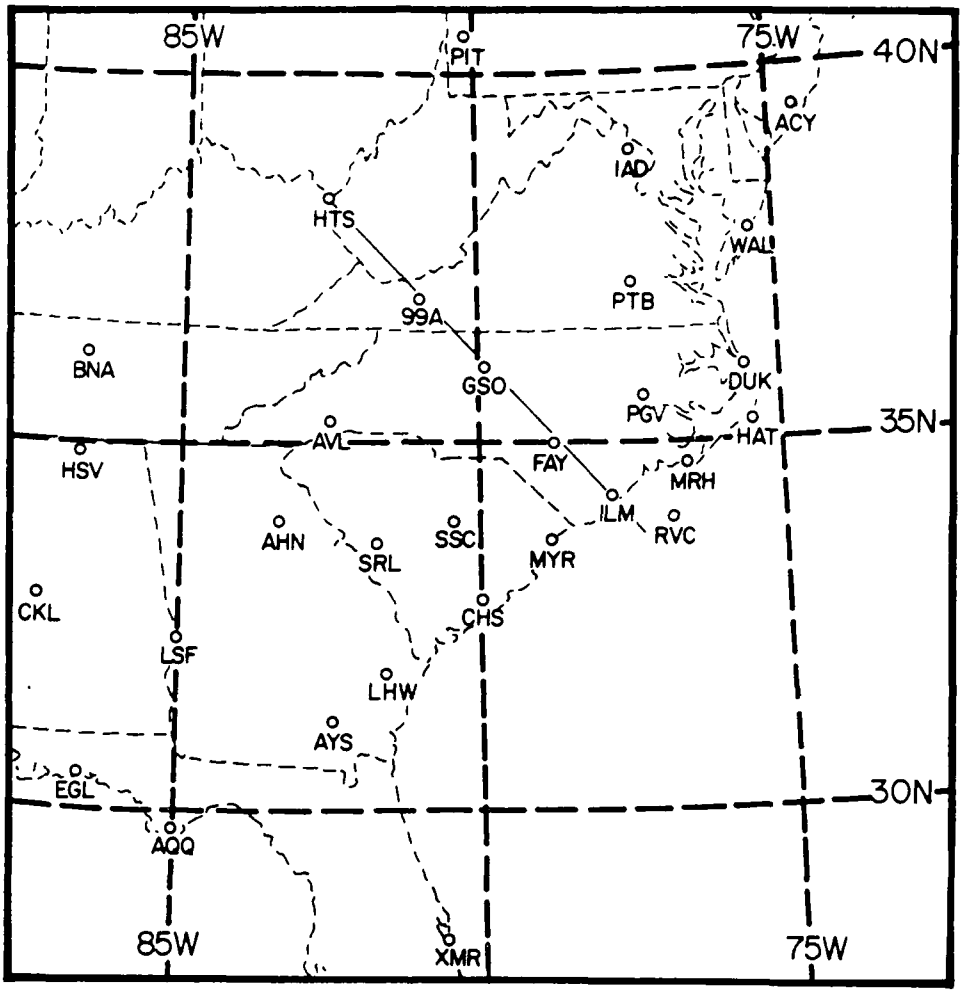

Figure 2.1. Inner and Regional GALE Area rawinsonde network. The Inner Area extends from LHW-SRL in the southwest to WAL in the northeast. The Research Vessel Cape Hatteras (RVC) is also shown. Cross-section line HTS-RVC is referred to in Fig. 3.9.

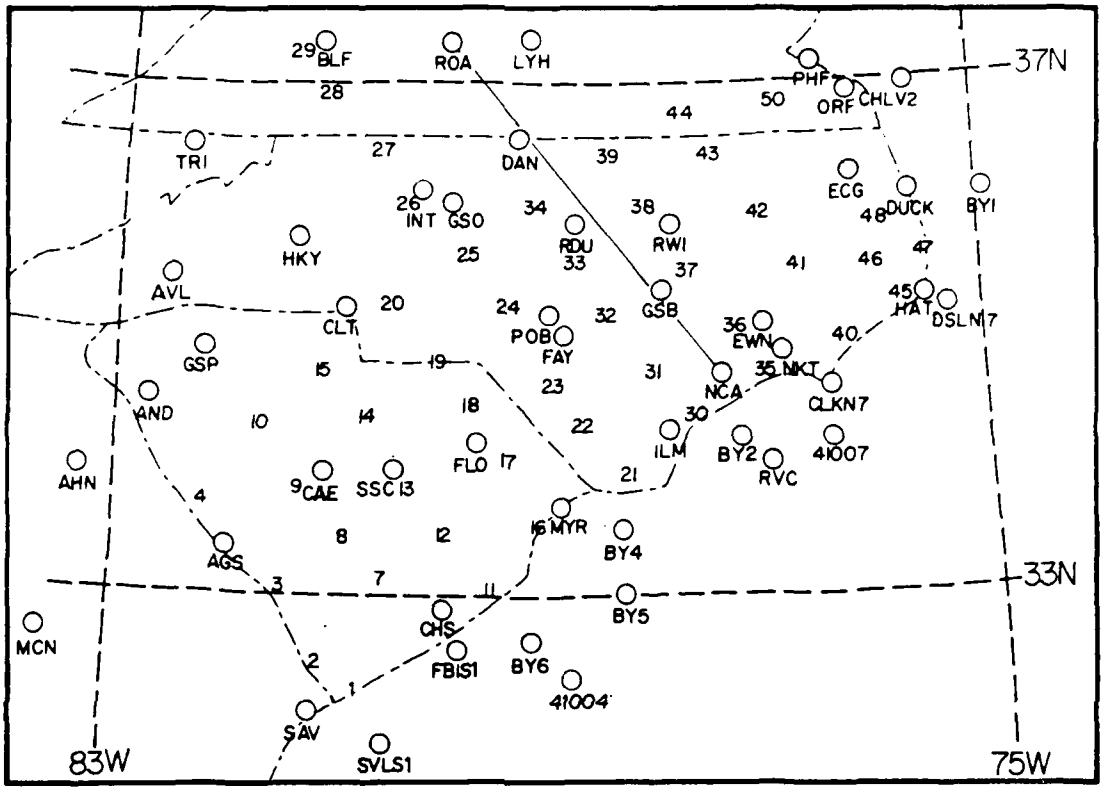

Figure 2.2. Location of surface observation sites, including the 50-station PAM-II network (numbered). Cross-section line ROA-NCA is referred to in Fig. 3.17.

weather scenarios. These tracks were designed to provide, but were not limited to, *in situ* measurements of mesoscale features and processes in precipitation regions and their environments, and information about the horizontal and vertical air-motion field.

e) Radar operations

An operational strategy for the GALE radars was to document the three-dimensional distribution of precipitation over the Inner GALE observational area. The standard NWS radar network included 10 radars that provided useful coverage of the Regional and Inner GALE Areas.

f) Satellite systems

The meteorological satellites in operation during GALE were GOES-6, NOAA-9, NOAA-6, DMSP F-6, DMSP F-7, and NIMBUS-7.

2.2 Barnes Objective Analysis Scheme

The analysis of meteorological fields, especially those to be used in computations, was aided by the Barnes (1964, 1973) objective analysis method. This widely-employed scheme accepts data from observation points and mathematically interpolates to any desired point in the geographical region. In particular, the scheme is used to obtain values at points in a two-dimensional grid array to be used in finite-difference calculations. If q represents any meteorological variable, the interpolated value is just the weighted mean ($\bar{q}$) of observations surrounding the point. That is,

$$\bar{q} = \sum_{i=1}^{N} w_i q_i \Big/ \sum_{i=1}^{N} w_i$$

Here, N is the total number of stations influencing a given grid point. The observation weights w are inverse distance (d) dependent and are defined by

$$w = \exp(-d^2 / k)$$

Here, k is the weight parameter and controls the rate at which the weight value decreases outward from the point of interpolation. Hence, k determines the degree of smoothing of

the data field: small k, little smoothing; large k, greater smoothing.

The selection of k is therefore crucial to the structural detail remaining in the interpolated field. The choice of this parameter value must strike a balance between an attempt to retain as much detail as the observation network density allows, and filtering out sources of random error. Structural detail is limited by the minimum resolvable wavelength. The GALE PAM-II stations have a mean spacing of about 68 km, while the upper air stations of the Inner GALE sounding (including NWS and CLASS) network have an average separation of about 180 km. These distances are about one-half those of the normal operational reporting networks. Theoretically, the Inner GALE networks can resolve features of twice the respective mean station separations, or about 140 km at the surface and 360 km aloft.

The weight parameter k is selected to reflect the degree of credibility given the amplitudes of the minimally-resolved waves, that is, the signal to noise ratio of the observations at small wavelengths. The specific k values used in this application suppress the amplitudes of the two-station-spacing waves to only 10 percent of their original amplitude (that is, a response function of 0.1) in the belief that error does make a significant contribution to the amplitudes of the higher frequency features. Sources of "error" include turbulent fluctuations with periods of several minutes (especially near the ground), biases introduced by local topography and obstacles at observation sites (again, especially important for surface stations), and features on scales smaller than the station spacing (e.g. gravity waves). The appropriate k values are 2000 and 7500 km^2 for surface and upper air analyses, respectively.

In spite of apparently strong smoothing, the interpolated fields still reflect features one would be inclined to accept if done subjectively by a skilled analyst. In particular, sharp discontinuities like frontal zones are still well represented in wind and temperature fields. Specific applications of the Barnes scheme will be described in the discussions of the results.

3. CASE STUDY OF A RAIN-SNOW LINE: 14-15 FEBRUARY 1986

3.1 Synoptic Overview

3.1.1 Satellite Imagery

Infrared imagery for 1200 GMT 14 February (Fig. 3.1a) depicts widespread cloudiness over the Tennessee and Ohio Valley. Note the comma-shape of the enhanced cloudiness extending northward from Lousiana, which is associated with a surface cyclone and developing cold front over the Mississippi Valley. Also note the elevated cloud top over southern Kentucky in the vicinity of a R-S line at the surface (indicated by the arrow). Six hours later (Fig. 3.1b) the cloud shield associated with this winter storm has moved eastward and has now overspread the Appalachians and extends across North Carolina. Elevated cloud tops over portions of Tennessee and Alabama are associated with heavier precipitation at the surface. At 2131 GMT (nearly three hours later) the highest cloud tops are located over western North Carolina and northward (Fig. 3.1c; note the different enhancement). By 0230 GMT (Fig. 3.1d), the cloud shield has continued to move eastward as the storm system has developed and areas of convective activity have broken out over the Atlantic. The upper-level clouds seem to leave the lower-level clouds behind as a region of lower cloudiness emerges over central North Carolina. Note the development of a cold front as clouds have vertically lined up across the Carolinas. By 0630 GMT (Fig. 3.1e), convection begins to develop over the Gulf Stream and all but the low clouds have moved out of the Carolinas.

3.1.2 Upper Air Analysis

The 300-mb analysis (not shown) at 1200 GMT indicates a jet streak with winds exceeding 55 m s^{-1} stretched southeastward from Montana to northern Texas. A second jet with wind speeds also over 55 m s^{-1} was located across the Great Lakes and New England states. The 500-mb analysis shows a trough extending southward from Iowa to eastern Texas (Fig. 3.2a). Cyclonic horizontal wind shear near the base of the trough axis contributed to a vorticity maximum over Oklahoma, with significant positive vorticity advection (PVA) ahead of the trough, especially over Arkansas and Missouri. A pool of colder air accompanied the trough, extending as far south as Arkansas and Oklahoma. The 850-mb analysis (not shown) at this same time indicates that strong warm air advection was occurring, especially over Kentucky and Tennessee, providing an indication that geostrophic adjustment and ascent was occurring over the Tennessee

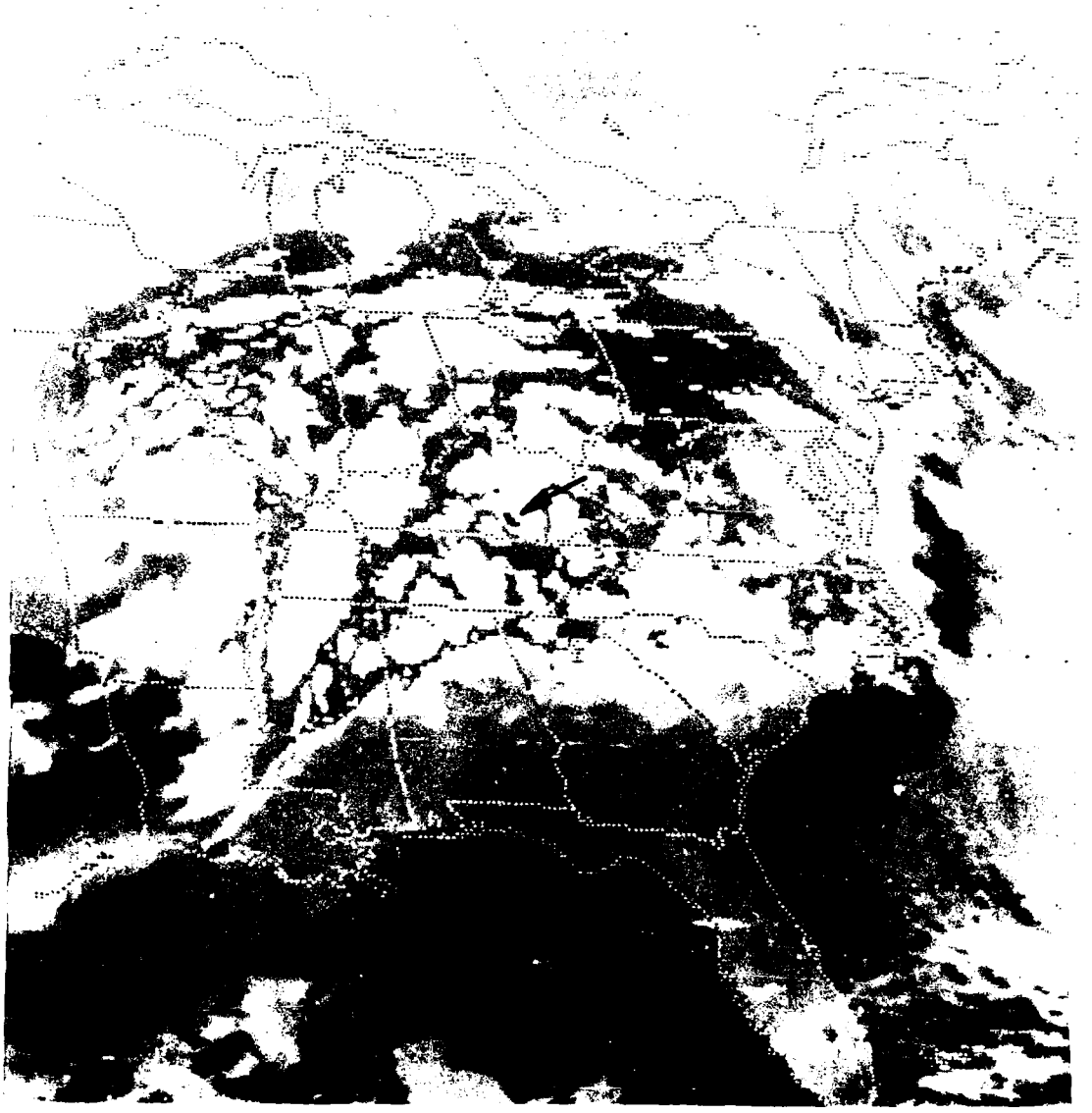

Figure 3.1a. Infrared satellite image at 1201 GMT 14 February 1986. Gray shades are applied using the infrared enhancement curve MB. The arrow indicates a region of elevated cloud top over southern Kentucky (see text).

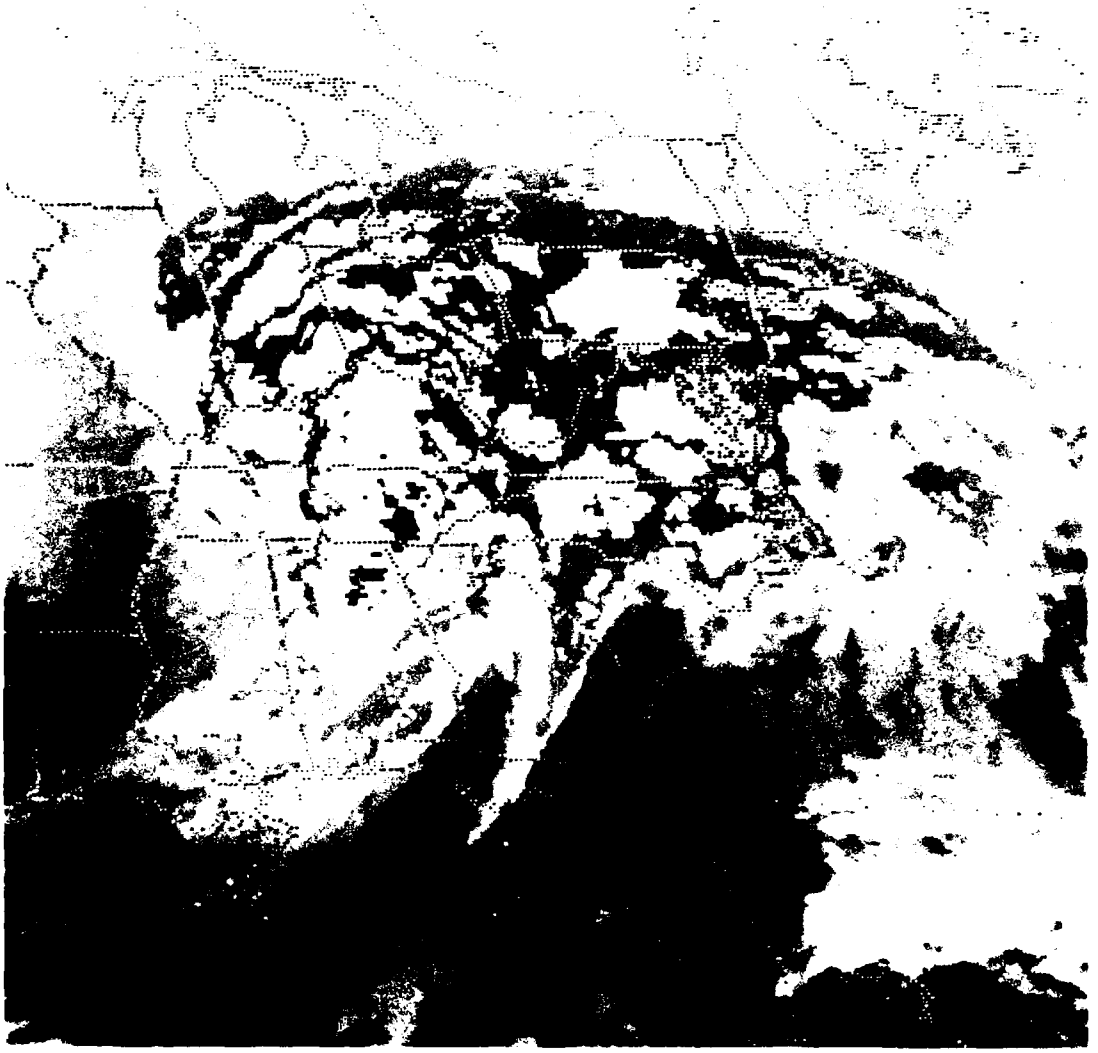

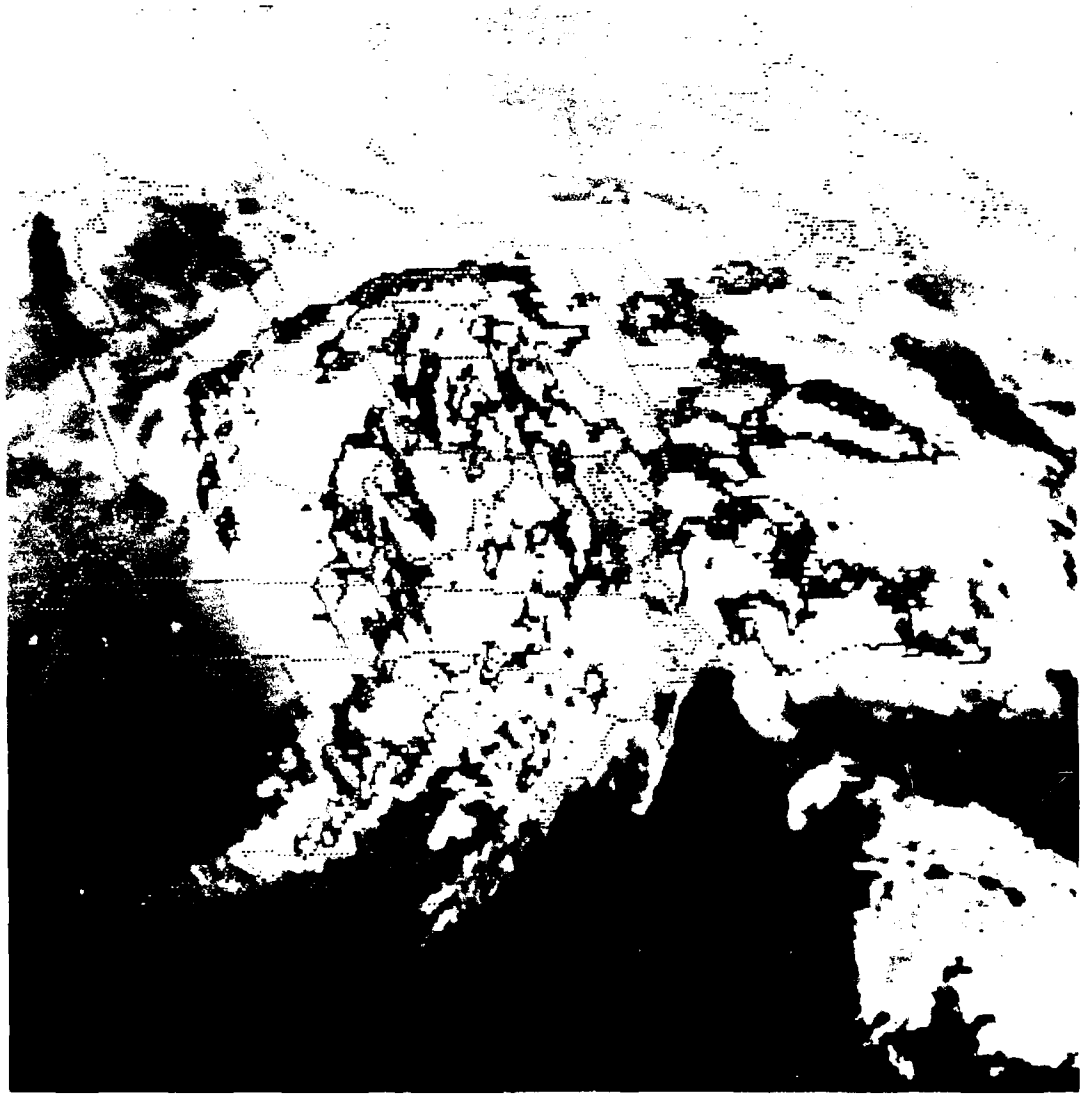

Figure 3.1c. Same as in Fig. 3.1a, except at 2131 GMT using the infrared enhancement curve CC.

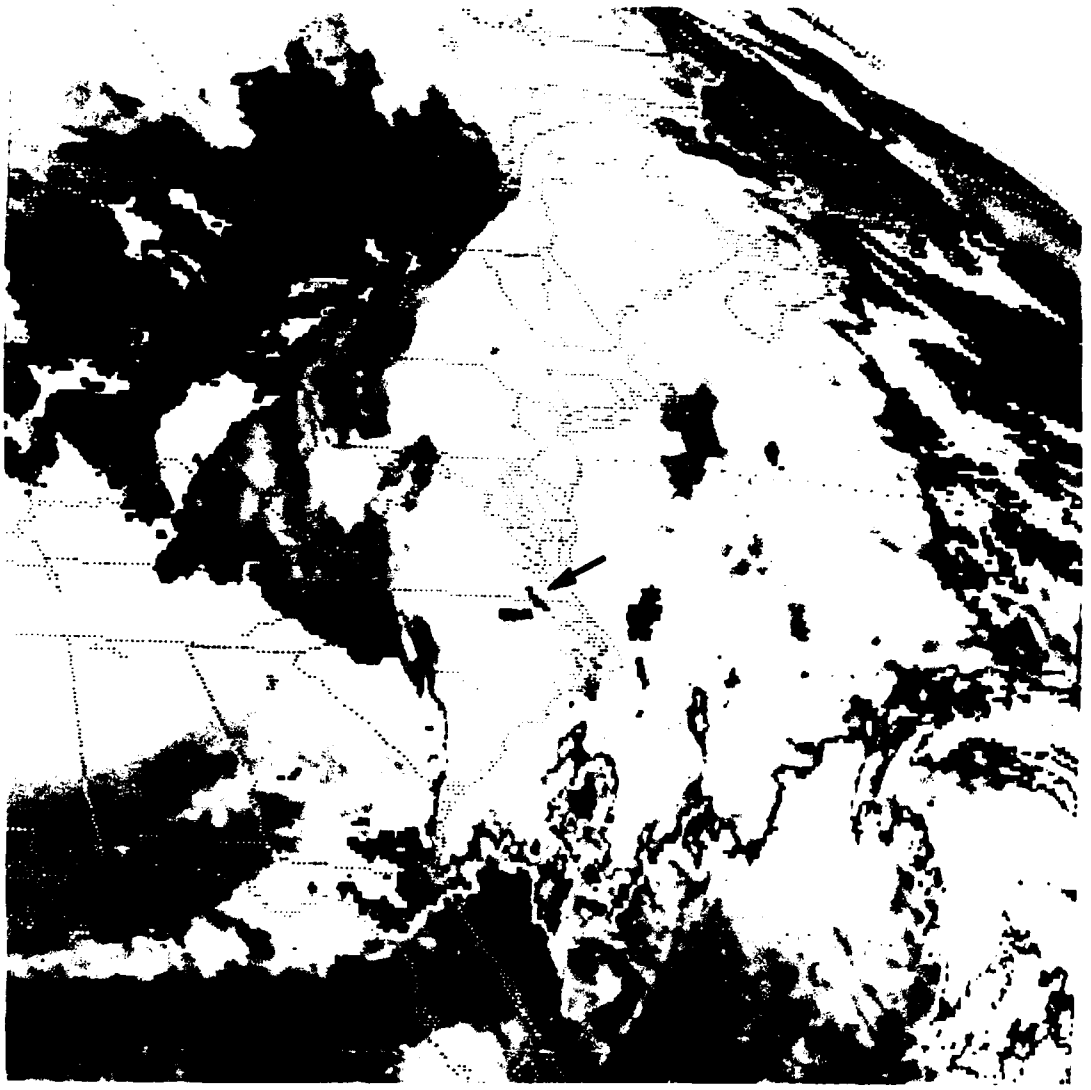

Figure 3.1d. Infrared satellite image at 0230 GMT 15 February 1986. Shading is applied using the infrared enhancement curve EC. The arrow indicates a region of elevated cloud top over North Carolina (see text).

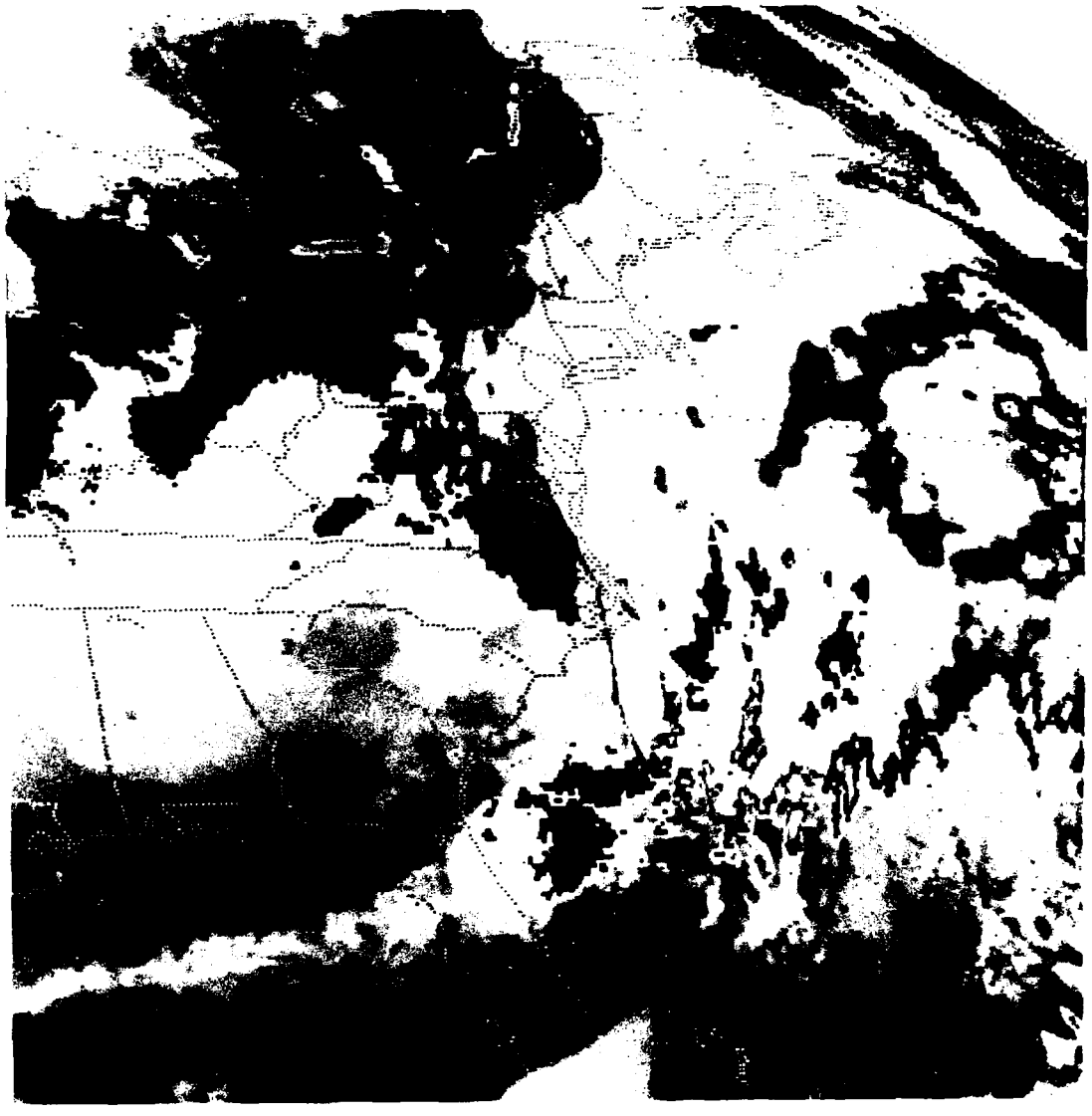

Figure 3.1e. Same as in Fig. 3.1d, except at 0630 GMT.

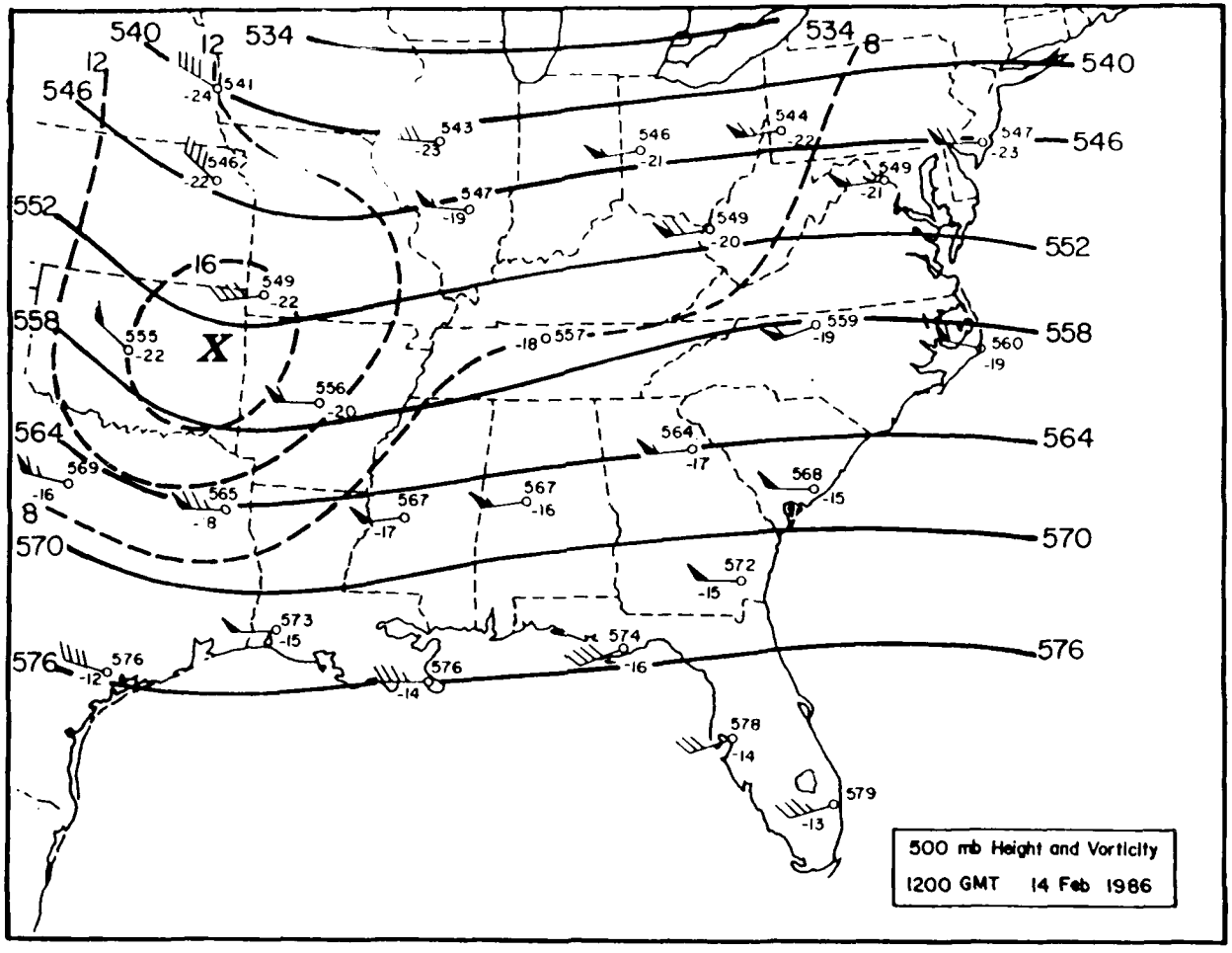

Figure 3.2a. Analysis at 500 mb for 1200 GMT 14 February 1986. Heights are solid (540= 5400 m) and the "X" denotes the location of vorticity maxima (x 10^{-5} s^{-1}). Station reports include temperature (°C) and wind velocity (barb = 5 m s^{-1}).

Valley.

By 0000 GMT 15 February, the two strong jets evident at the 300-mb level at 1200 GMT were still positioned on both the upstream and downstream sides of the trough. The 500-mb trough has moved eastward, extending southward from Indiana (Fig. 3.2b). The maximum of vorticity has moved northeastward, located over the Indiana-Kentucky border, with a broad area of PVA located over the Ohio Valley and eastward to the East Coast. The cooler air has now moved as far south as Georgia. At 850 mb (not shown) at this time, the initially widespread warm air advection was now mainly confined to the Carolinas and southern Virginia.

3.1.3 Surface Analysis

Figure 3.3a and 3.3b show the surface analyses for 1200 GMT 14 February and 0000 GMT 15 February. These analyses are based primarily on operational NWS surface data. However, PAM-II, ship, and buoy data supplemented the analyses over the eastern portion of the Carolinas and adjacent Atlantic Ocean.

The surface weather conditions for the East Coast at 1200 GMT were dominated by a cold anticyclone located just off the North Carolina coast. Subfreezing temperatures extended as far south as northern Florida and extremely dry air was entrenched over the Carolinas (Fig. 3.3a). A low centered over western Arkansas was located at the southern end of a cold front extending southwest from the Great Lakes region and a new low was forming over eastern Arkansas. The combined circulation of the high and low centers resulted in a broad area of southerly flow across the eastern one-third of the United States. The new low center moved slowly east-northeastward and weakened as it approached the Appalachian Mountains, and was appeared as a surface pressure trough over northeastern Tennessee by 0000 GMT 15 February (Fig. 3.3b). At 1200 GMT snow was falling as far east as western West Virginia and as far south as southern Kentucky while rain and freezing rain were falling over portions of Tennessee and Arkansas. By 0000 GMT, snow began falling in parts of South Carolina and as far east as the Atlantic seaboard, with temperatures still below freezing over most of the mid-Atlantic area. A R-S line, which was oriented nearly east-west at 1200 GMT, had shifted southeastward across the Appalachians into South Carolina by 0000 GMT (Fig. 3.3b).

3.1.4 24-hour Precipitation/Total Snowfall Accumulation

An analysis of precipitation amounts (Fig. 3.4a) for the mid-Atlantic region from

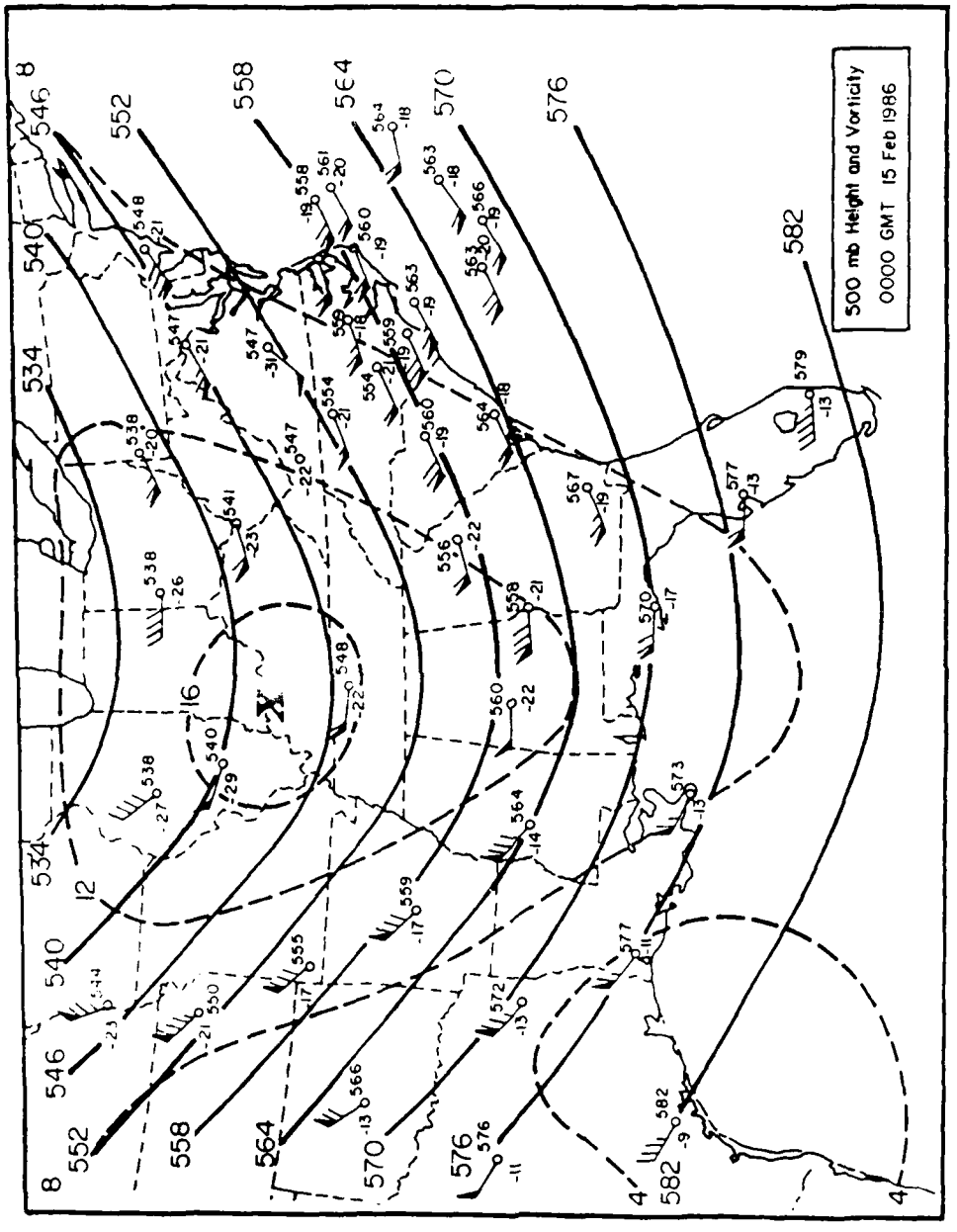

Figure 3.2b. Same as in Fig. 3.2a, except for 0000 GMT 15 February 1986.

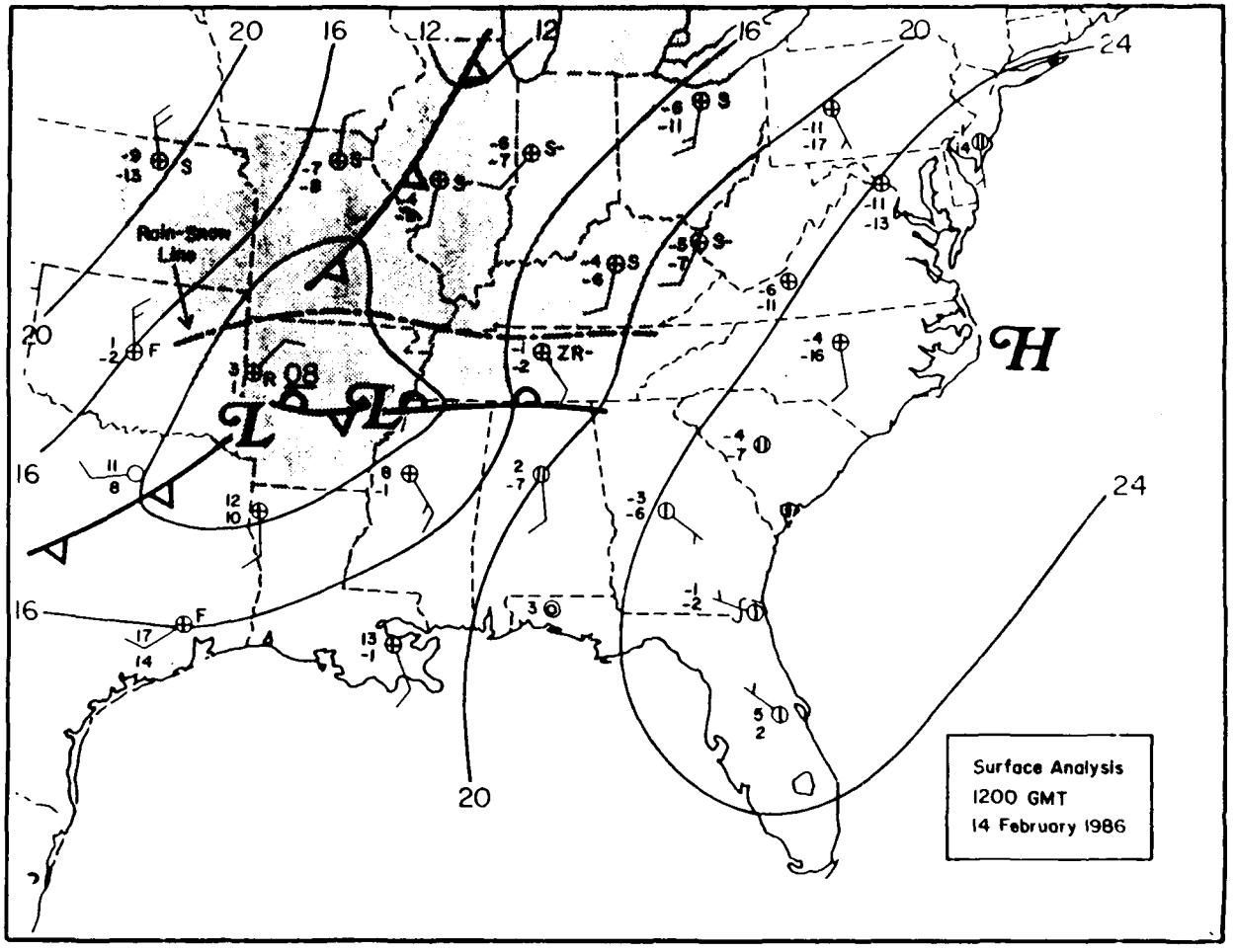

Figure 3.3a. Surface frontal analysis for 1200 GMT 14 February 1986. Station reports include temperature (°C), dewpoint temperature (°C), observed weather, cloud cover, and wind velocity (half-barb represents 2.5 m s^{-1}). Central pressure denoted by bold numbers (08 = 1008 mb). Shading depicts area of precipitation.

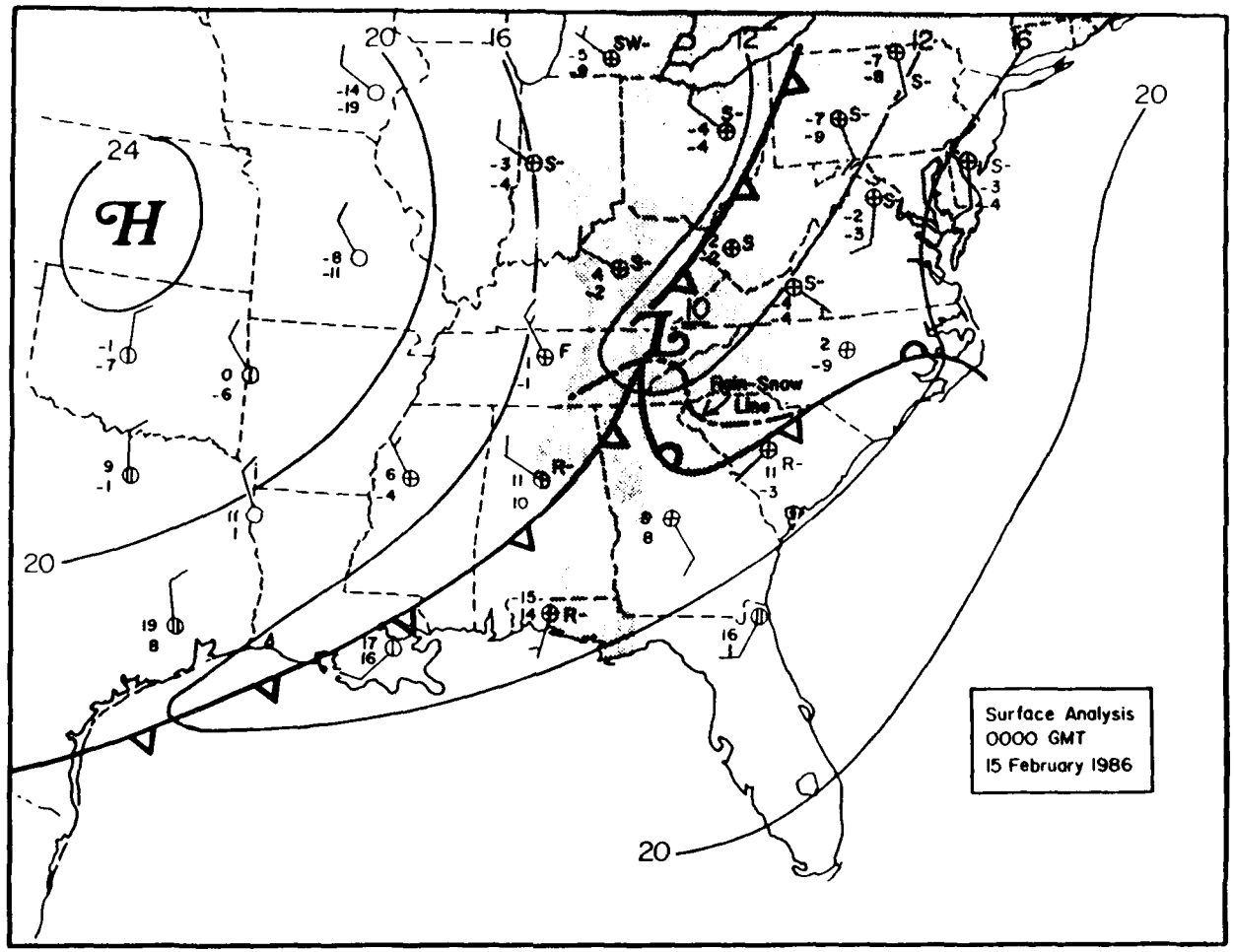

Figure 3.3b. Same as in Fig. 3.3a, except for 0000 GMT 15 February.

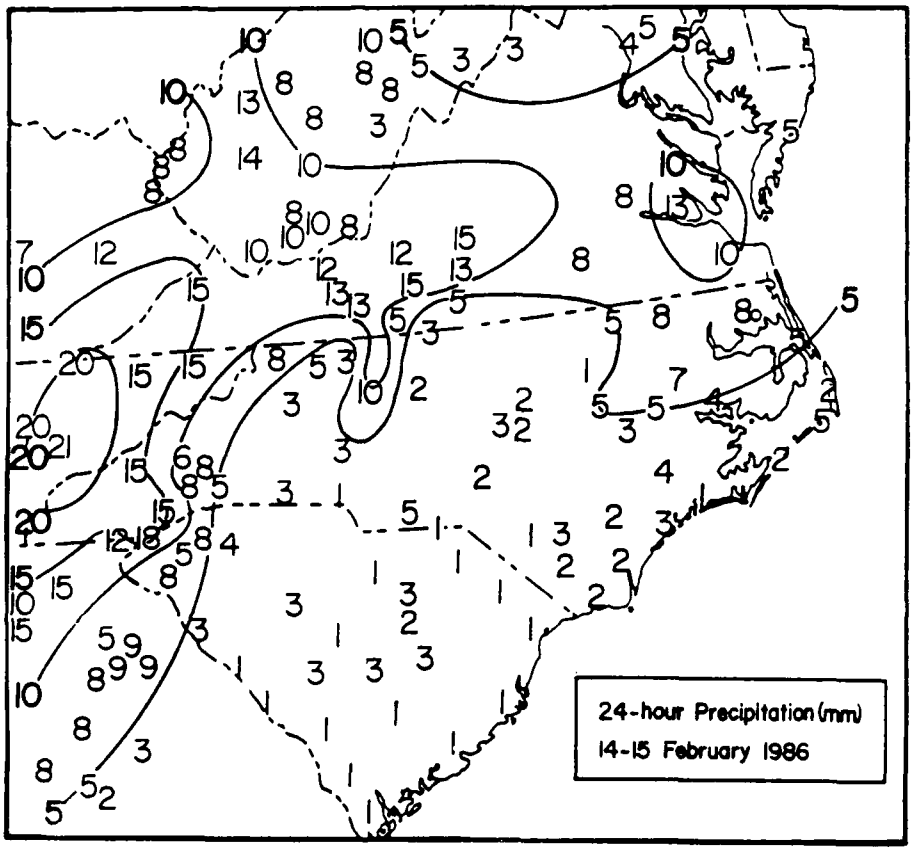

Figure 3.4a. Precipitation accumulation from 1200 GMT 14 February through 1200 GMT 15 February. Precipitation [and contours (bold)] is in millimeters.

1200 GMT 14 February to 1200 GMT 15 February 1986 depicts a maximum of precipitation over the mountainous regions of Virginia, east Tennessee, North Carolina, and West Virginia, and across the southeastern portion of Virginia.

Snowfall accumulation for the duration of this storm is shown in Fig. 3.4b. The heaviest snow fell over the Virginia mountains and extended eastward to the Virginia coast.

3.2 Mesoscale Analyses in the Vicinity of the Rain-Snow Line

3.2.1 Surface Analysis

On 15 February 1986 a R-S line formed *in-situ* over the Inner GALE Area. This feature was most fully developed from 0200 to 0400 GMT 15 February. The R-S line accompanied a cyclone that moved eastward across the Appalachians toward the North Carolina coast.

Figures 3.5a-d show the surface analyses for the Carolinas and eastern Georgia)part of the Inner GALE region) from 2100 GMT 14 February to 0600 GMT 15 February. At 2100 GMT, a stationary front had developed ahead of the surface low-pressure center in an inverted pressure trough, with a R-S line extending eastward from Tennessee across the North Carolina-South Carolina border (Fig. 3.5a). Generally weak radar echoes were being received, except for strong echo returns from northeastern Georgia. By 0000 GMT, the stationary front extended across the entire region (Fig. 3.5b). At this time, the R-S line was found farther eastward, nearly parallel to the frontal zone. Stronger radar echoes were found across portions of northeastern North Carolina and Georgia and western South Carolina (Fig. 3.5b).

A R-S line extended across the entire analysis region at 0300 GMT, again nearly parallel to the stationary front, which continued to show little movement north and south (Fig. 3.5c). The mesoscale nose of high pressure in Fig. 3.5c appears to be related to the R-S line. It is suggested that this feature may be enhanced as the result of a mesoscale circulation associated with the R-S line. Additional evidence for this mesoscale circulation is provided by the satellite image for 0230 GMT 15 February (Fig. 3.1d) which shows an elliptically-shaped elevated cloud top in the vicinity of the R-S line (indicated by the arrow). Strong radar signals have now moved into and just off the coast of the eastern Carolinas. By 0600 GMT (Fig. 3.5d), a low pressure center was analyzed in southeastern North Carolina. A R-S line can still be found, again nearly parallel to the

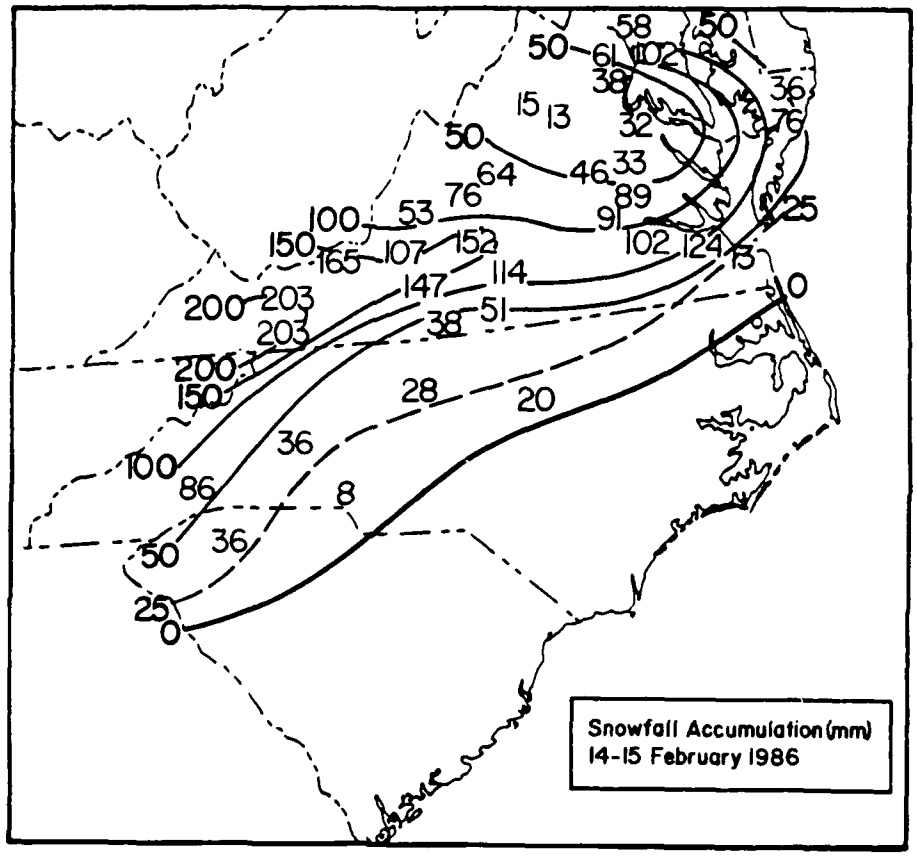

Figure 3.4b. Total snowfall accumulation for 14 to 15 February 1986. Snow amounts [and contours (bold)] are in millimeters.

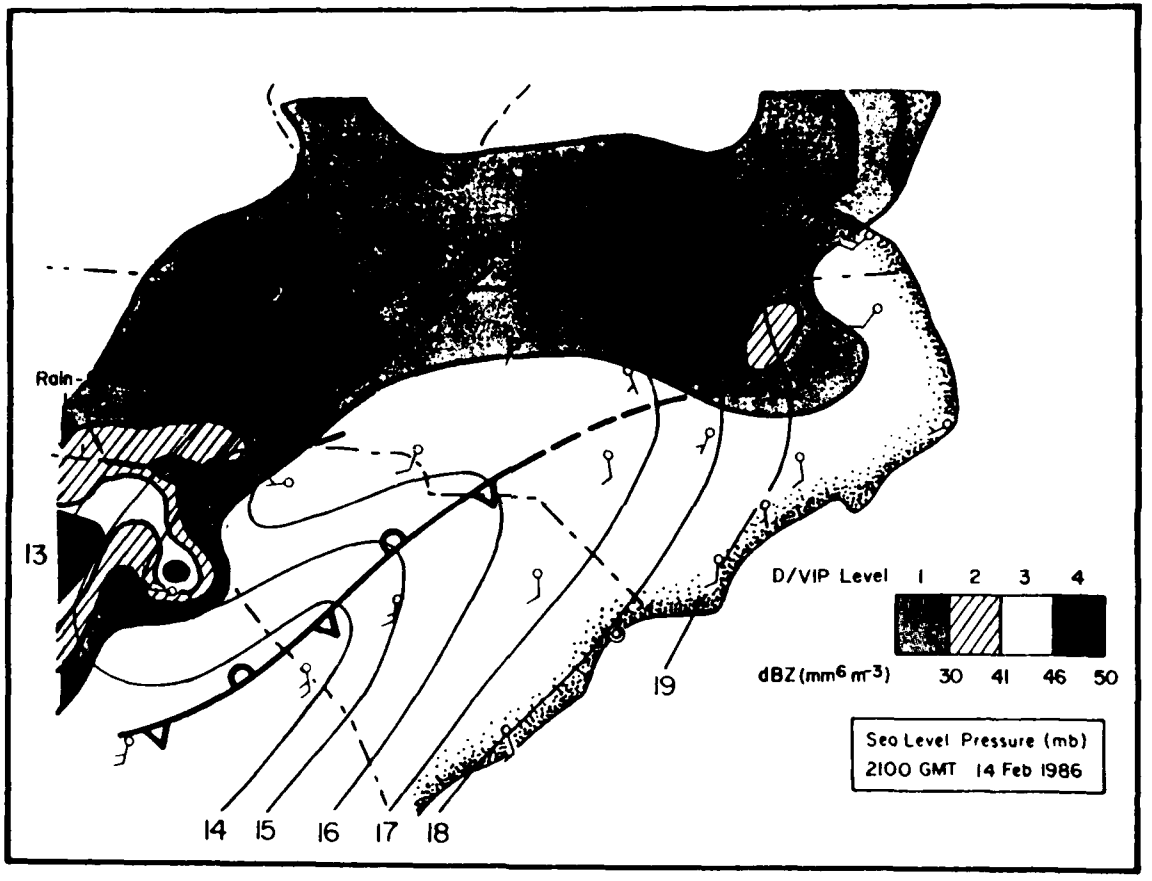

Figure 3.5a. Surface analysis for 2100 GMT 14 February 1986. Half-barb wind vectors indicate 2.5 m s^{-1}. The location of the rain-snow line, stationary front, radar intensities, and isobars (contours in mb - 1000) are indicated.

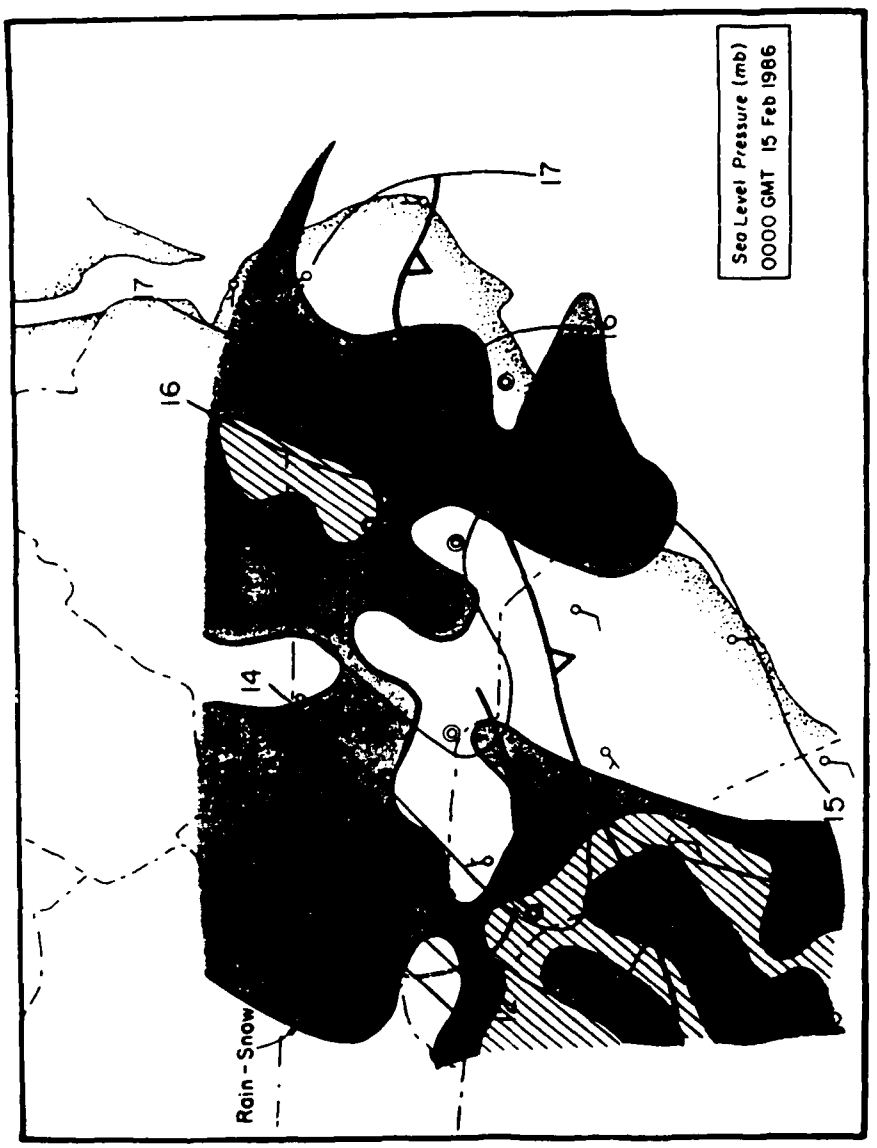

Figure 3.5b. Same as in Fig. 3.5a., except for 0000 GMT 15 February.

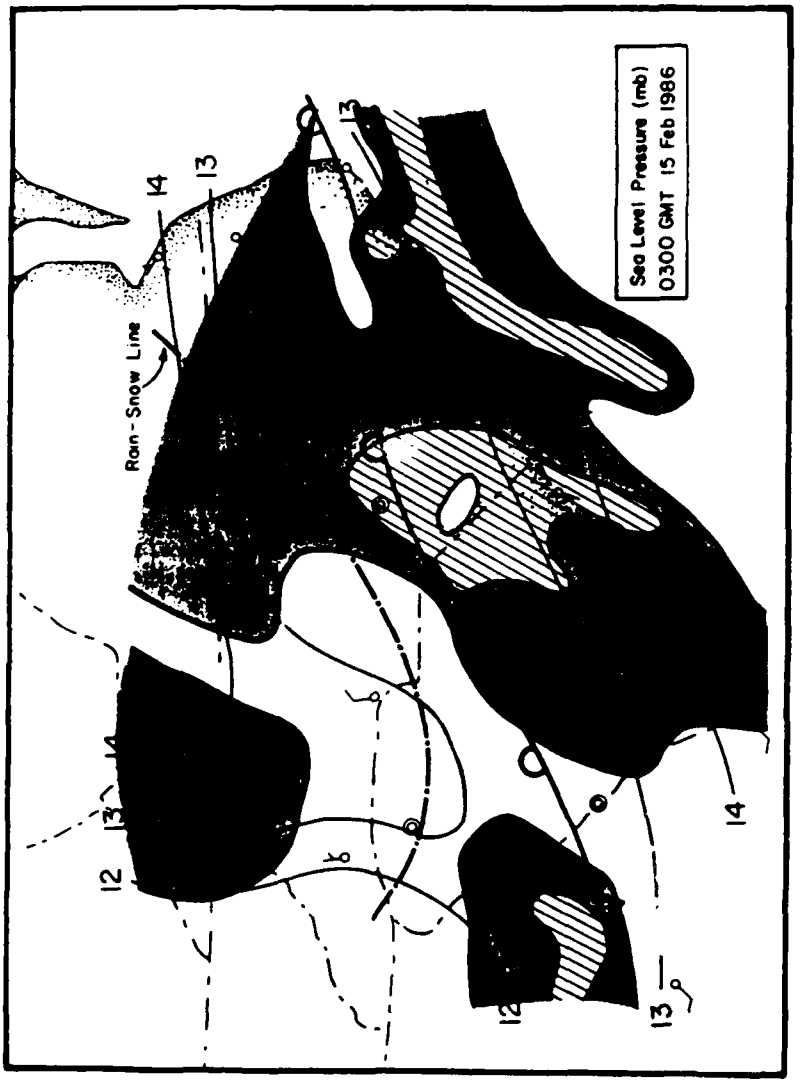

Figure 3.5c. Same as in Fig. 3.5a, except for 0300 GMT 15 February.

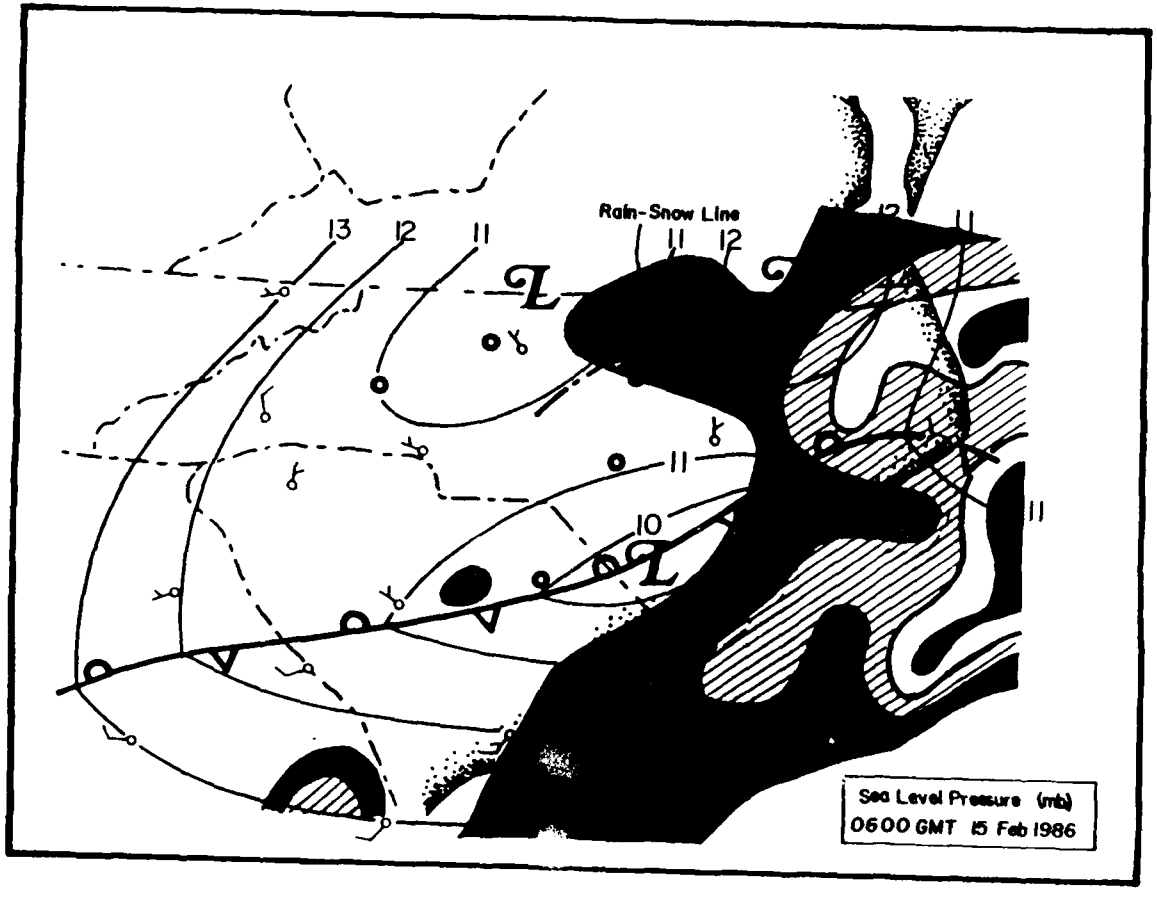

Figure 3.5d. Same as in Fig. 3.5a, except for 0600 GMT 15 February.

surface front, although precipitation has stopped across much of the Carolinas and Georgia. Strong radar returns can be found across eastern North Carolina and just offshore, where convective activity is increasing.

Figures 3.6a-d show the surface streamline and isotherm patterns for the Inner GALE region for the same times as in Fig. 3.5, with the R-S line and frontal positions superposed. PAM-II wind and temperature data were the primary sources for these analyses, although supplementary NWS hourly observations were also used. The PAM-II winds were one-hour time-averaged to remove higher frequency fluctuations in the data. This is justified since the R-S line and front were quasi-stationary. The time average was centered at the desired analysis time.

Broad southerly flows prevails at 2100 GMT, with warm advection occurring over most of the eastern Carolinas (Fig. 3.6a). A tongue of warm air existed over eastern South Carolina which remained quasi-stationary. Only the extreme eastern edge of the R-S line at 0000 GMT extends into the main body of the PAM-II network, where a weak anticyclonic wind shift can be found (Fig. 3.6b). Confluence in the streamlines can be found at the stationary front across parts of North and South Carolina. Warm air advection dominates at this time, although a small region of cold advection is located over east-central and south-central North Carolina. By 0300 GMT, the temperature gradient has increased across northeastern North Carolina (Fig. 3.6c). Confluence along the stationary front at this time supports the frontogenesis. By 0600 GMT (Fig. 3.6d), the front has further intensified and streamline confluence is even more evident.

Stewart and King (1987) examined the temporal variability of surface temperature and pressure as they related to the R-S boundary. In a limited attempt to find if similar variability existed during this R-S line event, a time series of surface parameters for Raleigh-Durham (RDU), North Carolina was plotted (Fig. 3.7). RDU was chosen since it was in the vicinity of the R-S line and, as a result, experienced many different precipitation types.

Dry-bulb temperatures remained constant just before and during the fall of snow and ice pellets around 1900 GMT (Fig. 3.7). A gradual dry-bulb temperature increase followed the cessation of precipitation during the afternoon (see Fig. 3.6a), but largest 1 h declines occurred during the second onset of snow, consistent with what was found by Stewart and King (1987). Dry-bulb temperatures remained constant after 0000 GMT, except for a small increase around 0300 GMT, when the rain and drizzle stopped and all snow was reported. Wet-bulb temperatures showed a general increase during and after the early fall of snow and ice pellets and reached the dry-bulb temperature around 0100

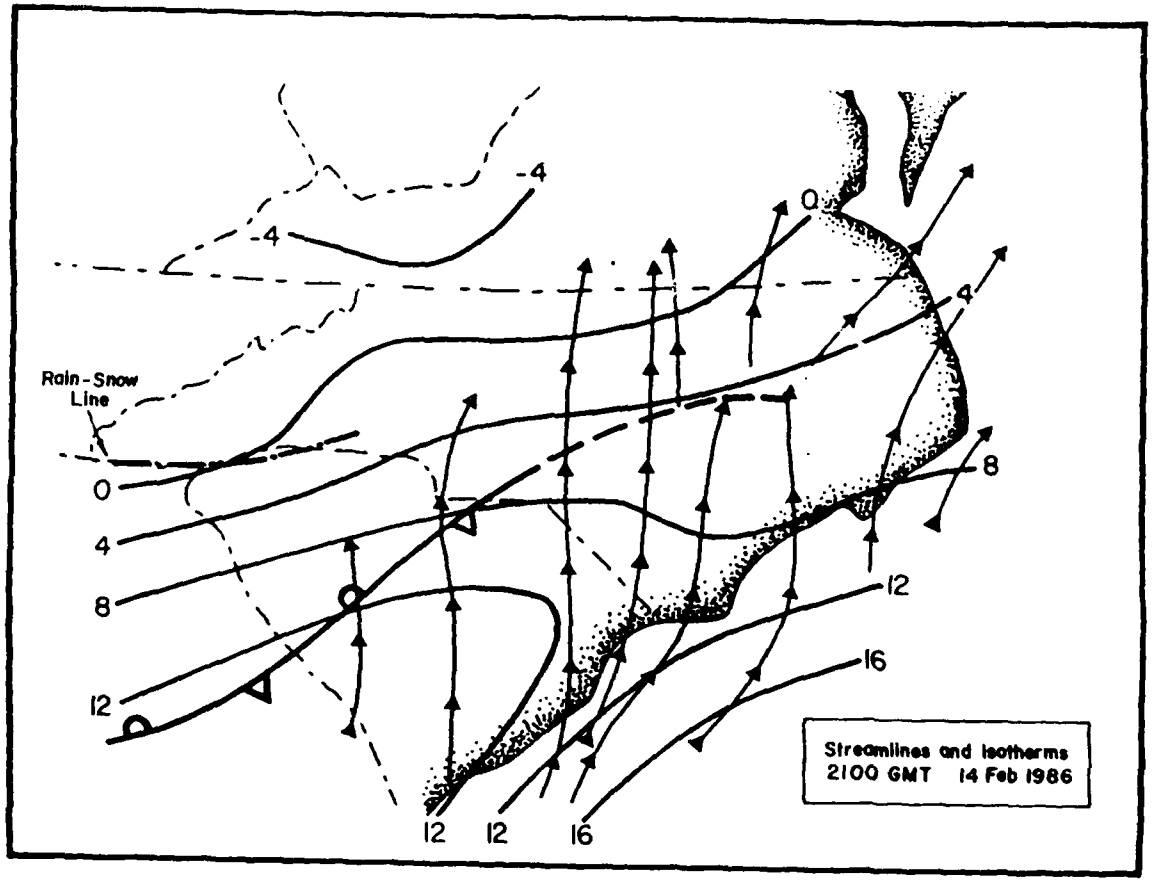

Figure 3.6a. Surface wind direction and temperature (°C) analysis for 2100 GMT 14 February. The location of the rain-snow line and front are also indicated.

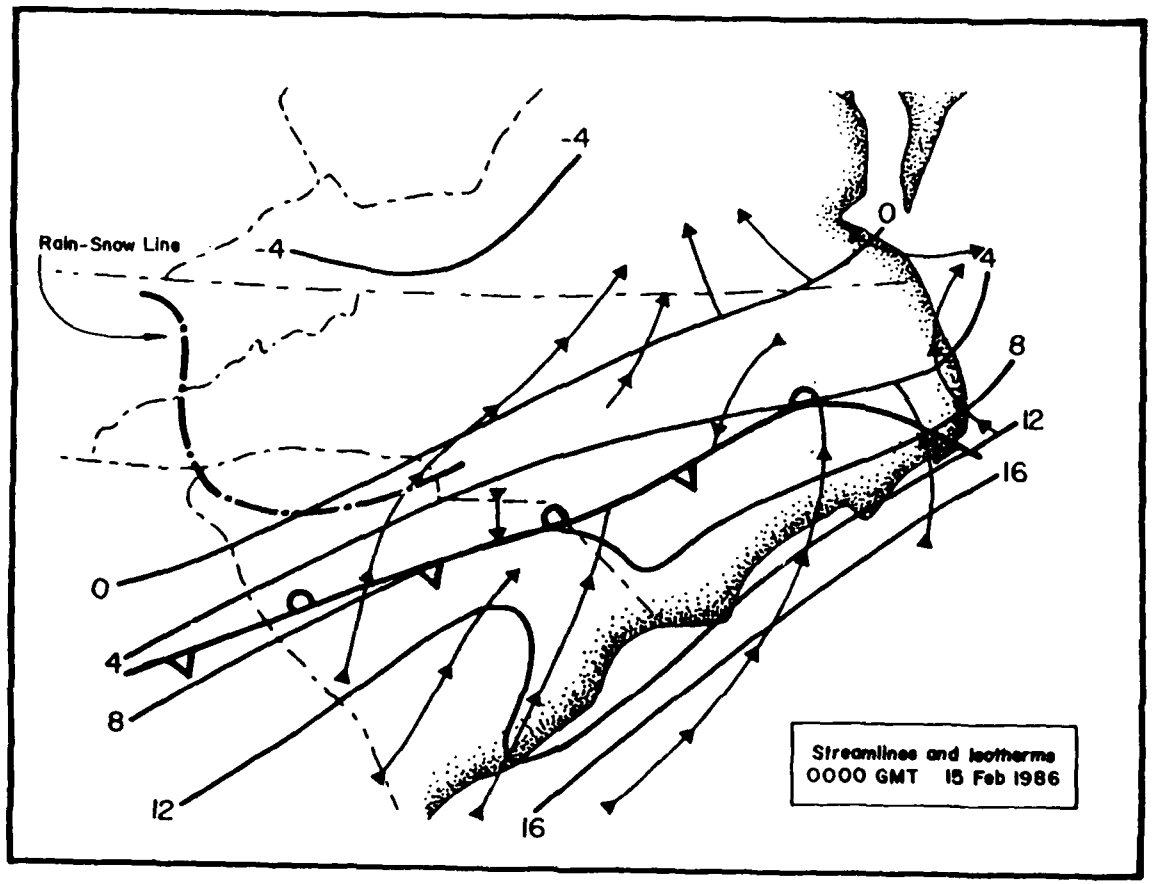

Figure 3.6b. Same as in Fig. 3.6a, except for 0000 GMT 15 February.

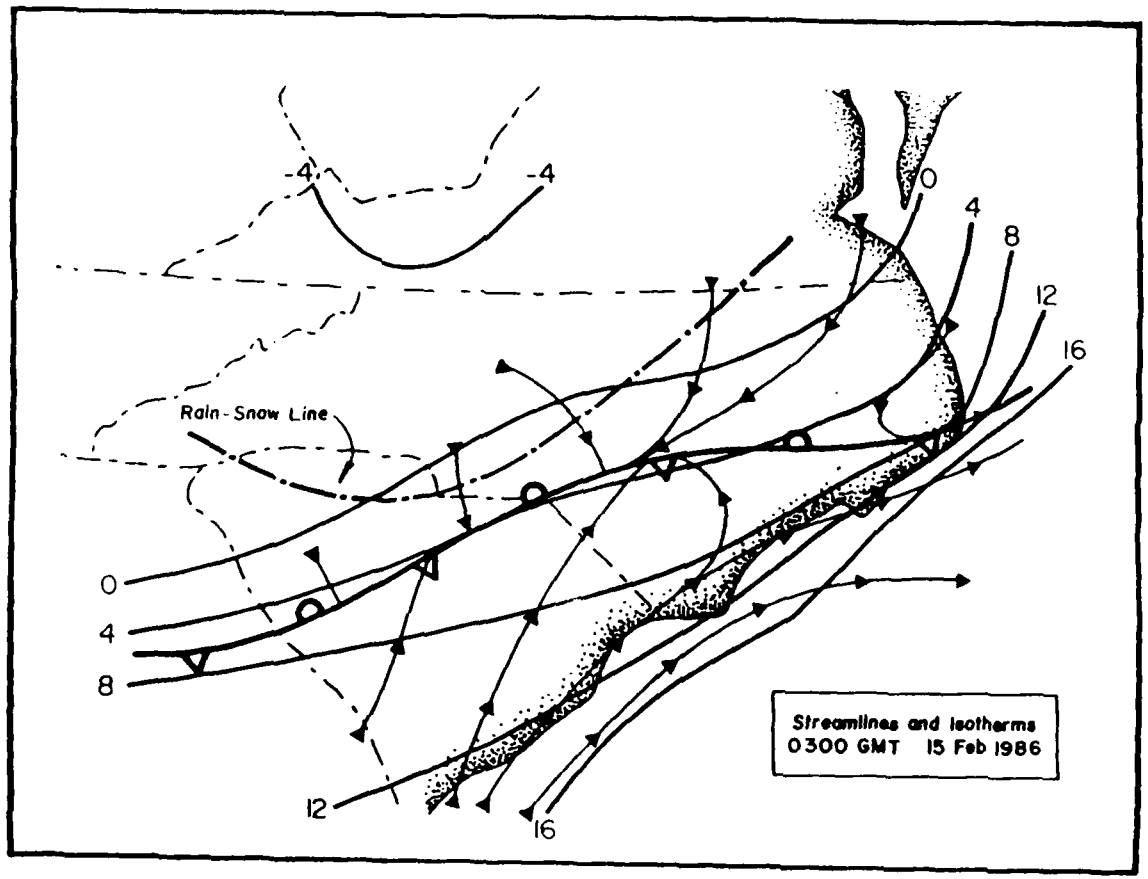

Figure 3.6c. Same as in Fig. 3.6a, except for 0300 GMT 15 February.

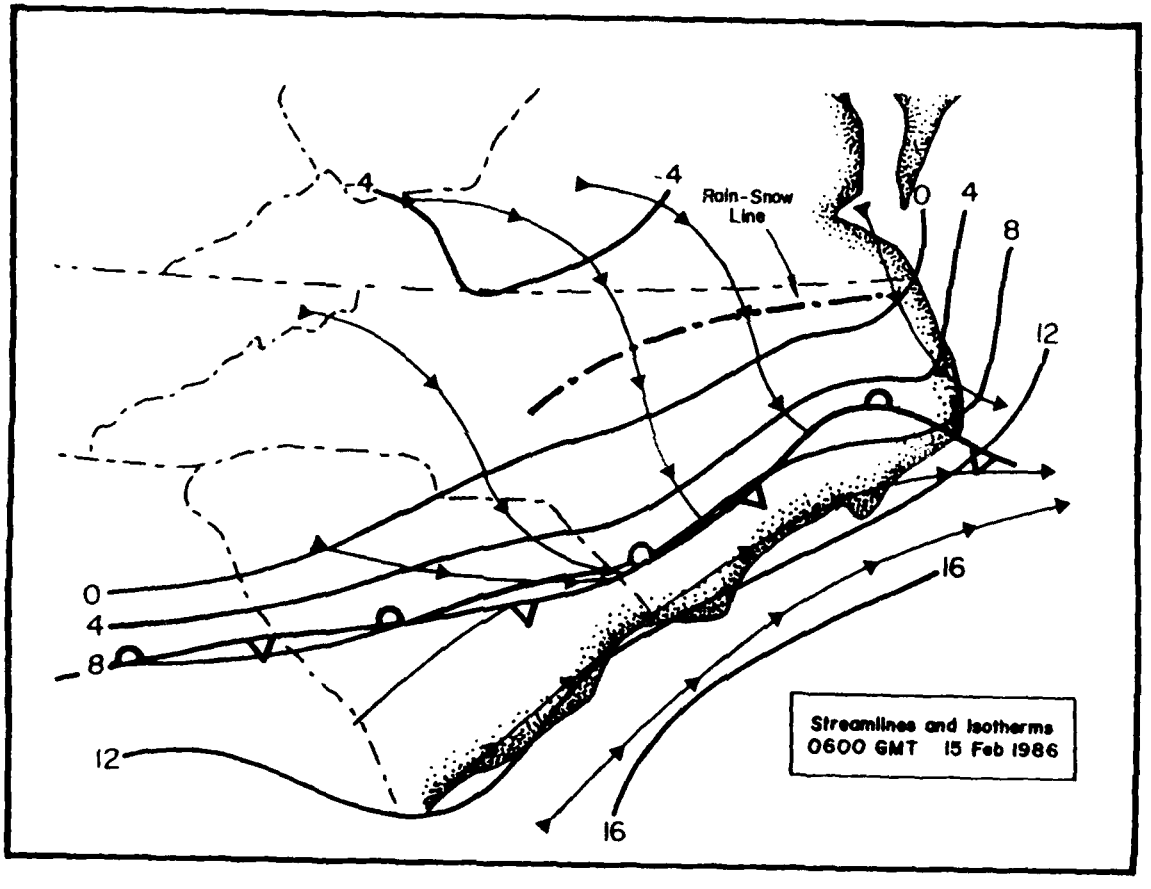

Figure 3.6d. Same as in Fig. 3.6a, except for 0600 GMT 15 February.

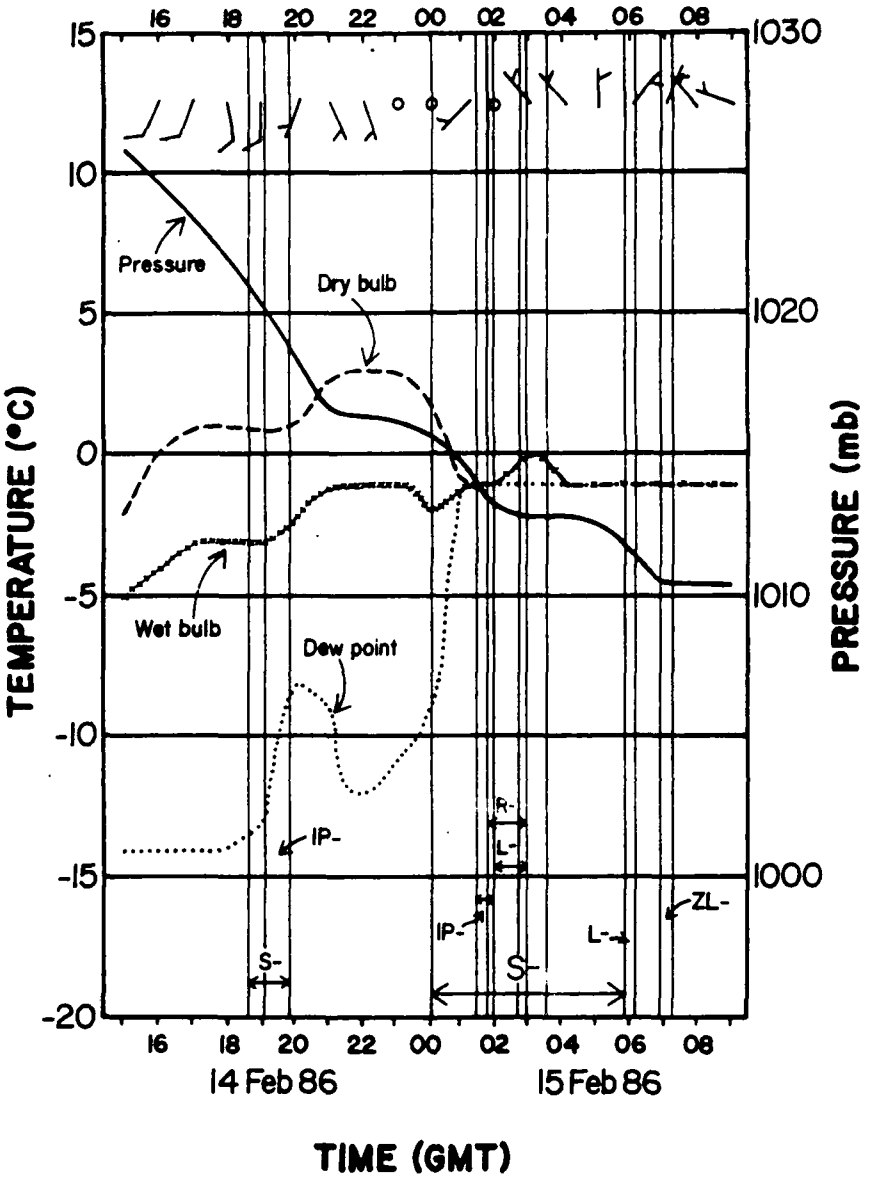

Figure 3.7. Surface parameters plotted as a function of time at Raleigh-Durham, NC on 14 and 15 February 1986. Half-barb wind vectors indicate 2.5 m s^{-1}. The symbol L denotes drizzle, ZL denotes freezing drizzle, R denotes rain, S denotes snow, and IP denotes ice pellets. The dash accompanying one of these symbols represents light.

GMT. The wet-bulb temperature dipped slightly just before the second episode of snow, but then rose just after snow began around 0000 GMT. The dew-point temperature rapidly increased during the initial fall of snow and ice pellets, decreased after the mixed precipitation had ended, then increased dramatically during the onset of another snow episode, reaching the dry-bulb temperature at 0100 GMT. The large decrease of dry-bulb temperature and increase of the dew-point temperature suggests that evaporative cooling was occurring.

According to Stewart and King (1987), pressure changes are linked to precipitation transitions. For RDU in this mixed precipitation event, some relationship between pressure and precipitation type transitions was also found. At the time when ice pellets fell with snow near 1900 GMT and 0130 GMT, there was a slightly larger decline in the pressure trace (see Fig. 3.7). There was a slight rise in pressure after the end of rain and drizzle with snow around 0300 GMT. Stewart and King found that, at one of the two sites that reported both snow and rain, the largest pressure drop occurred during the transition from snow to rain. In the present case, while the pressure continued to fall at the time of transition from snow to drizzle near 0600 GMT, a larger decline in pressure occurred after the drizzle had ended. Therefore, the evidence shows that RDU's pressure generally decreased during instances of snow and rain and during the transition from snow to drizzle.

3.2.2 Isentropic Analysis

Analyses of pressure, wind vectors, and moisture on a 285°K isentropic surface are shown in Figs. 3.8a-d for 2100 GMT 14 and 0600 GMT 15 February 1986. The 285°K surface was chosen because of its location within the frontal boundary as analyzed in the plane of the cross-section shown in Fig. 3.9.

At 2100 GMT significant cross-isobaric flow and evidence for ascent is indicated over the Carolinas, Georgia, and Alabama (Fig. 3.8a). Very dry air existed at this level across North Carolina, corroborated by a sounding at Greensboro (Fig. 3.18). A similar flow pattern is found at 0000 GMT (Fig. 3.8b). However, mixing ratios have doubled over North Carolina. By 0300 GMT, the region of strongest cross-isobaric flow has moved slightly eastward and decreased somewhat. Moisture has continued to increase along the coast of the Carolinas (Fig. 3.8c). By 0600 GMT (Fig. 3.8d), most of the flow was along isobaric surfaces or descending to levels of higher pressure.

At this point it is interesting to compare the isentropic analysis for 0000 GMT 15

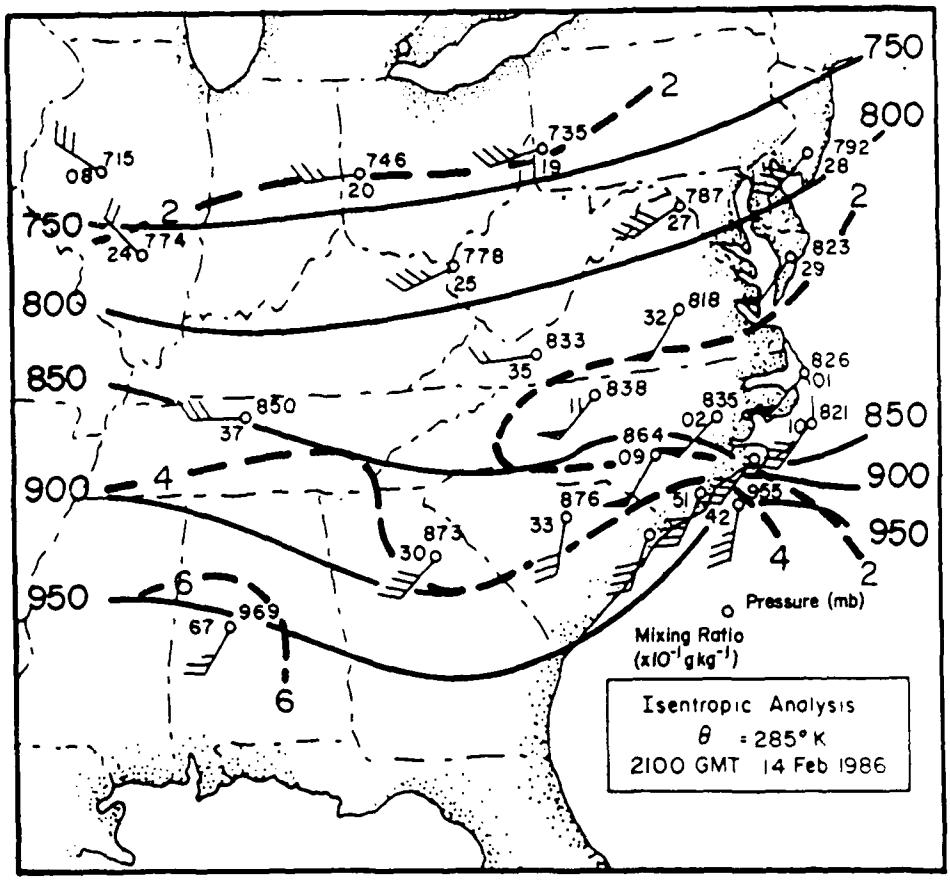

Figure 3.8a. Isentropic analyses of pressure, wind, and mixing ratio on the 285-K surface at 2100 GMT 14 February 1986: pressure (solid contours, mb); mixing ratio (heavy dashed, g kg^{-1}); wind (barb = 5 m s^{-1}, pennant = 25 m s^{-1}).

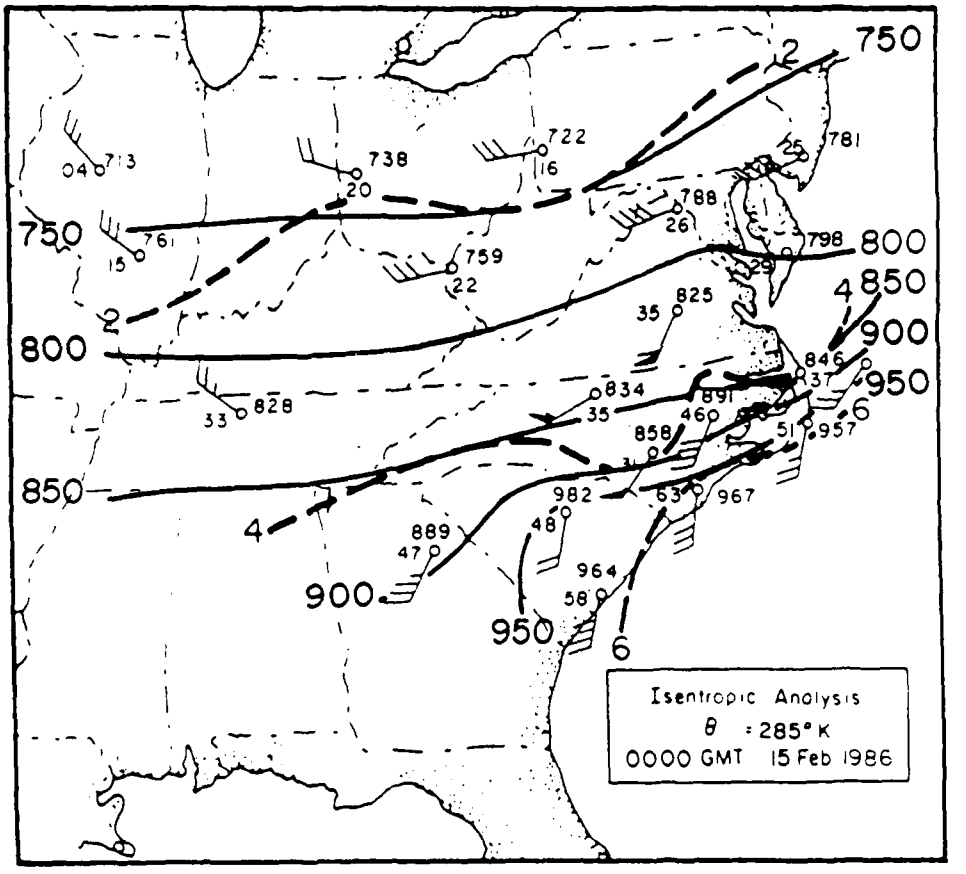

Figure 3.8b. Same as in Fig. 3.8a, except for 0000 GMT 15 February.

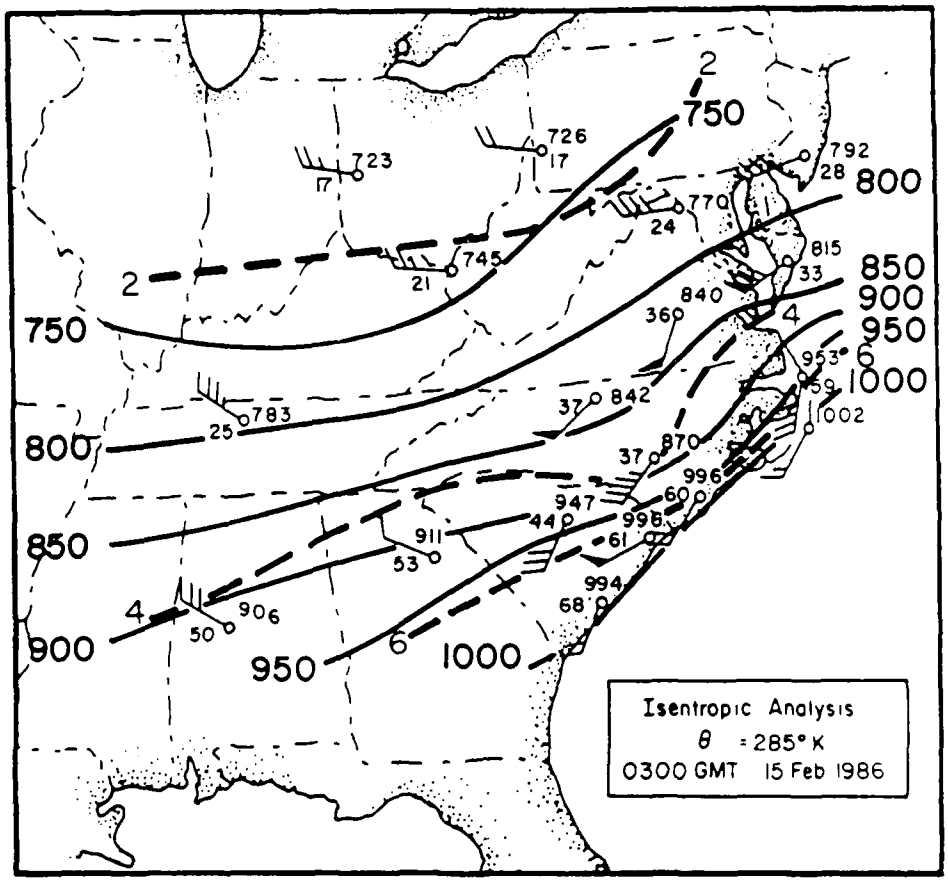

Figure 3.8c. Same as in Fig. 3.8a, except for 0300 GMT 15 February.

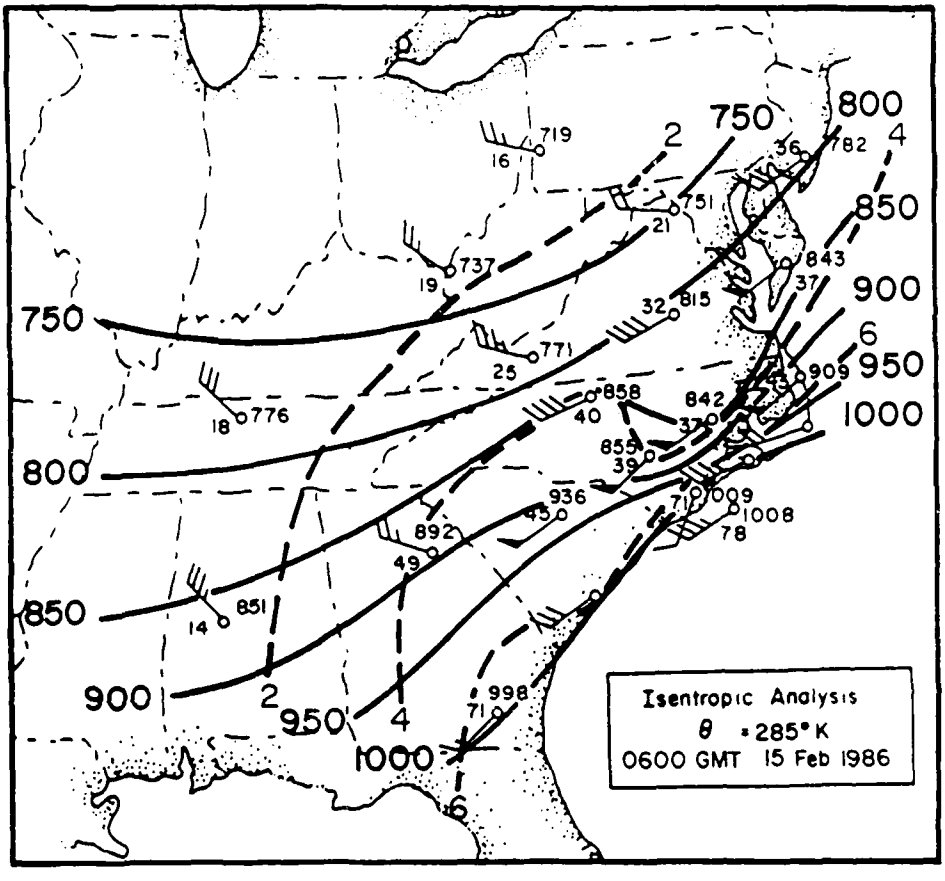

Figure 3.8d. Same as in Fig. 3.8a, except for 0600 GMT 15 February.

February with that by Homan and Uccellini (1987); in particular, the vertical velocity (ω) on the 284°K θ-surface (their Figs. 10b and 11b). We shall accept that the pressure tendency and diabatic contributions to ω act to cancel as the authors suggest. Then,

$$\omega \equiv dp/dt = V_H \cdot \nabla_\theta P$$

Here, V_H is the horizontal velocity and $\nabla_\theta P$ is the pressure gradient on the θ-surface. Using Homan and Uccellini's results at a location in the vicinity of CLASS station PGV (Greenville, NC), $V_H \approx 15$ m s^{-1} from the SSW and $\nabla_\theta P \approx 41$ mb/° latitude. Therefore, the vertical velocity is calculated to be -3.5 μb s^{-1}.

For comparison, a similar computation based on the 285°K θ-surface shown previously in Fig. 3.8b provides a $V_H \approx 20$ m s^{-1} from the SSW and $\nabla_\theta P \approx 50$ mb/° latitude. These values lead to $\omega \approx -8.0$ μb s^{-1}, or more than twice the ascent found by Homan and Uccellini.

The principal reason for the difference in vertical velocities is the scale of the analyses. Homan and Uccellini had only the customary radiosonde network, so that their analyses and computations must be representative of the synoptic scale. The computation based on the Inner GALE network, however, provides resolution on the meso-ß scale. Evidently, the increased observation density of the GALE sounding network has revealed additional atmospheric structure.

3.2.3 Vertical Cross Sections

To illustrate the vertical atmospheric structure during this R-S line event in more detail, the soundings from Huntington, WV (HTS), 99A, Greensboro, NC (GSO), Fayetteville, NC (FAY), Wilmington, NC (ILM), and RVC were projected onto the cross-section line shown in Fig. 2.1, oriented nearly perpendicular to the front and R-S line.

Analysis of the field of potential temperature and temperature for 2100 GMT on 14 February appear in Fig. 3.9a. Several common layers were found over HTS, 99A, GSO, and FAY: a well-mixed surface boundary layer which extended 50 to 75 mb up above the earth's surface, a stable layer 50 to over 100 mb deep in the lower troposphere, and a layer with small conditional stability occupying the region above the stable layer

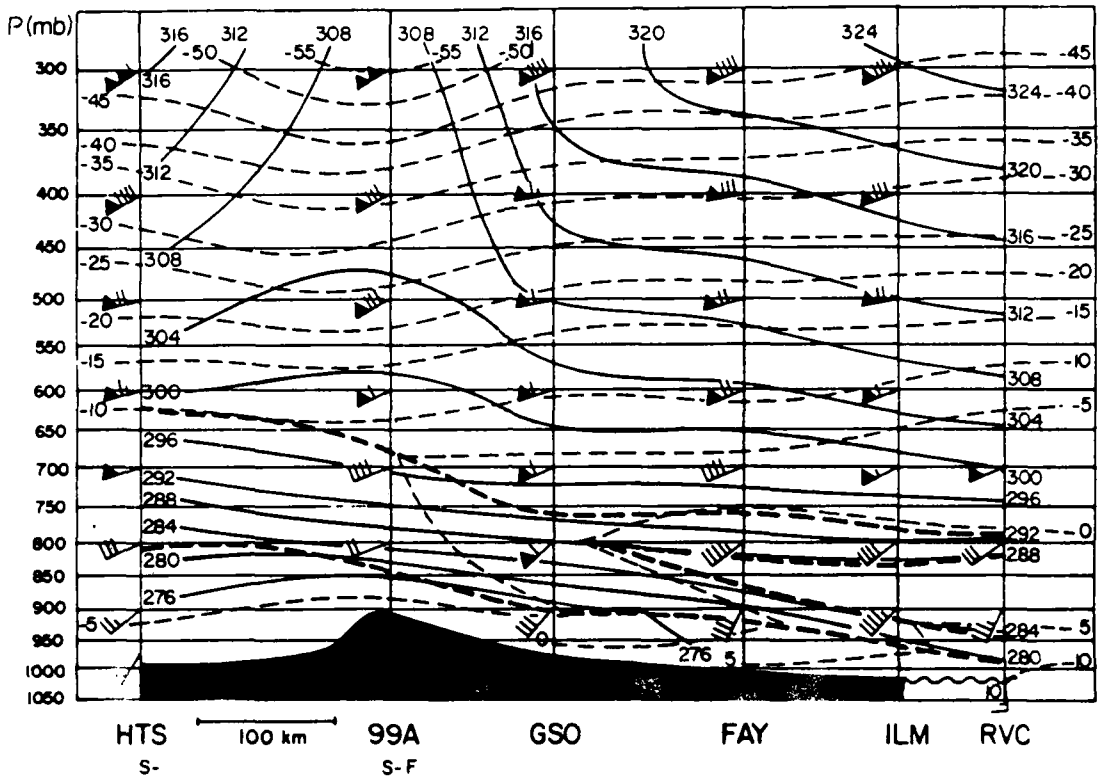

Figure 3.9a. Cross-section from Huntington, WV (HTS) to the Research Vessel Cape Hatteras (RVC) (see Fig. 2.1 for location) at 2100 GMT 14 February 1986. Thin solid lines depict potential temperature (K), thin dashed depict isotherms (°C), heavy dashed lines indicate the tropospheric frontal and stable layer boundaries, and wind vectors with pennant = 25 m s^{-1}, barb = 5 m s^{-1}, half-barb = 2.5 m s^{-1}. Observed weather is indicated below the station identifier.

through the middle troposphere. A layer of stronger stability in the upper troposphere up to 300 mb was also present, except over 99A, where conditional instability prevailed in the upper troposphere. At RVC and ILM, a more complicated structure was observed. A low-level stable layer with a base about 50 mb from the surface was observed, a second stable layer about 50 mb deep could be found near 800 mb, and a layer of potentially unstable air existed between the stable layers. Above the upper stable layer, stronger stability existed up to the middle troposphere. Between 500 and 600 mb, neutrally stable air could be found, whereas relatively stable air was present in the upper troposphere over ILM and RVC. Temperatures at the surface were below freezing just to the northwest of GSO (left in the figure) and snow was falling at HTS and 99A at this time. The R-S line did not yet intersect this cross section, and the strong inversion capping the cold air north of FAY had not yet extended to the ground as a surface front.

Figure 3.9b shows the wind component along the developing surface front normal to the plane of the cross section. The majority of the total wind parallels the developing frontal surface. Along-front winds generally increase with height, especially through the sloping stable layers (as expected from thermal wind considerations).

An analysis of the cross-frontal wind component and relative humidity (RH) appear in Fig. 3.9c. A local maximum of winds crossing the front towards the north can be found in the lower troposphere over GSO, FAY, ILM, and RVC. However, in the 400 to 600 mb region, the cross-front component of the winds reverses over these same stations. A tongue of high RH (> 90%) extends across the lower to middle troposphere over HTS, 99A, and, to some extent, GSO. Layers of dry air (RH < 30%) are observed in the lower troposphere over GSO, FAY, ILM, and RVC.

Figure 3.10a shows the isentropic and isothermal analyses, along with the frontal position, for 0000 GMT 15 February. A broad, nearly horizontal stable layer associated with the frontal zone extends across the lower troposphere over HTS, 99A, GSO, and FAY, and finally reaches the surface between FAY and ILM. A branch of this stable layer reaches the surface near ILM. The stable layer around 800 mb over RVC and ILM shows continuity with a layer at the same altitude three hours earlier. Decreasing potential (and equivalent potential) temperatures with height across portions of the lower troposphere over ILM and RVC indicated the potential for convective instability existed. The 0°C isotherm has moved between GSO and FAY at this time, while the surface front has continued to intensify toward the ENE and was positioned between FAY and ILM (Fig. 3.10a). Aloft, the 0°C isotherm again strongly tilts back toward GSO through the

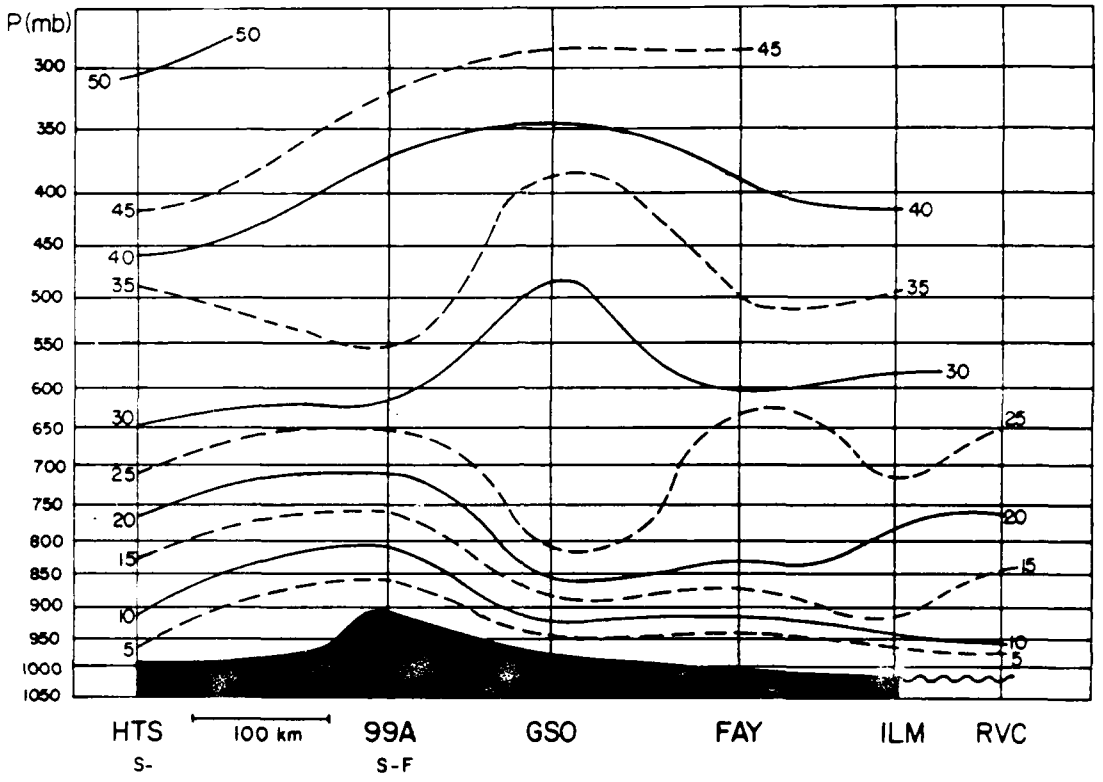

Figure 3.9b. Cross-sectional analysis of along-frontal wind speeds (m s^{-1}) between HTS and RVC at 2100 GMT 14 February 1986.

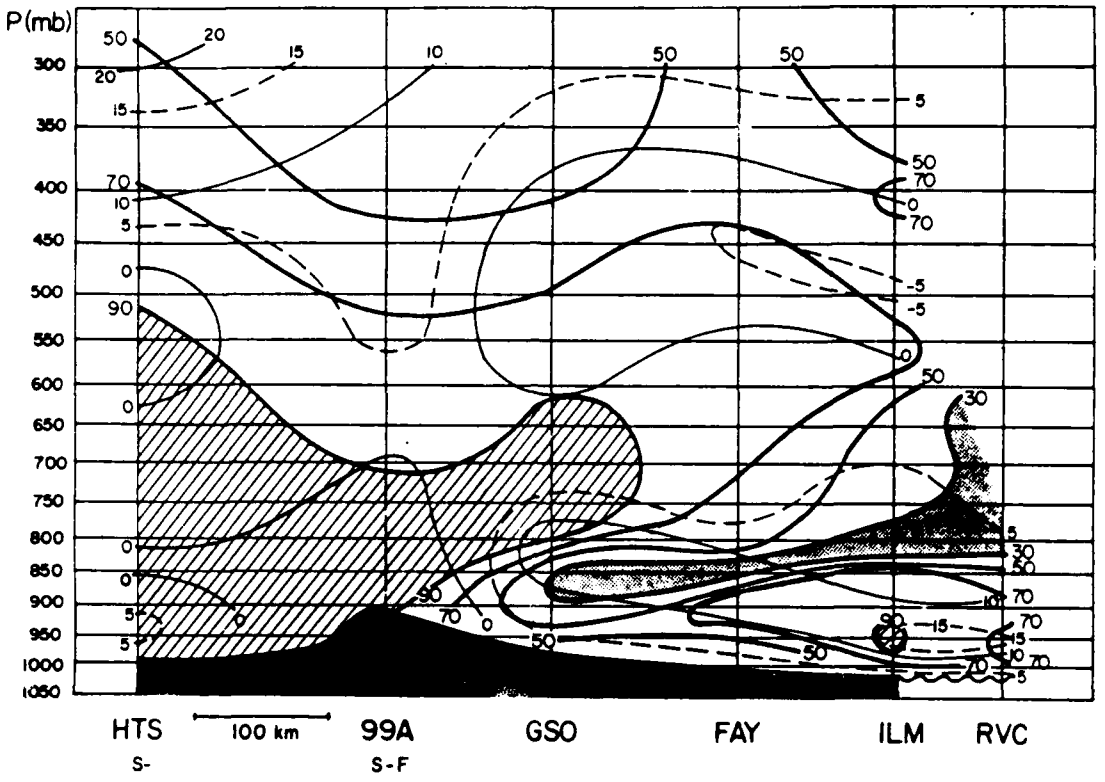

Figure 3.9c. Cross-sectional analysis of cross-frontal wind speeds (m s^{-1}) and relative humidity (RH)(hatched areas indicate RH ≥ 90‰, dotted areas indicate RH ≤ 30‰) between HTS and RVC at 2100 GMT 14 February 1986.

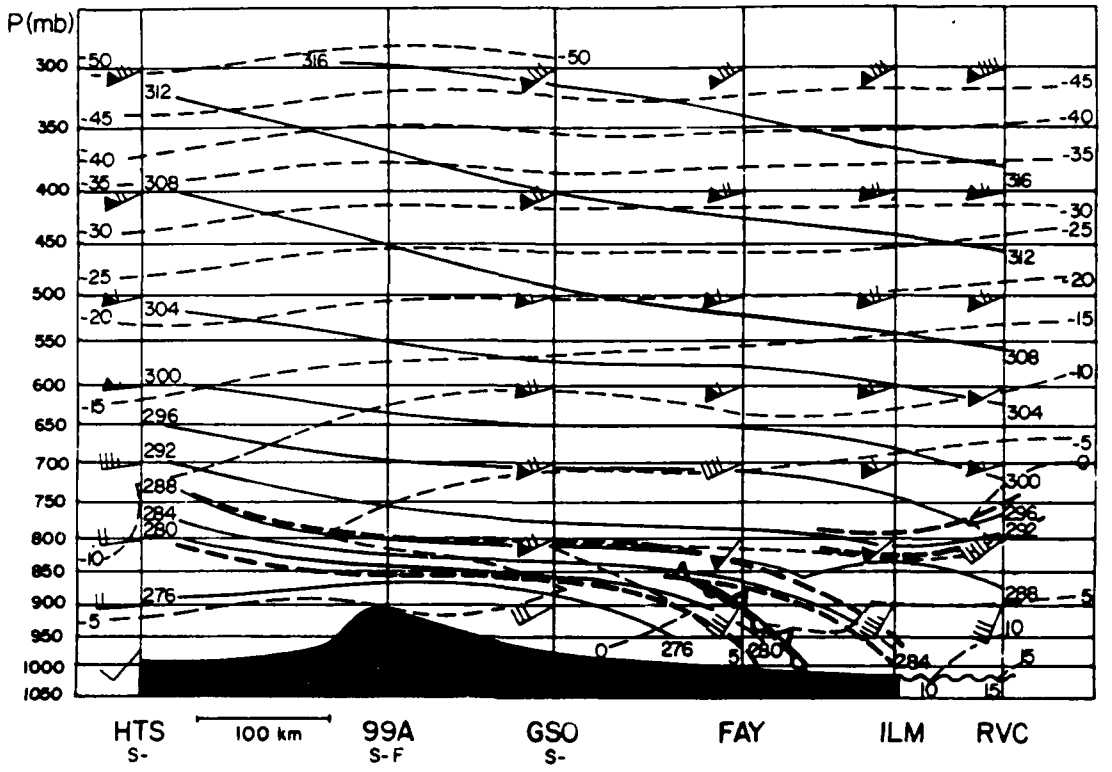

Figure 3.10a. Same as in Fig. 3.9a, except for 0000 GMT 15 February. The frontal position is also shown.

stable layer, while the temperature pattern above the stable layers was nearly unchanged.

Figure 3.10b shows the along-front wind analysis and frontal location. Note the strong wind shear in the lowest 200 mb over GSO, FAY, ILM, and RVC. Emanuel (1979) showed that symmetric instability results in two-dimensional mesoscale motions. For an assessment of the possibility of symmetric or slantwise instability, the fields of potential temperature and M (M = u + fx; u = along-front wind speed, f = Coriolis parameter, x = horizontal distance), pseudo-angular momentum, were mapped together on the cross section. According to theory, the potential for symmetric instability exists where the slope of the M-surface is shallower than that of the θ-surface. The shaded area in Fig. 3.10b shows that the area for symmetric instability exists in the lowest 150 mb; the same area where the strong wind shear was observed.

An analysis of the cross-frontal wind components and RH is presented in Fig. 3.10c. The highest values of southerly cross-frontal winds can be found in the lower troposphere over FAY, ILM, and RVC. Winds flowing across the front toward the south are occurring in a region that is ascending up through the middle troposphere over ILM and RVC. Two regions of very low RH can be found: one over ILM and RVC between 850 and 800 mb, another extends some 200 mb deep over RVC. On the other hand, the moist tongue near 900 mb has shifted southeastward over portions of FAY and ILM.

Figure 3.11a presents the isentropic and isothermal analyses, as well as the positions of the R-S line and front, for 0300 GMT 15 February. The vertical extent of the lower stable layer has generally increased. The surface frontal position has moved slightly northwestward toward FAY. A stronger temperature gradient has developed between FAY and ILM; the temperature difference between them has increased from 2°C to 5°C. A strong temperature inversion has persisted in the stable layer associated with the frontal zone.

Note in Fig. 3.11b the strong wind shear at low levels, and the 30 m s^{-1} wind maximum above the front. The potential for instability, as given by slope differences between the M- and isentropic-surfaces, is indicated by the shaded area. This region is of nearly the same extent as at 0000 GMT (Fig. 3.10b).

Figure 3.11c shows that the moist air (RH > 90%) has shifted little since 0000 GMT, except for a thin layer of high RH near 700 mb over ILM and RVC. Extremely dry air (RH $\leq$ 15%) still characterizes the lower troposphere over ILM. However, the air over RVC has become more moist, as indicated by the higher RH between the surface and 800

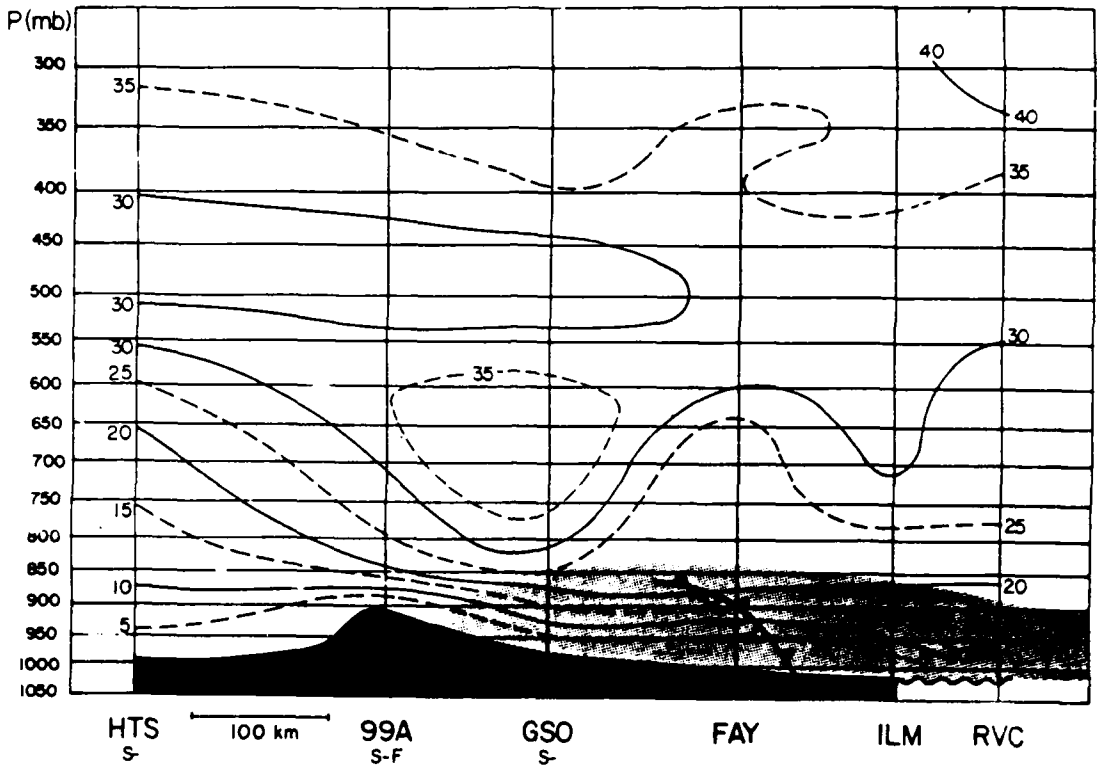

Figure 3.10b. Same as in Fig. 3.9b, except for 0000 GMT 15 February. Frontal position and area of symmetric instability (stippled) are also shown.

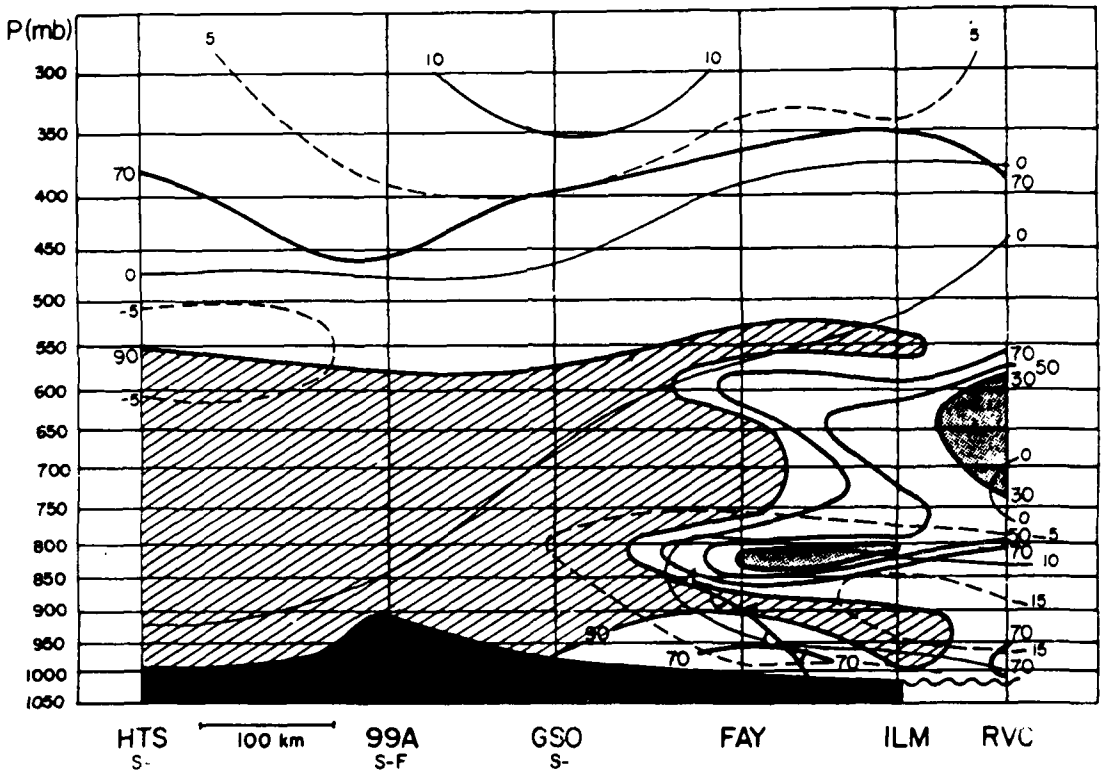

Figure 3.10c. Same as in Fig. 3.9c, except for 0000 GMT 15 February. The frontal position is also shown.

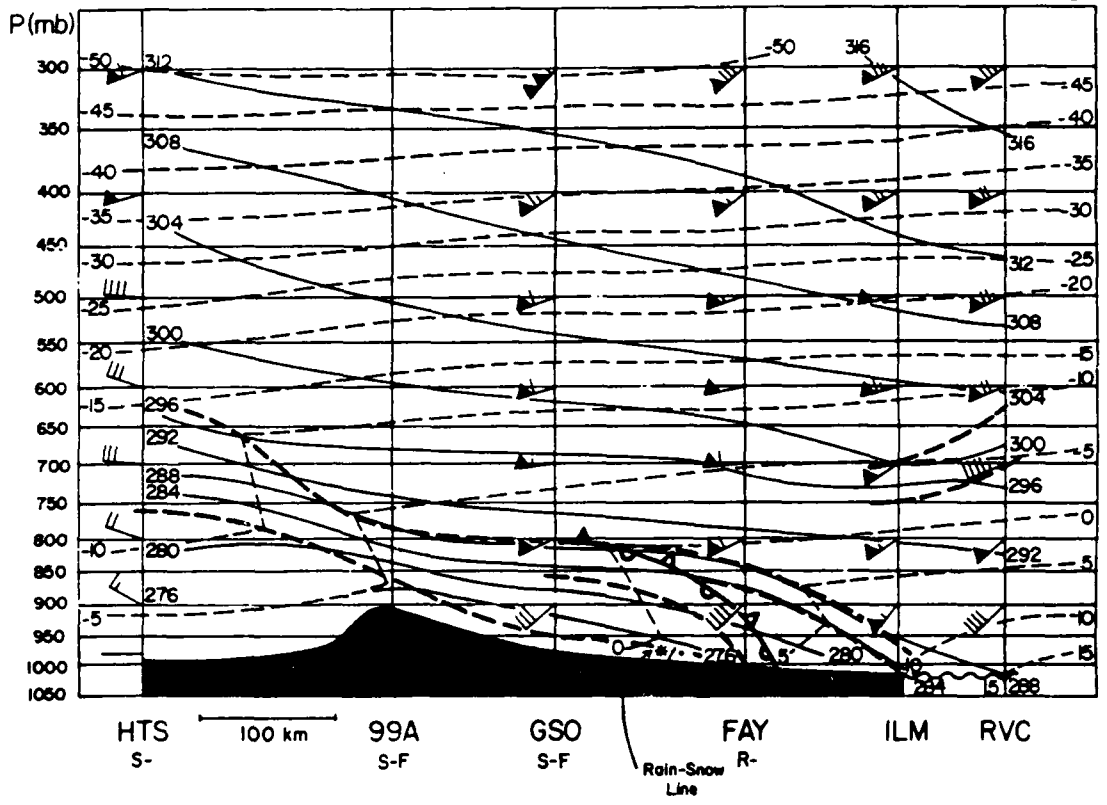

Figure 3.11a. Same as in Fig. 3.10a, except for 0300 GMT 15 February. The rain-snow line position is also shown.

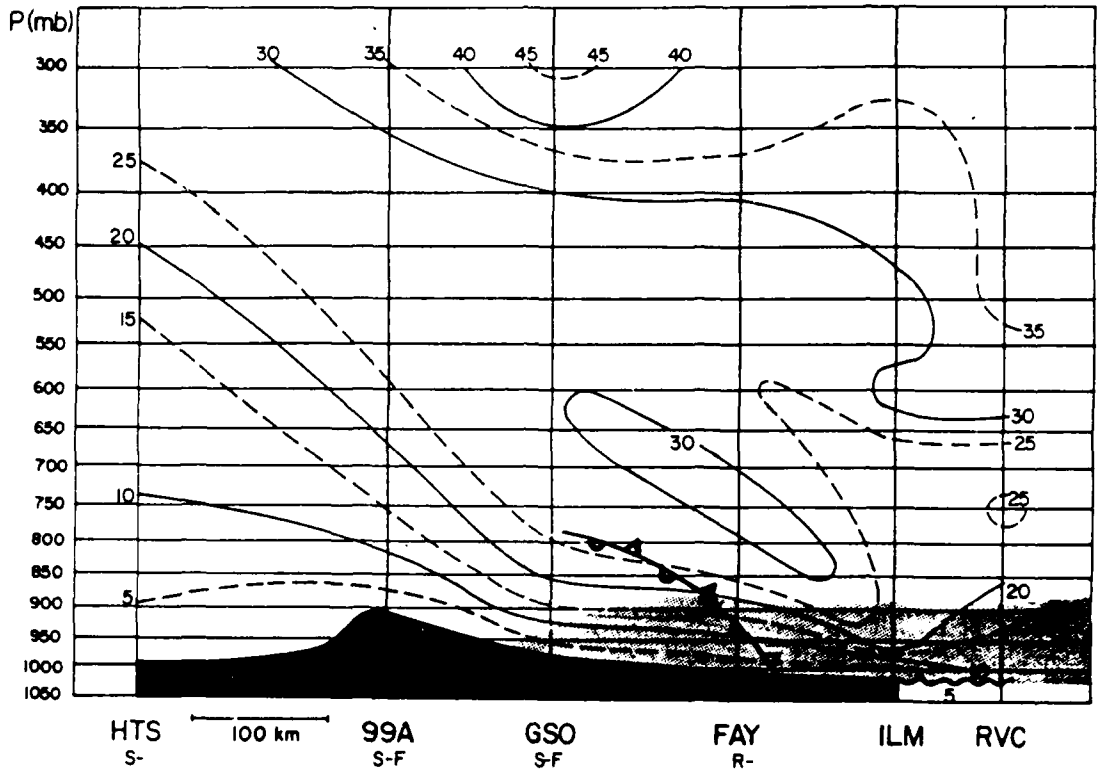

Figure 3.11b. Same as in Fig. 3.10b, except for 0300 GMT 15 February.

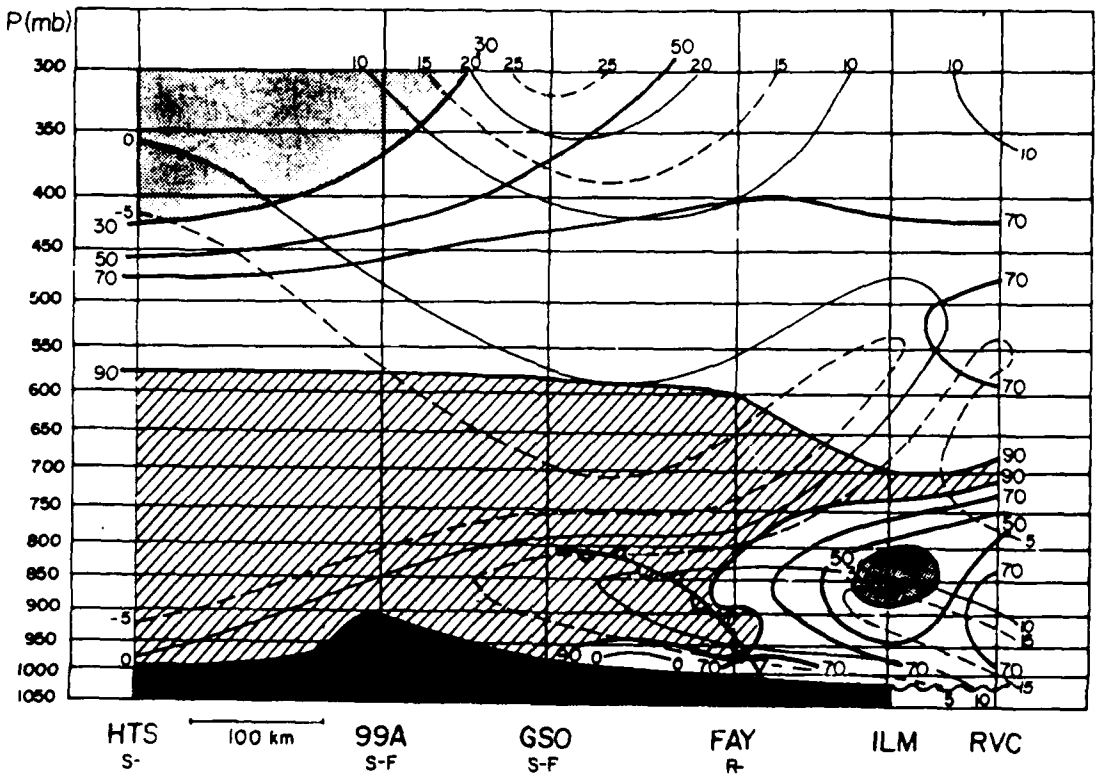

Figure 3.11c. Same as in Fig. 3.10c, except for 0300 GMT 15 February.

mb. The wind components toward the southeast have increased and are at a lower altitude from FAY north.

The last figures in this cross-section sequence are shown in Fig. 3.12a-c. The isentropic analysis for 0600 GMT (Fig. 3.12a) is more complicated than previously. The stable layer associated with the frontal zone now extends upward from the surface over 99A, GSO, and FAY. A second branch of this stable layer extends the length of the cross section, its top ranging 620 mb over HTS to 860 mb over RVC. A narrow branch of stable air sloped downward and reached the surface over ILM. A shallow layer of conditionally unstable air exists southeast ahead of the frontal zone, above the lower stable layer and below the upper stable layer over 99A, GSO, and FAY. A layer of conditionally unstable air over ILM and RVC extended from near the surface to approximately 850 mb. The 0°C isotherm has continued to shift toward FAY. The temperature gradient between FAY and ILM continued to strengthen, with a 10°C temperature difference developing between them.

Strong along-frontal wind shear has moved over FAY, ILM, and RVC by this time (Fig. 3.12b), and is once again located over the frontal surface. The along-front wind maximum has moved from over GSO at 0300 GMT to above ILM. The air over ILM and RVC has moistened significantly since 0300 GMT, while drier air has moved into the middle troposphere over the length of the cross section (Fig. 3.12c).

3.2.4 Surface Divergence Fields

The existence of a mesoscale circulation associated with the gradient of melting along the R-S line was investigated using the PAM-II data. The divergence field was calculated using PAM-II wind data averaged over a one hour interval and centered at 0300 GMT 15 February. These data were interpolated to grid points by the Barnes objective analysis program described earlier. The horizontal divergence is defined by

$$\delta = \partial u/\partial x + \partial v/\partial y$$

where u and v are wind components in the x and y grid directions, respectively. The grid distance is about 34 km and centered differences thus obtained over 68 km. The latter is comparable to the average separation between PAM-II stations. It should be mentioned that the data available to the Barnes program include the GALE buoy network and the

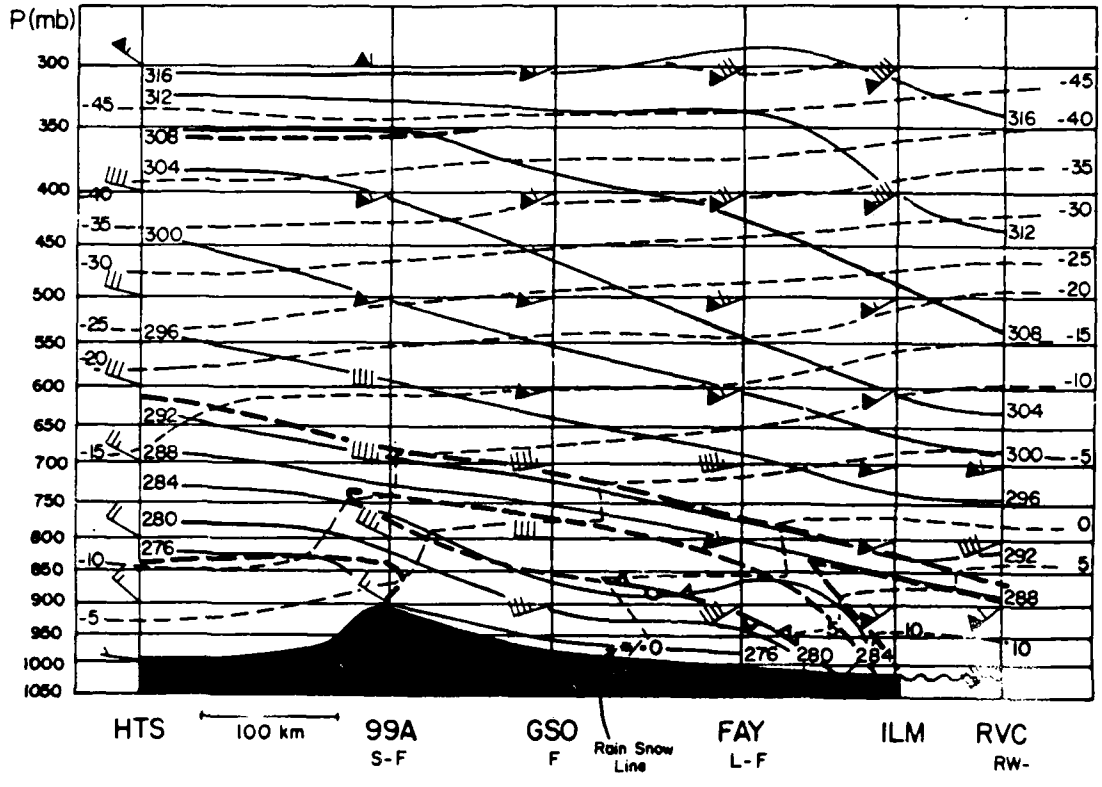

Figure 3.12a. Same as in Fig. 3.9a, except for 0600 GMT 15 February. The frontal and rain-snow line positions are also shown.

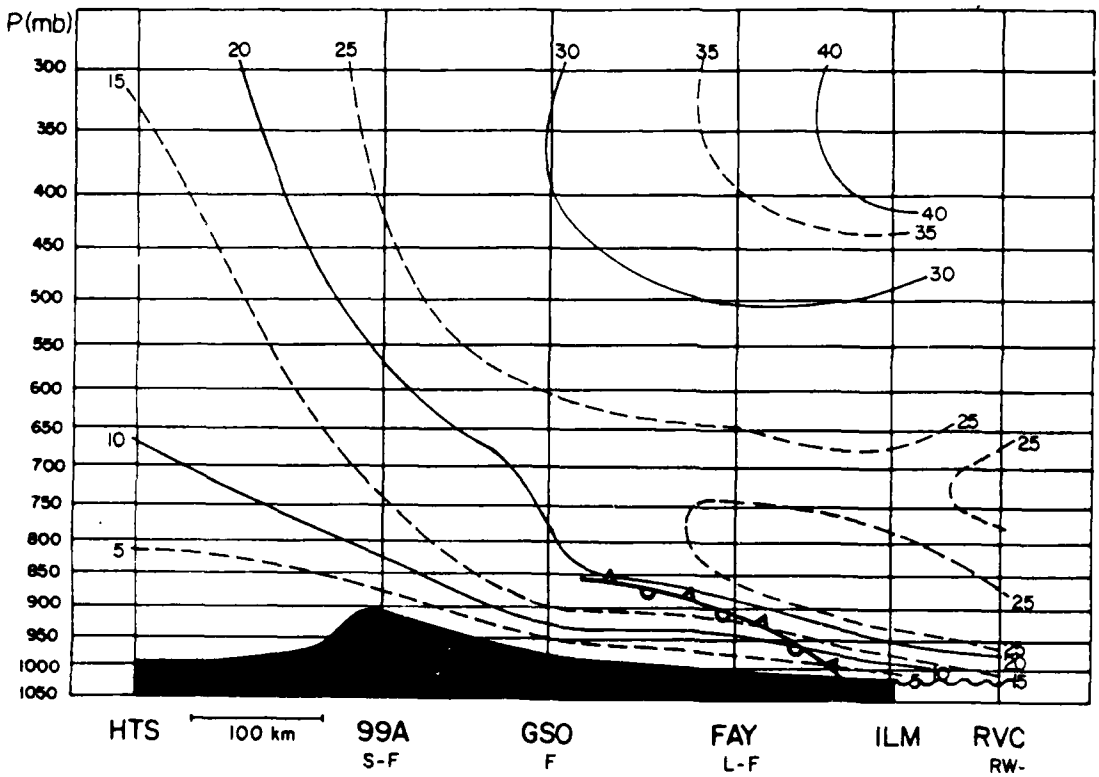

Figure 3.12b. Same as in Fig. 3.9b, except for 0600 GMT 15 February. Frontal position also shown.

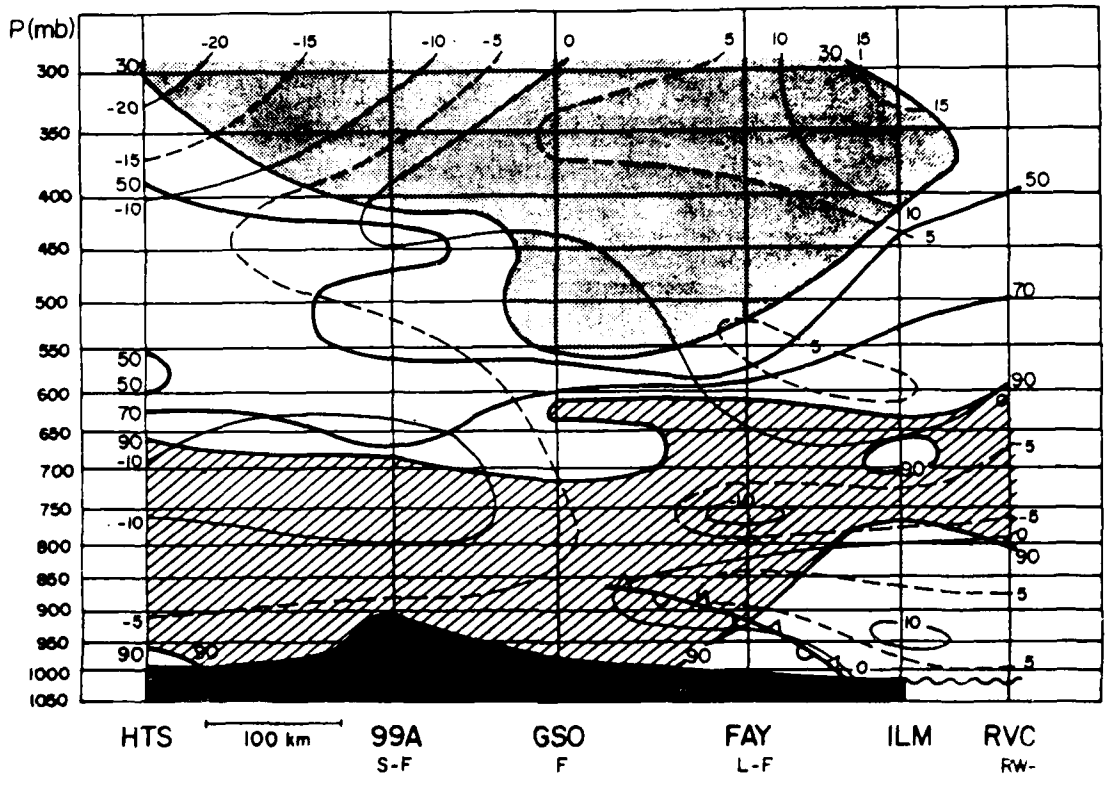

Figure 3.12c. Same as in Fig. 3.10c, except for 0600 GMT 15 February.

R/V RVC. These over-water data are crucial to the meaningful computation of meteorological fields along the coast and the near-shore waters.

Figure 3.13 depicts the frontal and R-S line positions, along with the divergence field, for 0300 GMT 15 February. The frontal zone is seen to lie generally in the region of convergence as expected for such a well-formed feature. The R-S line is seen to separate the areas of strong convergence along the front from an area of weak divergence on the northwest, implying ascent on the southeast side and descent on the northwest side side of the R-S line. This is consistent with the rising and sinking branches of the mesoscale circulation described by Lin and Stewart (1986) [See Fig. 1.2], and provides evidence for the existence of a mesoscale circulation in the vicinity of the R-S line.

3.2.5 Upper Level Divergence and Vertical Velocity

The three-dimensional structure in the vicinity of the R-S line and the frontal zone are further explored by means of computed fields based on upper air soundings over the Inner GALE network. This would include any ship and dropwindsonde observations offshore. These soundings are available at three-hourly intervals and over a mesoscale observation network. Again, the Barnes objective analysis scheme was used to interpolate the data to a 34 km grid. Divergence was calculated on constant pressure levels, available at 10 mb intervals.

Vertical velocity was calculated by vertical integration of the continuity equation (kinematic method; Holton, 1979) in isobaric coordinates, that is:

$$\omega_U = \omega_L + \bar{\delta}\,\Delta p$$

Here, ω_U and ω_L are the vertical velocities at the upper and lower pressure levels ΔP (> 0) apart. The layer mean divergence $\bar{\delta}$ is obtained as the simple average of δ at the two levels. The integration commences at the ground level where

$$\omega_L = \mathbf{V}_H \cdot \nabla P_s$$

The terrain induced ascent or descent is calculated as the the lower boundary condition. The gradient of the terrain pressure (P_s) is determined from a Barnes analysis of U.S. Standard Atmosphere pressure altitudes at several surface stations, PAM-II, and buoy locations, plus some bogus (artificial) points along the crest of the Appalachians. The

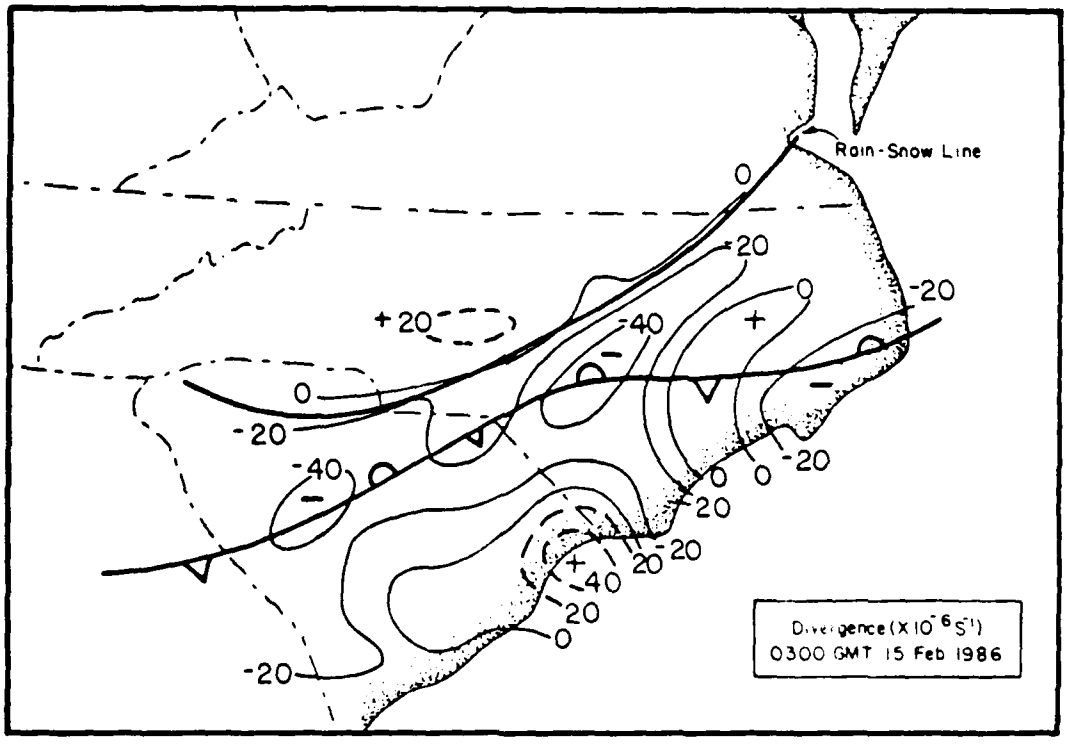

Figure 3.13. Analysis of surface divergence using the PAM-II wind data averaged over 1 hour centered at 0300 GMT 15 February 1986. Divergence (dashed contours) and convergence (solid contours) analyzed every 20 x 10^{-6} s^{-1}. The surface front and rain-snow line are also shown.

pressure topography thus obtained realistically represents the terrain over the computation domain. The Inner GALE Area is gently sloped and the terrain ω can be expected to be small. Indeed, the terrain ω at 0300 GMT on 15 February shows $\omega \sim -0.1$ $\mu b\ s^{-1}$ (upslope) in the light southerly flow southeast of the front, and downslope flow $\sim +0.3$ $\mu b\ s^{-1}$ in the westerly winds between the front and the western edge of the PAM-II network. (The reader may find it useful to recall that 1 microbar per second ($\mu b\ s^{-1}$) is approximately equivalent to 1 cm s^{-1} in the lower troposphere.)

Our computations of vertical velocity at pressure levels above the surface has shown that the results do depend on the particular levels used to compute the layer mean divergence $\bar{\delta}$. For purposes of this study it is deemed adequate to compute $\bar{\delta}$ in 50-mb ($\approx$ 400 m) layers. The first layer (from the surface to 950 mb) is somewhat thicker near the coast where surface pressures were around 1012 mb. The 950-mb level intersects the ground west of GSO, well beyond the western edge of the main body of the PAM-II network.

Computations at 0300 GMT were performed up to 700 mb. A few horizontal patterns are shown in Fig. 3.14. The 950-mb divergence pattern (Fig. 3.14a) should be compared with the surface divergence (Fig. 3.13). The large surface divergence near MYR (Myrtle Beach) on the South Carolina coast is found at 950 mb and, as expected, produces downward vertical motion ($\omega \approx 3$ $\mu b\ s^{-1}$) over this region. This feature is possibly related to downdrafts in the heavier precipitation area [D/VIP (Digital Video Integrator and Processor) Level ≥ 2; $\approx$ 30-41 dBZ) found by radar (see Fig. 3.5c). The convergence along the North Carolina coast at both the surface and 950 mb contributes to ascending motion which extends into central North Carolina.

It is interesting to note that these coastal details in ω seem consistent with the sign of ω implied from the 285-θ-surface near 950 mb (see Fig. 3.8c). The winds at MYR and ILM together with the pressure gradient suggest descent at the former station and ascent at the latter station. The broader-scale ascent over central South Carolina (≈ -1 $\mu b\ s^{-1}$) in Fig. 3.14a is also implied in the θ-surface data.

At 850 mb (Fig. 3.14b), approximately one kilometer higher, the general pattern of convergence/divergence over South Carolina is similar to that at 950 mb. Over North Carolina, the prominent convergence seen in the central part of the State has decreased to near zero. The vertical motion patterns at 850 and 950 mb, especially over North

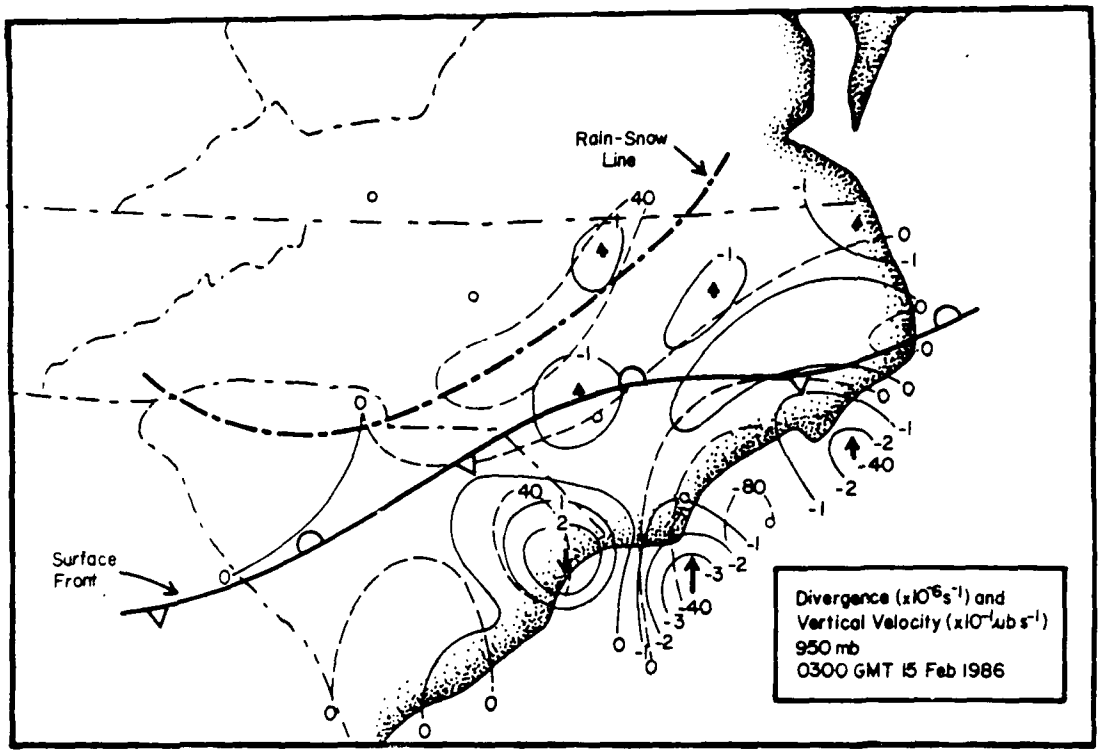

Figure 3.14a. Analysis of divergence (x 10^{-6}) and vertical velocity (x10^{-1} μb s^{-1}) at 950 mb for 0300 GMT 15 February 1986. Divergence (dashed contours) analyzed every 40 x 10^{-6} s^{-1} and vertical velocity (solid contours) analyzed every 1 μb s^{-1}. The rain-snow line and surface front are also shown.

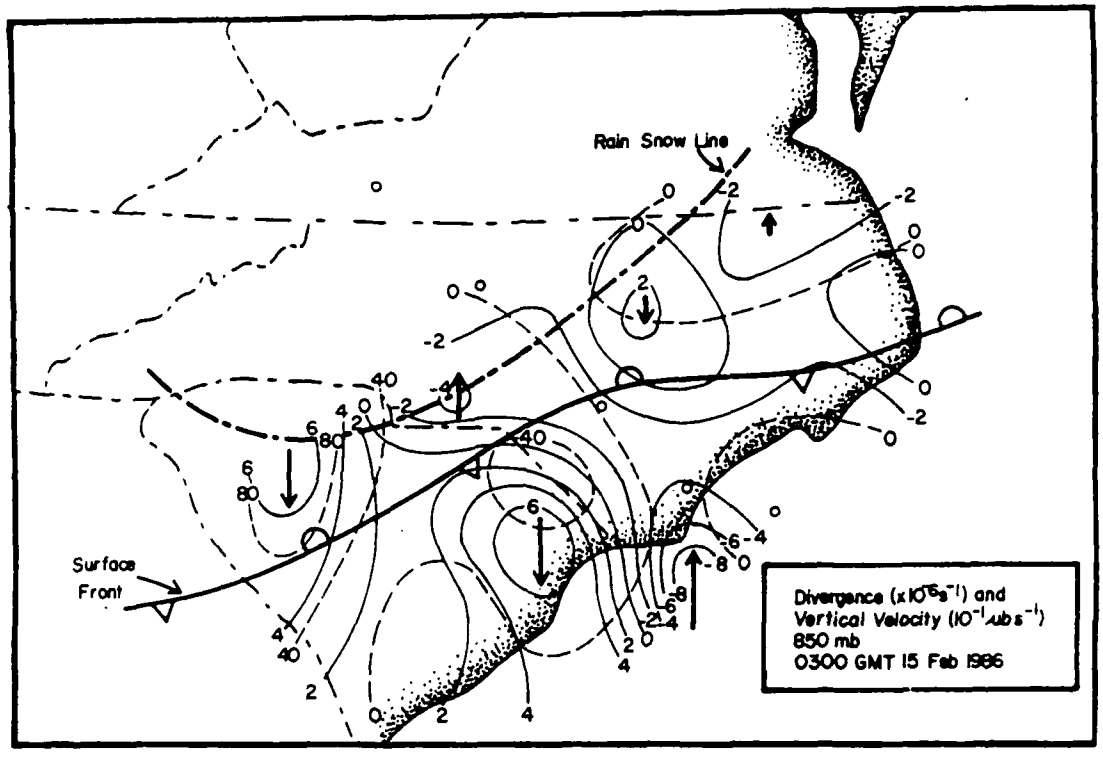

Figure 3.14b. Same as in Fig. 3.14a, except at 850 mb.

Carolina, seem related to the precipitation inferred by radar returns (Fig. 3.5c). Ascent of -2.0 to -3.0 $\mu b\ s^{-1}$ corresponds to the heavier precipitation just north of the NC-SC border and along the coast to near HAT. The lack of radar echoes near HAT may be explained by the sinking motion occurring between HAT (Cape Hatteras) and DUK (Duck), NC.

The implied ascent near GSO shown in Fig. 3.8c is again in agreement with the kinematic ω. The small area of subsidence at 850 mb in east-central North Carolina is not clearly revealed by the θ-surface, but the wind nearly parallels the isobars so that $\omega \approx 0$ is indicated.

Figures 3.15a and b show the divergence and vertical velocity from the surface up to 700 mb superposed on the 0300 GMT cross section shown in Fig. 3.11a. The pattern of divergence is complex. Among the more prominent features are the relatively large convergence values ($\delta \approx -70 \times 10^{-6}\ s^{-1}$) at 950 mb over RVC and northwest of the frontal zone ($\delta \approx -50 \times 10^{-6}\ s^{-1}$) near FAY. Between the the convergent value over RVC and the stable layer that slopes to the surface at ILM, a small divergent area area is found. This feature is evidence that the GALE enhanced sounding network, together with an appropriately tuned Barnes analysis scheme, is able to resolve features with meso-β scale wavelengths.

A level of non-divergence near 800 mb extends from 99A to RVC, with alternating convergent/divergent patterns above this level. These patterns may reflect a Dines-like compensation within the lower troposphere.

The vertical motion field produced by the divergence pattern is displayed in Fig. 3.15b. The cross section is dominated by ascending motion, the strongest (-6 $\mu b\ s^{-1}$) occurring over the sloping stable layer in the warmer air between FAY and RVC. As mentioned earlier, this is the region of highest radar reflectivity (see Fig. 3.5c), so this rising motion may be responsible for enhanced precipitation in this area. It is interesting to note that Fig. 3.5a shows "no echoes" around GSO and D/VIP 1 (< 30 dBZ) activity over southwestern Virginia around 99A. Station 99A has definite ascent (up to $\omega \approx -5\ \mu b\ s^{-1}$), while the area over GSO possesses a minimum ω ($< -2\ \mu b\ s^{-1}$). Overall, there does seem to be the anticipated relationship between the kinematic vertical velocities and the precipitation pattern based on radar returns, lending some credence to the ω

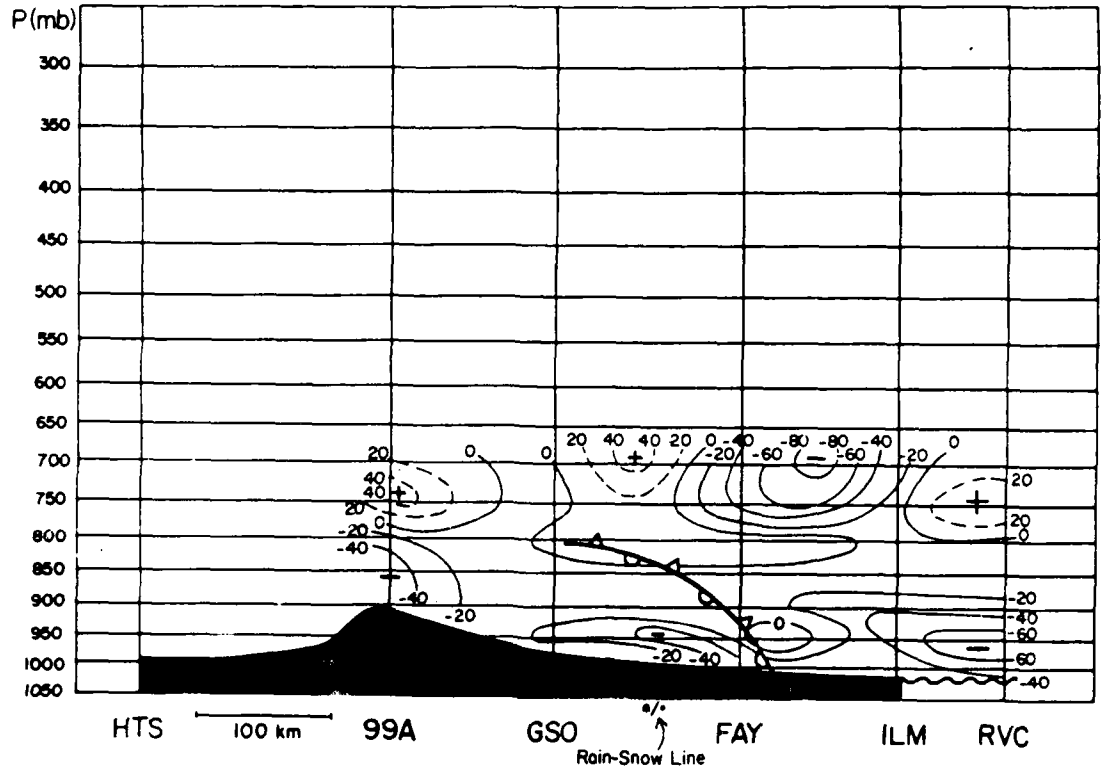

Figure 3.15a. Analysis of divergence for the cross section of Fig. 3.11. Divergence analyzed every 20 $x10^{-6}$ s^{-1}. The surface front and rain-snow line are shown.

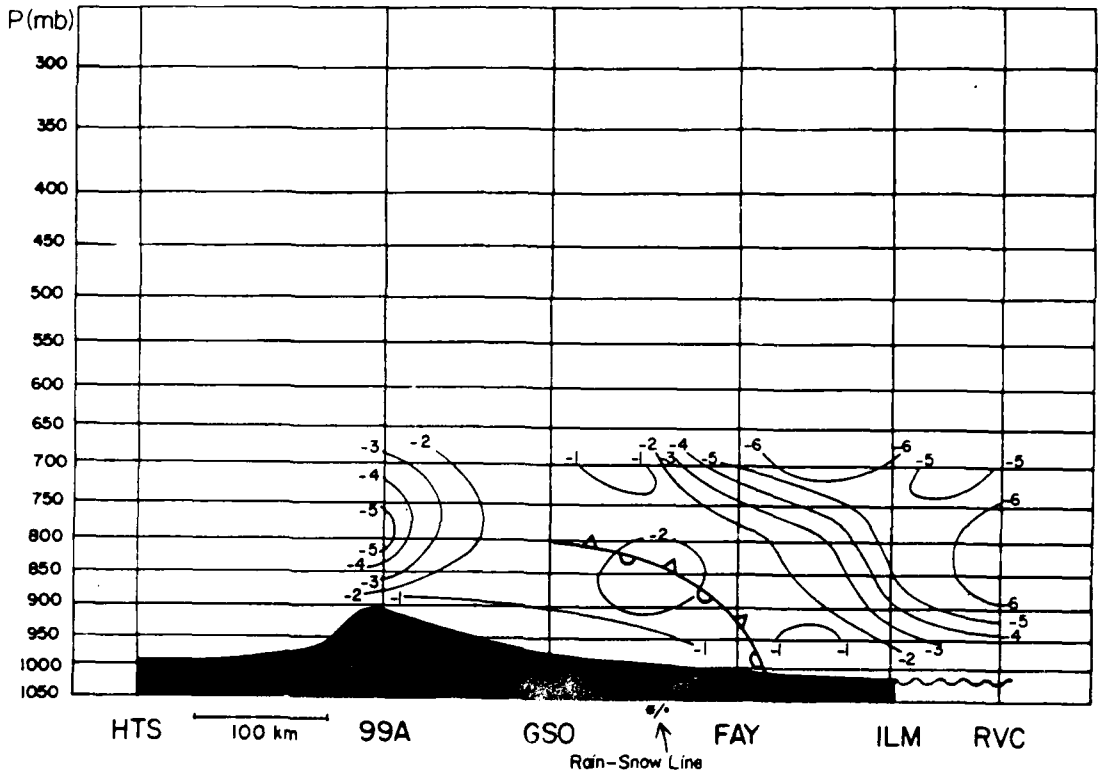

Figure 3.15b. Analysis of vertical velocity for the cross section of Fig. 3.11. Vertical velocity analyzed every 1 μb s^{-1}. The surface front and rain-snow line are also shown.

computation.

The relationship of the R-S line, which is located about 50 km to the northwest of FAY, to the divergence and vertical velocity fields is not clear. The close proximity of the R-S line to the stationary front may be causing difficulty in disintangling the kinematics associated with each feature. The GALE sounding network may be inadequate to resolve the circulation pattern associated with the R-S line from that associated with the front.

3.2.6 Thermodynamic Processes

The interaction of the R-S line and the stationary front developing to its south is of interest in this case study. Frontogenetic processes can be expected to influence the location of the R-S line, while diabatic processes, through the latent heat of melting or sublimation, may modulate the frontal gradient and mesoscale dynamics within the precipitation area. Figure 3.16 shows evidence of frontogenesis in the development of a 13°C temperature gradient in the region between Goldsboro, NC (GSB) and RVC, located north and south of the frontal position, respectively (see Fig. 2.2). Frontogenesis and the *in situ* formation of the R-S line are furtner illustrated in Fig. 3.17 which shows the surface temperature and precipitation type for five stations that lie along the line "ROA-NCA" in Fig. 2.2.

A limited experiment in the computation of the thermodynamic processes in the vicinity of the rain-snow line is described in this subsection. One starts with the First Law of Thermodynamics in isobaric coordinates, namely,

$$\frac{\partial T}{\partial t})_P = - V_H \cdot \nabla_P T + (\kappa \frac{T}{p} - \frac{\partial T}{\partial p})\omega + \frac{H}{c_p} . \qquad 3.1$$

The temperature tendency on any pressure surface is a function of three processes represented by the three terms on the right hand side of equation 3.1. The first term is the horizontal temperature advection. The second represents adiabatic contributions, where the quantity in the brackets is the static stability in which the first term is the dry adiabatic lapse rate in this coordinate system. Here $\kappa = R/c_p = 0.286$; R is the gas constant; and c_p is the specific heat at constant pressure. The third term on the right side represents diabatic sources and sinks of heat, where H is the heating rate.

The First Law will now be combined with a pressure kinematic replacement for the pressure tendency. [The general principles of pressure kinematics are described in

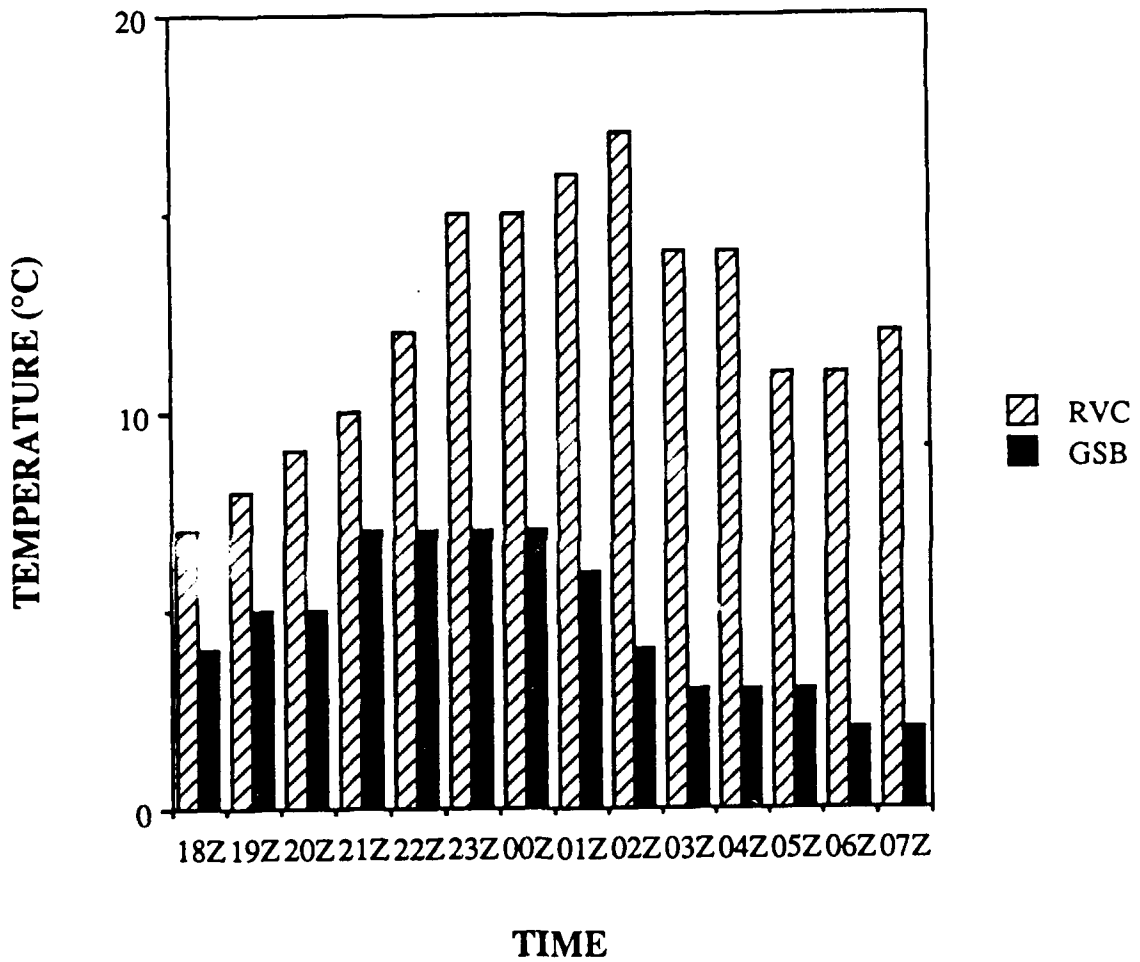

Figure 3.16. Time series from 1800 GMT 14 February to 0700 GMT 15 February 1986, showing surface temperature at the Research Vessel Cape Hatteras (RVC) and Goldsboro (GSB), NC (see Fig. 2.2 for location).

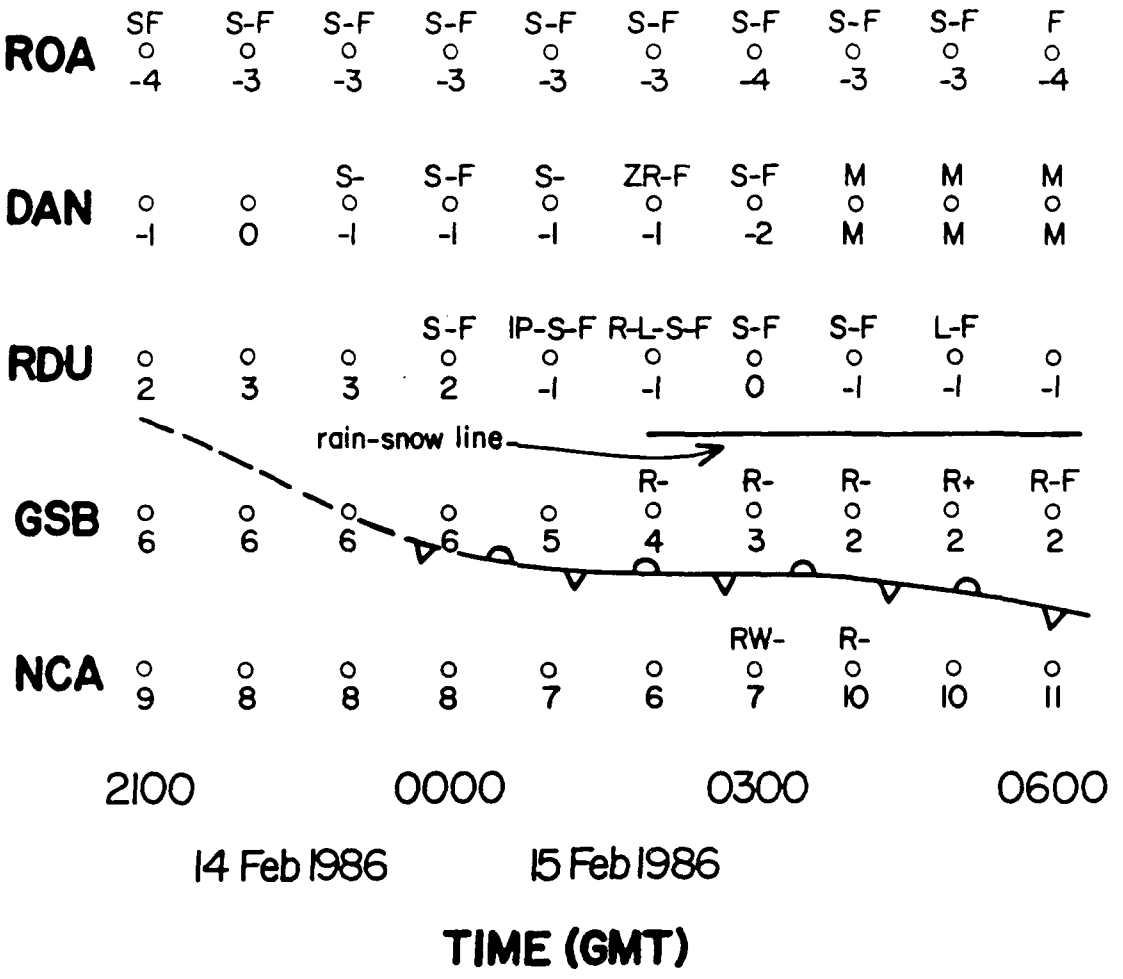

Figure 3.17. Time series of reported surface weather and temperature (°C) between Roanoke (ROA), VA and Jacksonville (NCA), NC along a projection line shown in Fig. 2.2. The location of the rain-snow line and stationary front are indicated. M denotes missing data.

Petterssen (1956, Chapter 3).] The 0°C isotherm will be used as a proxy for the R-S line. Then, in a coordinate system moving with this (or any) isotherm on a constant pressure surface,

$$\frac{\delta T}{\delta t} = \frac{\partial T}{\partial t})_P + \mathbf{C} \cdot \nabla_p T = 0 \qquad 3.2$$

The time derivative on the left side of Eq. 3.2 represents that on the moving isotherm, and **C** is the isotherm velocity measured normal to the isotherm orientation. Thus, exactly,

$$\frac{\partial T}{\partial t})_P = -\mathbf{C} \cdot \nabla_p T = 0 \qquad 3.3$$

Substitution into the Eq. 3.1 leads to

$$(\mathbf{V}_H - \mathbf{C}) \cdot \nabla_p T - (\kappa \frac{T}{p} - \frac{\partial T}{\partial p})\omega = \frac{H}{c_p} \qquad 3.4$$

The first term on the left side of Eq. 3.4 represents temperature advection relative to the moving isotherm. In the following, the diabatic term will be treated as a residual of the sum of the relative advection and adiabatic terms. In reality, the residual will also contain the effects of computation error, and to a lesser extent, the contribution of kinetic energy and frictional conversion of energy to heat. The latter two may be justifiably ignored.

As an example of this type of energy budget computation, the necessary numerical values were obtained at a grid point on the 970 mb surface at 0300 GMT very near the 0°C isotherm, where it intersects the cross section of Fig. 3.15. This location is in central North Carolina approximately between GSO and FAY.

The values to be used in the relative advection computation are, approximately:

$C = 2.0$ m s^{-1} from 340° (6-h average movement)

$V_H = 20$ m s^{-1} from 210°

$\nabla_p T = 3.5$°C/° latitude from 340°.

In the computation of the adiabatic term,

T = 273 K , P = 970 mb, $\partial T/\partial p = 0$ (isothermal over lowest 50 mb), and $\omega = -1.1$ $\mu b\ s^{-1}$.

Substitution into the thermodynamic equation gives

$$-22.2 \times 10^{-5}\ K\ s^{-1} + 8.8 \times 10^{-5}\ K\ s^{-1} \approx -13.4 \times 10^{-5}\ K\ s^{-1} = H/c_p .$$

This result says that warm relative advection is partially compensated by adiabatic cooling due to ascent, with the net result that diabatic cooling performs the rest of the compensation. Here,

$$H = -3.2 \times 10^{-5}\ cal\ g^{-1}\ s^{-1}$$

and

$$\partial T/\partial t = -1.5\ K\ (3\ h)^{-1}$$

due solely to diabatic processes.

The sequence of three soundings at neighboring station GSO during the passage of the R-S line is presented in Fig. 3.18. The three-hourly soundings between 2100 GMT 14 and 0300 GMT 15 February reveal cooling to have occurred below 850 mb prior to the onset of light snow at 0000 GMT. The cooling averages about -2 K $(3h)^{-1}$. It is proposed that this cooling due to melting, or possibly even of sublimation of falling snow into the very dry air found beneath the clouds at 2100 GMT, is detected in the above computation. After snow commences, the diabatic process ceases to be important and the dominant warm advection produces the observed warming below 850 mb between 0000 and 0300 GMT.

4. CLIMATOLOGY OF RAIN-SNOW LINES

4.1 Introduction

A R-S line climatology for North Carolina has been undertaken to investigate the spatial and temporal variability of this major winter forecast problem. As stated earlier, there are a number of reasons for the difficulty in forecasting the location and evolution of R-S lines. This climatology attempts to put the case study into an historical perspective.

Little research has been documented with respect to the atmospheric features and characteristics associated with R-S lines. Stewart (1985), Stewart and King (1987), and Stewart and McFarquhar (1987) have performed empirical and numerical studies on the atmospheric features, scales, and motion associated with R-S boundaries. Forbes et al.

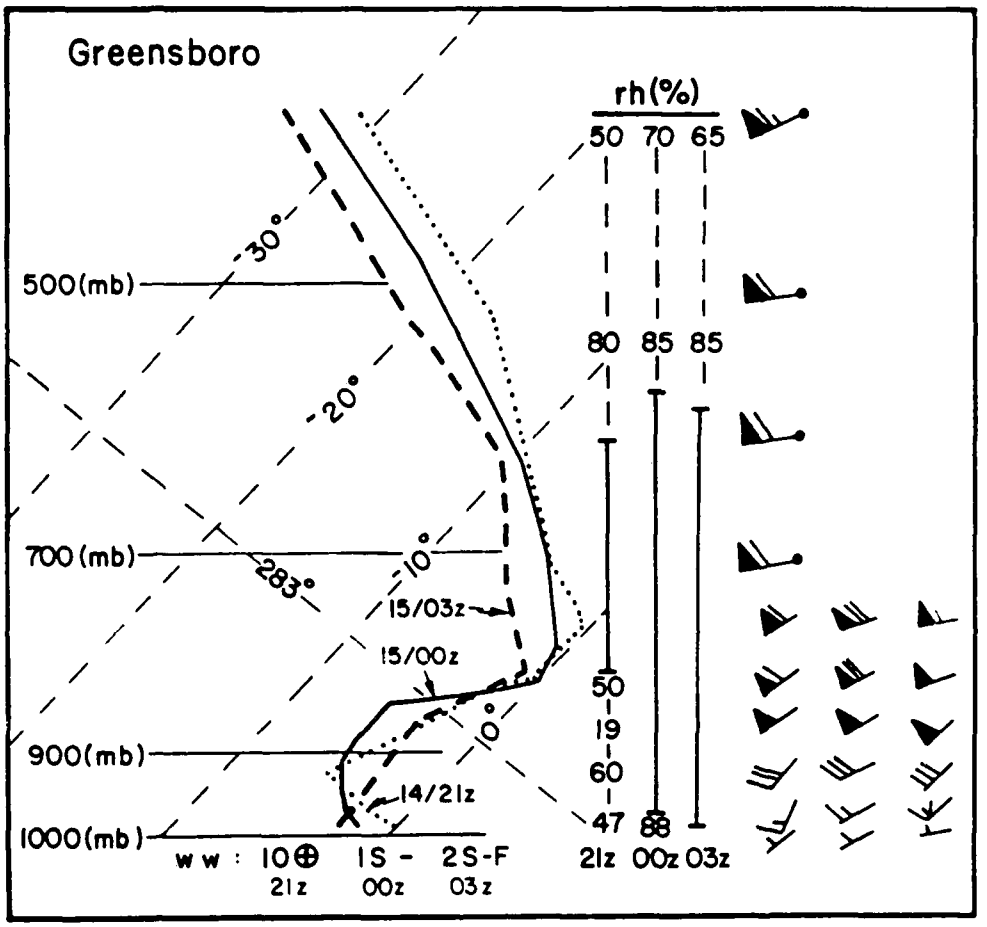

Figure 3.18. Skew-T diagram showing temperature soundings taken at Greensboro, NC at 2100 GMT on 14 February, and 0000 and 0300 GMT on 15 February 1986. Relative humidity (in %) shown to the right of the soundings with solid vertical lines indicating saturation. Wind vectors with pennant = 25 m s^{-1}, full barb = 5 m s^{-1}, and half-barb = 2.5 m s^{-1}.

(1987) have investigated the dynamics associated with ice storms. However, the majority of winter storm research has focused on snowstorms (e.g., Bosart, 1981; Kocin and Uccellini, 1985a,b; Sanders and Bosart, 1985).

Since surface data were available, a supplementary goal of the climatology was to identify possible correlations between surface meteorological variables and precipitation types. Surface elements have long been known to aid in the forecast of precipitation types. Young (1978), while investigating freezing precipitation events in the southeastern U.S., found that a forecast of the most probable precipitation type could be obtained by using surface and 850 mb temperature. Matsuo et al. (1981) and Stewart and King (1987) have documented statistical evidence linking snow and rain with surface temperature and relative humidity. Bocchieri and Maglaras (1983) found the surface air and dewpoint temperatures to be important predictors of precipitation type (see Table 1). Lumb (1960, 1961, 1963) and Booth (1973) found the wet-bulb temperature to be important for rain-snow discrimination in the British Isles. Lumb indicated that cooling by evaporation during precipitation of moderate intensity can reduce the wet-bulb depression to a small fraction of its original value within an hour or two; as saturation is approached, the temperature of the air should approach the wet-bulb temperature. Penn (1957) also noted the effect of evaporational cooling, depicting this effect as being especially pronounced when very dry air is present in the low levels with wet-bulb temperatures at or below freezing.

4.2 Goals/Objectives

The goals of the climatology are to:

i) investigate possible relationships between the surface cyclone and R-S line position

ii) document preferred regions for R-S lines across North Carolina

iii) investigate correlations between surface meteorological variables and the various precipitation types that occur in the vicinity of R-S lines

4.3 Data, Methods, and Discussion

For the purposes of this climatology, only those significant snowfalls (≥ 5 cm/24 h) reported at a first-order NWS office in North Carolina (Asheville, Cape Hatteras, Charlotte, Greensboro, Raleigh-Durham, and Wilmington) during the period January 1966 to April 1987 were considered.

The climatology has two major focuses. The first involved determining the location

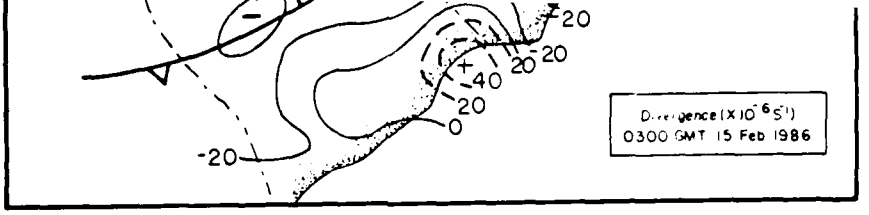

Figure 3.13. Analysis of surface divergence using the PAM-II wind data averaged over 1 hour centered at 0300 GMT 15 February 1986. Divergence (dashed contours) and convergence (solid contours) analyzed every 20 x 10^{-6} s^{-1}. The surface front and rain-snow line are also shown.

of the first appearance of a R-S line with respect to the parent surface cyclone producing the precipitation. The Climatic Data National Summary, Daily Weather Map, and available National Meteorological Center facsimile surface charts were used to locate the surface cyclone location, while three-hourly surface data gained from the Local Climatological Data (LCD) and Surface Weather Reports for selected stations in North Carolina, South Carolina, and Virginia (Fig. 4.1) were used to identify the position of the R-S line.

Some interesting remarks can be made about these snowfall events. These snowfalls occurred from November through April (Fig. 4.2), with a distinct maximum in January and February. In the cases where both a R-S line and parent cyclone could be identified, it was found that the location of the first R-S line in North Carolina relative to the position of the parent surface cyclone can be as distant as the northeast Gulf of Mexico or within the state of North Carolina itself (Fig. 4.3). In Fig. 4.3, the date corresponding to the cyclone number can be found in Appendix A.

To see if the position of the surface cyclone would seem has a bearing on the location of the R-S line, the surface cyclone positions identified in Fig. 4.3 were stratified into four geographic regions:

A. East of the Appalachians (EAST)
B. West of the Appalachians (WEST)
C. Atlantic Ocean (ATLANTIC)
D. Gulf of Mexico (GULF)

Figures 4.4a-d show the location of the R-S lines relative to the surface cyclone position. Generally, for surface cyclones east of the Appalachians, R-S lines seem to fall most often in the western portion of North Carolina (Fig. 4.4a). For cyclones west of the

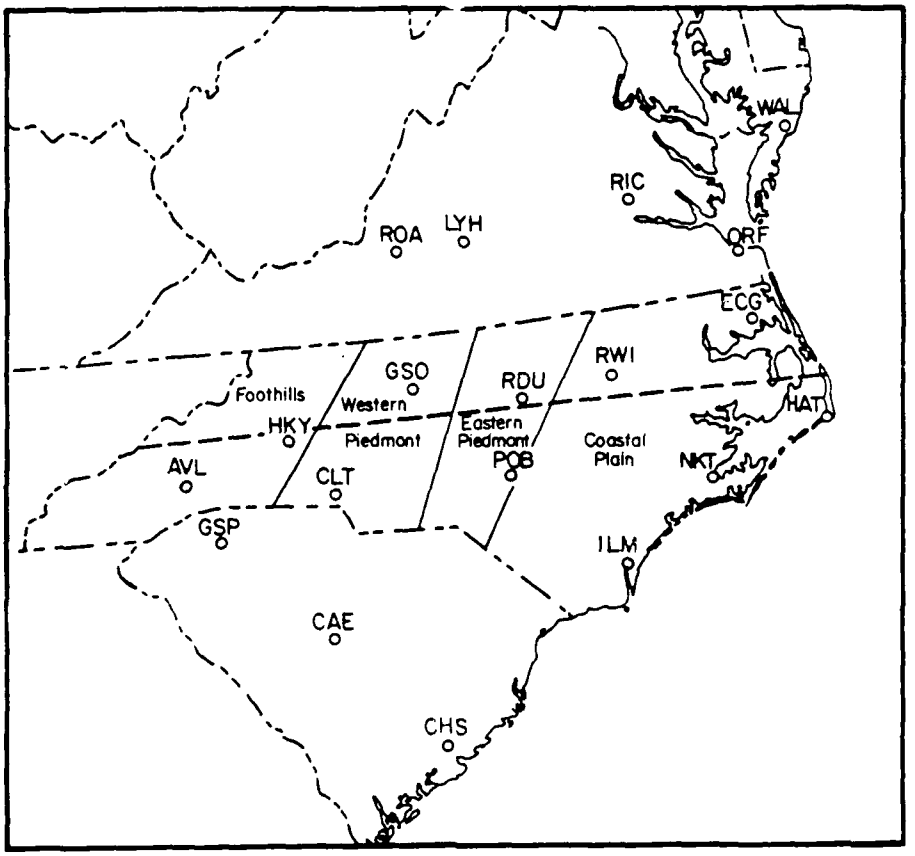

Figure 4.1. Weather forecast zones in North Carolina as defined by the National Weather Service, except that the "Foothills" include the mountainous areas. Key stations in the R-S line climatology are also shown.

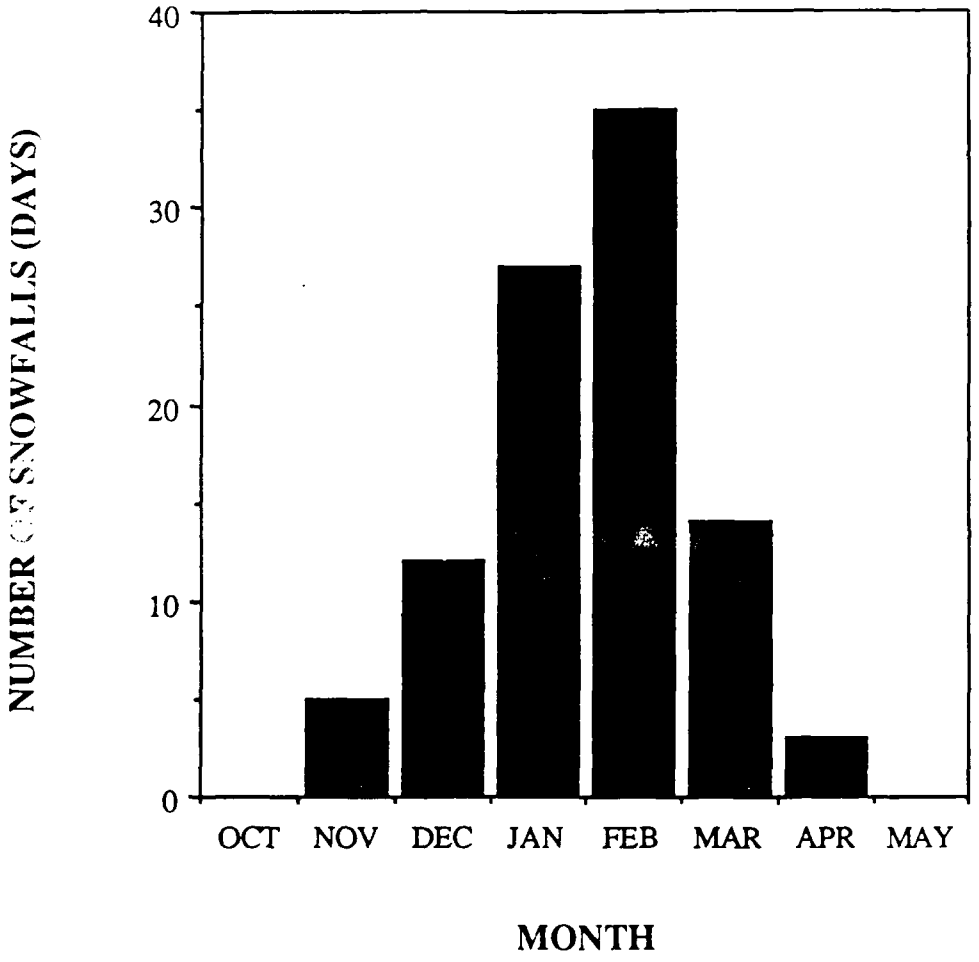

Figure 4.2. Histogram of the number of days per month on which significant snow accumulations (> 5 cm/24 h) occurred during the period from 1966-1987.

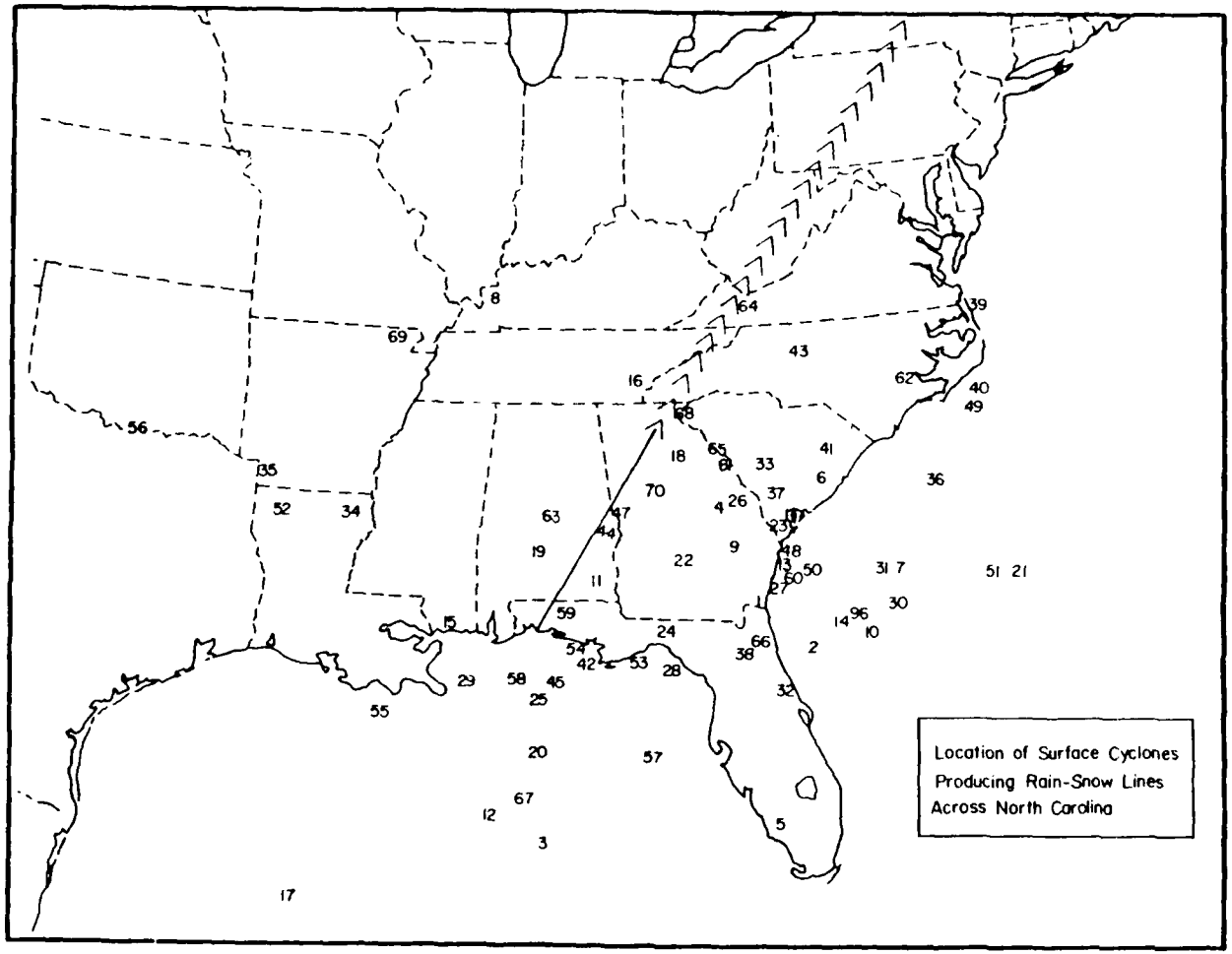

Figure 4.3. Location of the surface cyclones producing rain-snow lines across North Carolina for the dates listed in Appendix A. The axis of the Appalachian Mountains and an imaginary extension to the Gulf of Mexico are drawn for geographical region definition (see text).

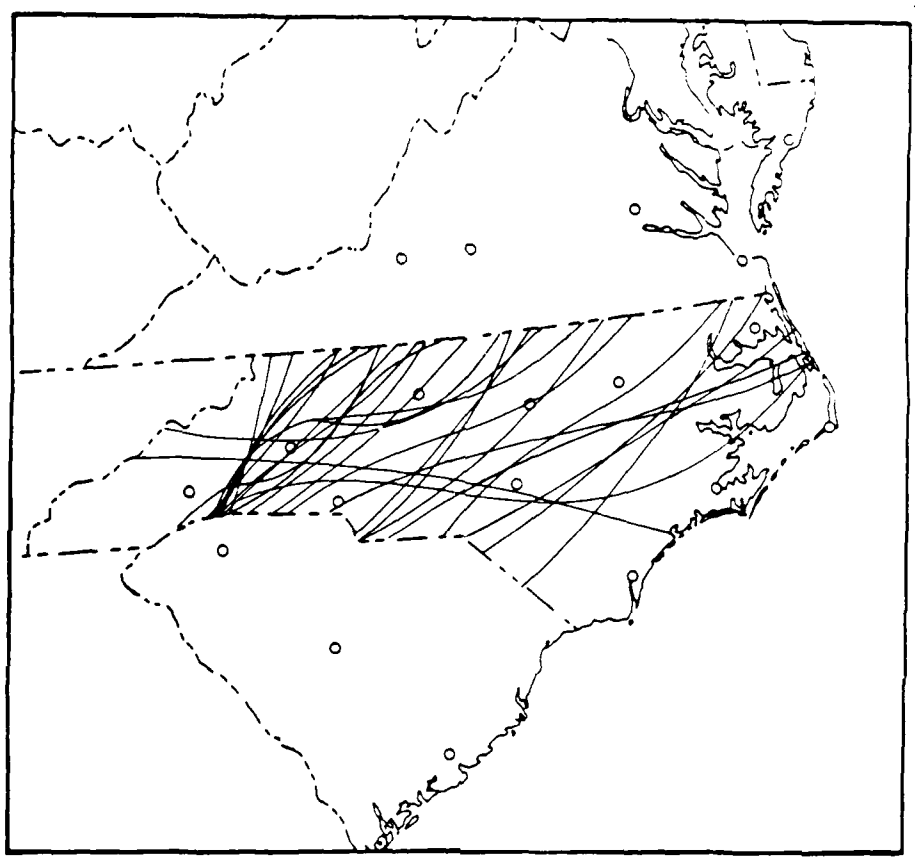

Figure 4.4a. Rain-snow line positions in North Carolina for the surface cyclones in Fig. 4.3 that are located over land east of the Appalachians.

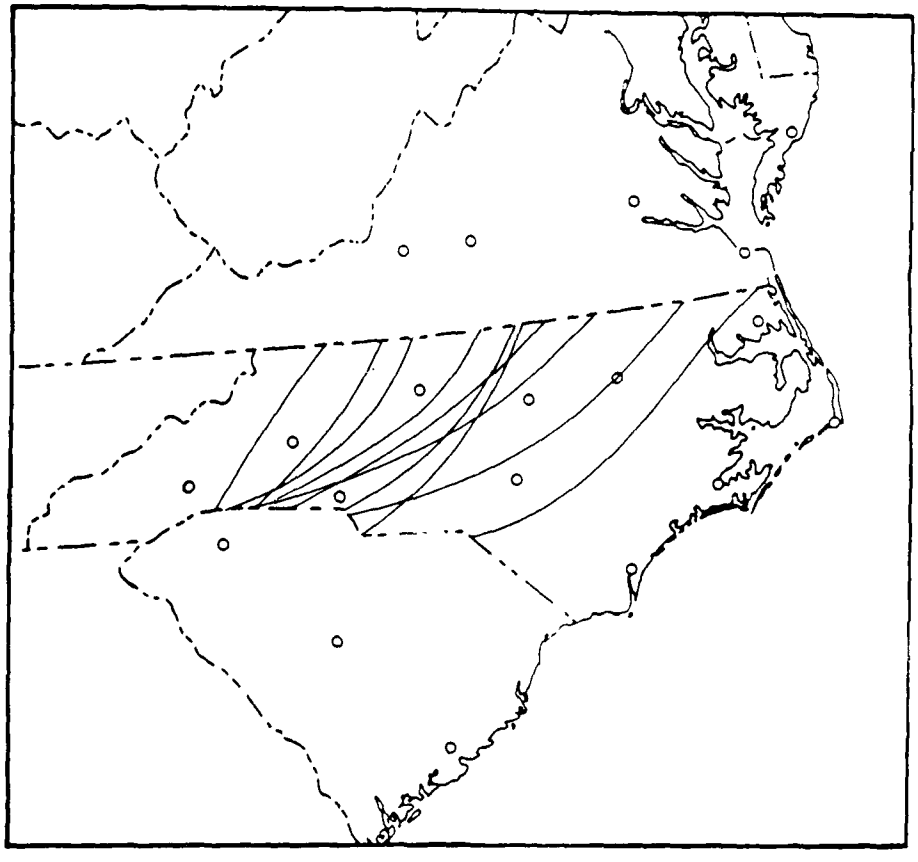

Figure 4.4b. Same as in Fig. 4.4a, except for cyclones over land west of the Appalachians.

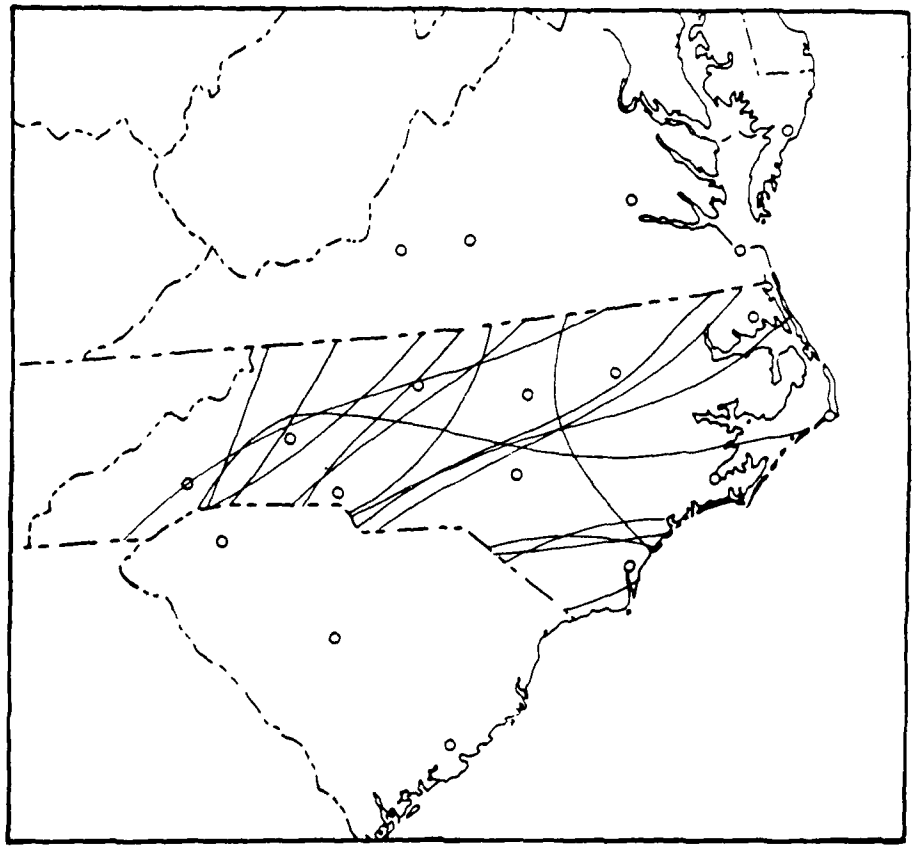

Figure 4.4c. Same as in Fig. 4.4a, except for cyclones over the Gulf of Mexico

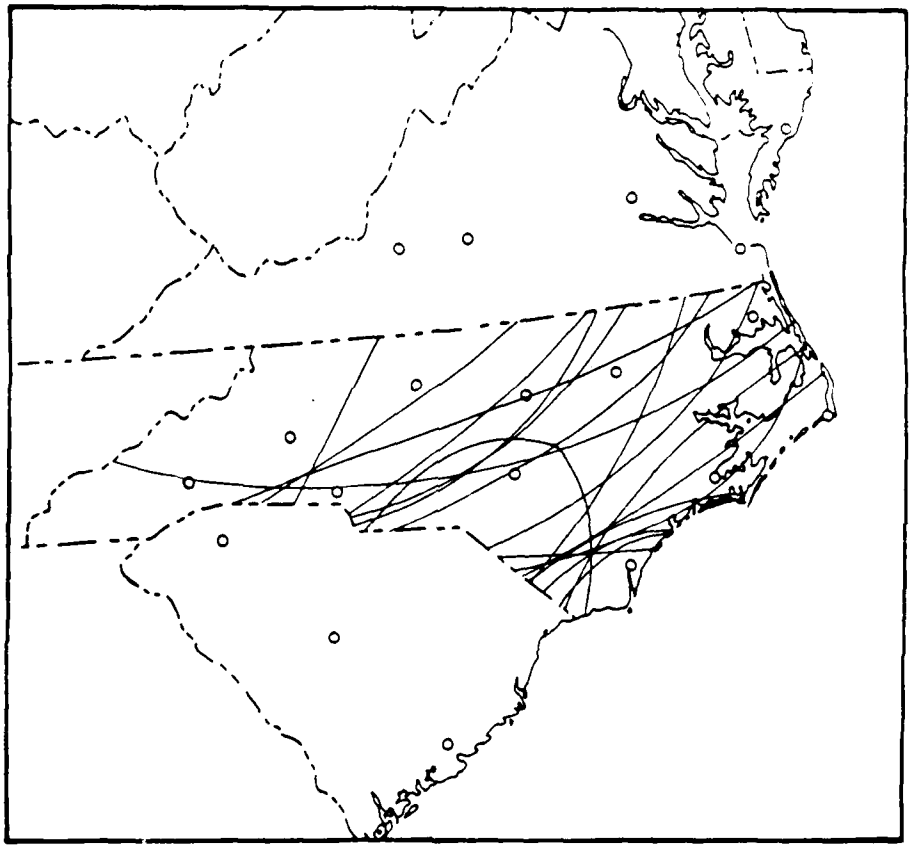

Figure 4.4d. Same as in Fig. 4.4a, except for cyclones over the Atlantic Ocean.

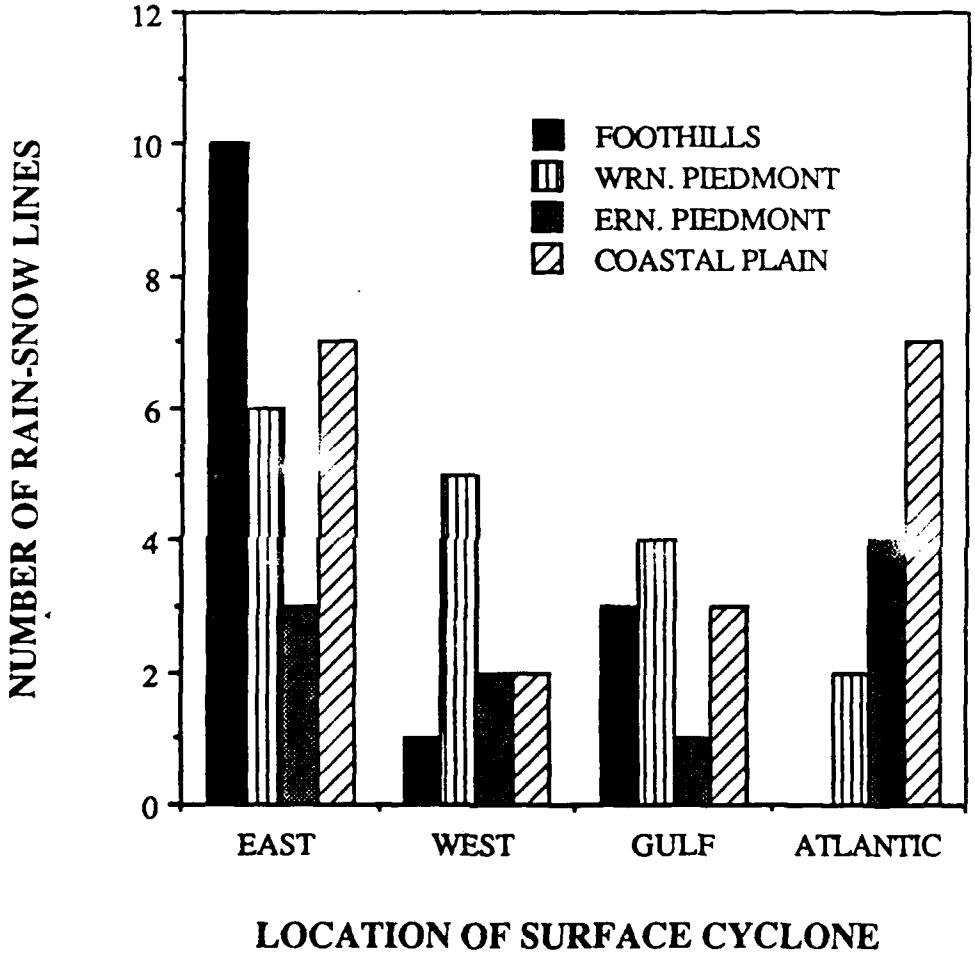

Figure 4.5. Histogram of the number of rain-snow lines occurring in a given region of North Carolina with respect to the location of its parent surface cyclone.

The second part of the climatology deals with the correlation between surface variables (temperature, wet-bulb temperature, dew-point temperature, and wind direction) and precipitation type observed in the vicinity of a R-S line. The types of precipitation investigated included frozen (sleet or ice pellets), freezing (freezing rain/drizzle), and mixed [combination of snow and/or ice pellets (sleet) and rain or drizzle], and were identified from the LCD and Surface Weather Reports of the aforementioned surface variables for the dates listed in Appendix A. Figures 4.6a-d illustrate the range of temperature and wind direction associated with the three categories of precipitation type. The air temperatures (± 1°F) associated with the maximum occurrence of frozen, freezing, and mixed precipitation were found to be 32°F (0°C), 32°F, and 35°F (2°C); wet-bulb temperatures of 32°F, 29°F (-2°C), and 32°F; dew-point temperatures of 29°F, 29°F, and 32°F. Winds out of the northeast (020-070°) were observed most often for all three precipitation types. Table 4.1 depicts the ranges of the surface variables associated with precipitation types in this study.

TABLE 4.1. Range of temperature of the surface variables and percentage of stations reporting the indicated wind direction [N=northerly (290°-070°); NE=northeasterly (020°-070°)] for various precipitation types.

	TEMPERATURE			WIND	
PRECIPITATION TYPE	DRY BULB	WET BULB	DEW POINT	DIRECTION	
FROZEN	12°- 40°F	11°- 39°F	3°- 38°F	N	NE
	(-11°- 4°C)	(-12°- 4°C)	(-16°- 3°C)	87%	68%
FREEZING	14°- 37°F	14°- 36°F	9°- 35°F	N	NE
	(-10°- 3°C)	(-10°- 2°C)	(-13°- 2°C)	86%	68%
MIXED	29°- 43°F	30°- 41°F	14°- 40°F	N	NE
	(-2°- 6°C)	(-1°- 5°C)	(-10°- 4°C)	78%	58%

Generally, it was found that stations reporting frozen, freezing, and mixed precipitation (as defined above) are found to have surface

i) temperatures of 0°C ± 2°, but as cold as -11°C and as warm as 5°C

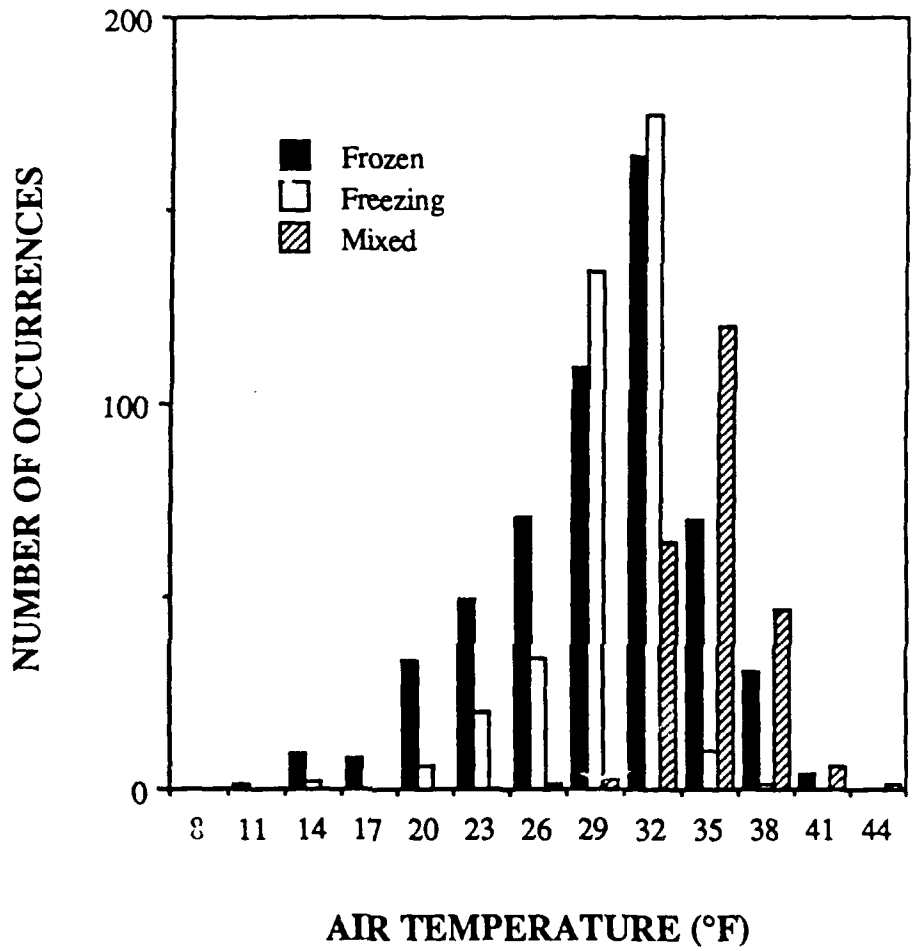

Figure 4.6a. Histogram of the number of occurrences of frozen, freezing, and mixed precipitation (see text for definitions) for a given surface air temperature (°F).

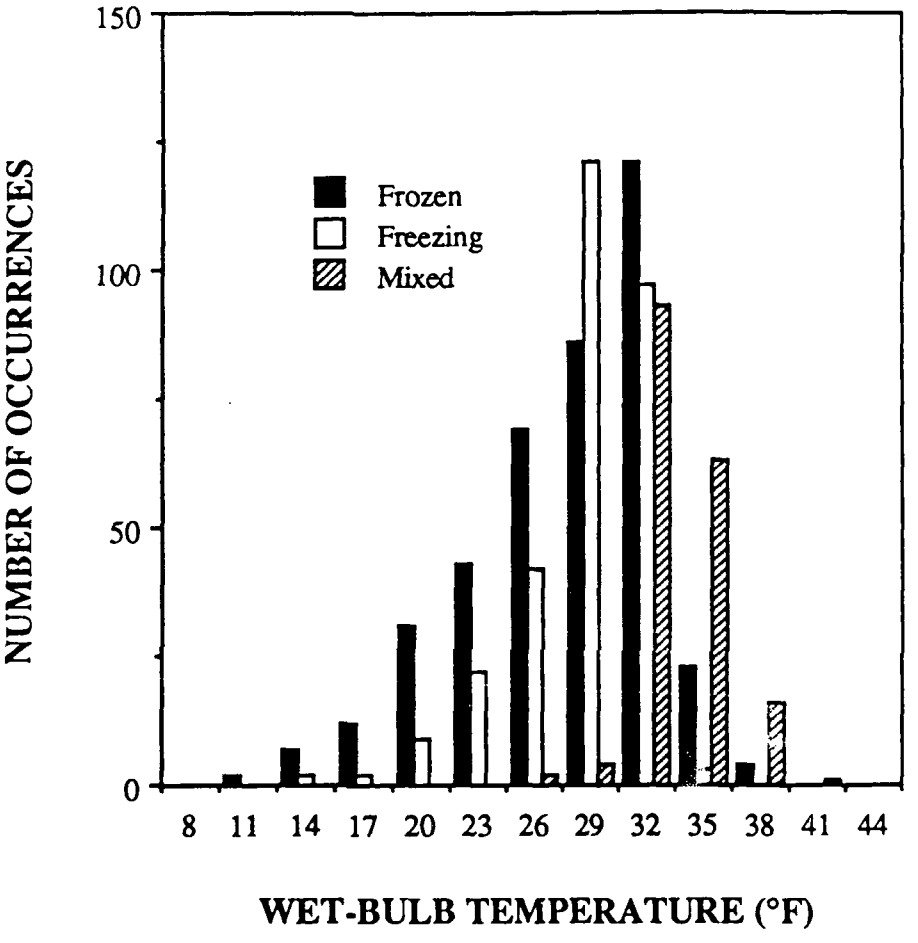

Figure 4.6b. Same as in Fig. 4.6a, except for wet-bulb temperature.

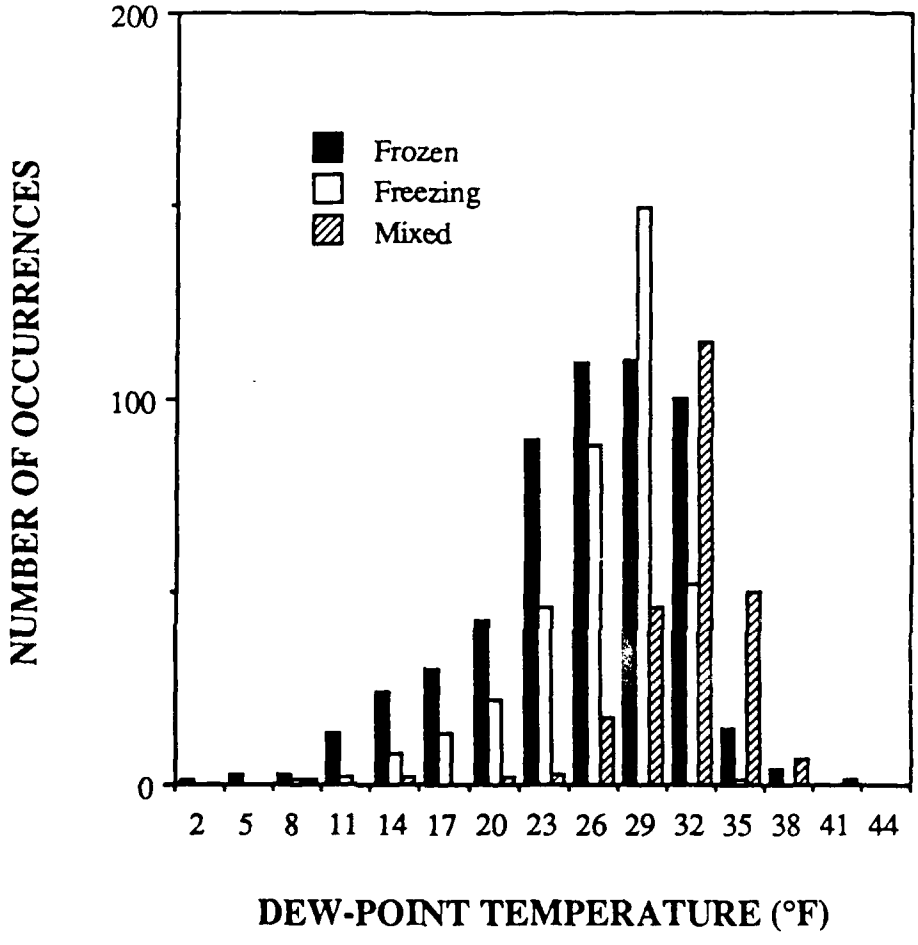

Figure 4.6c. Same as in Fig. 4.6a, except for dew-point temperature.

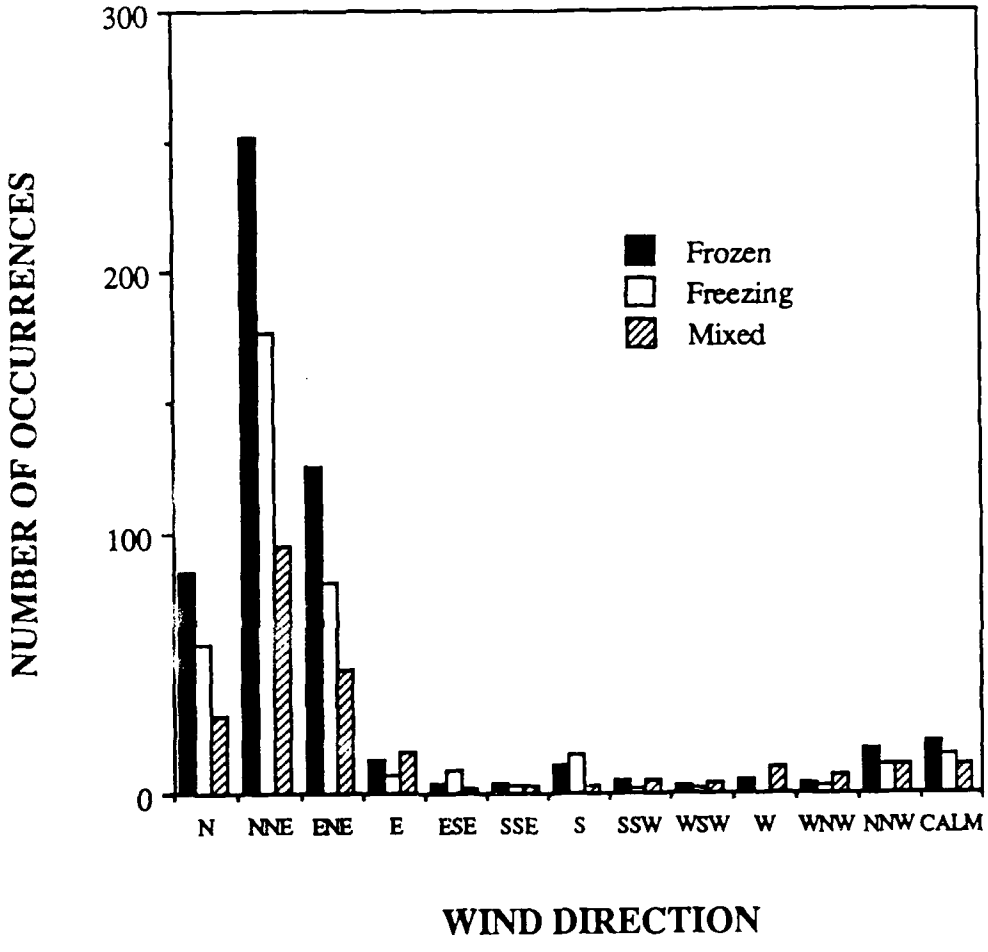

Figure 4.6d. Same as in Fig. 4.6a, except for wind direction (i.e. S = winds from 170-190°).

ii) wet-bulb temperatures of 0°C ± 2°, but as cold as -12°C and as warm as 5°C

iii) dew-point temperatures of 0°C ± 2°, but as cold as -16°C and as warm as 4°C

iv) winds out of the northeast (020-070°) over 65% of the time, with a northerly component (290-070°) reported nearly 85% of the time.

5. SUMMARY

The presence of a R-S line within the GALE data network during IOP 6 resulted in an opportunity to study the evolution of a R-S line and an associated front, using a special mesoscale data set. Standard operational and special surface and upper-air observations taken during the GALE field project were the primary sources of data for this research.

A 500-mb trough, with an associated vorticity maximum, propagated northeastward across the GALE observation area. A surface cyclone moved eastward across the Appalachians, bringing snow, ice pellets, freezing rain, and rain to the Inner-GALE Area. Rising motion and warm air advection combined to saturate portions of the lower troposphere, which, combined with cold and dry air near the surface, enabled a variety of precipitation types to fall. The heaviest precipitation and snowfall occurred in the Virginia mountains.

There were three distinct phases in the development of the R-S line and a stationary front to the southeast. From 2100 GMT 14 February to 0000 GMT 15 February, the R-S line and surface front developed *in situ* over the Inner GALE region. Between 0000 GMT and 0300 GMT 15 February, both the R-S line and frontal zone became better defined. This simultaneous enhancement was linked due to their mutual dependence on the temperature distribution. From 0300 GMT to 0600 GMT 15 February, both the R-S line and surface stationary front began to move east, propagating together as the thermal field continued to evolve.

The results of Stewart and King (1987) were compared to the weather sequence at RDU during the approach and passage of the R-S line. The largest 1 h decline of dry-bulb temperature occurred during an onset of snow, consistent with Stewart and King. However, Stewart and King found the largest pressure decrease after the transition from snow to rain. While the pressure did decrease during and after the snow to drizzle transition, the largest pressure drop occurred after the drizzle had stopped.

Analyses of the 285°K isentropic-surface during this R-S line event were presented.

Strong ascent was indicated over the eastern Carolinas during most of the period, but moves offshore by the end of the period of interest. Rising motion caused the initially dry air to become saturated over the Carolinas by the middle of the period (≈ 0000 GMT 15 February). A comparison of our isentropic analyses, which included the special GALE rawinsonde sites, with that of Homan and Uccellini (1987), found that a more detailed vertical motion pattern emerged, with some vertical velocities more than twice that found by these authors.

An analysis of a vertical cross section nearly normal to the R-S line and stationary front revealed other features. Several stable layers below 800 mb existed for the duration of the R-S line event, with instability inferred (from both the vertical gradient of potential temperature and symmetric instability theory) over ILM and RVC beginning around 0000 GMT 15 February. The 0°C isotherm moved slowly southeastward with time and showed a strong northward tilt throughout the period. A maximum of along-front winds towards the ENE was found above the frontal zone in the lower to middle troposphere. Maximum southerly cross-frontal winds were found just ahead and above the frontal zone. With time, warm advection and rising motion contributed to the moistening of the lower to middle troposphere over FAY, ILM, and RVC.

At the surface, fields of divergence were generated using the Barnes objective analysis scheme. At 0300 GMT 15 February, it was shown that the divergent/convergent pattern and satellite signature found in the vicinity of the R-S line was consistent with the theorized mesoscale circulation found by Lin and Stewart (1986).

The three-dimensional atmospheric structure in the vicinity of the R-S line was further explored by means of Barnes-generated fields of divergence and vertical velocity. Divergence was calculated on constant pressure levels, whereas vertical velocity was derived from vertical integration of the continuity equation. Since the Inner GALE Area has a small surface slope, a vertical velocity of zero was chosen at the surface boundary. The patterns of divergence and vertical velocity at 950 and 850 mb seem to be consistent with isentropic surface analyses and precipitation patterns based on radar reflectivity.

An experiment to quantify the thermodynamic processes in the vicinity of the R-S line was undertaken. Using the First Law of Thermodynamics, a coordinate system following the 0°C isotherm (chosen to represent the R-S line) was employed. The results indicate that cooling due to melting and/or sublimation was occurring at the R-S line. After its passage, warm air advection increased the low-level temperatures in this case.

A 22-year climatology of R-S lines occurring in North Carolina revealed that only a

weak relationship existed between the R-S line location within the State and location of the parent cyclone. Also compiled were the frequency distributions of the occurrence of frozen, freezing, and mixed precipitation types versus dry- and wet-bulb temperature, dewpoint-temperature, and wind direction. Histograms for each show modal values of temperature and moisture variables at 0°C for the frozen and freezing types, and mixed mixed precipitation occurred most frequently at somewhat warmer temperatures. All precipitation types occurred most frequently with surface winds from NNE to ENE.

6. CONCLUSIONS

Based on work on the GALE case described above, the following conclusions can be drawn:

i) Evidence for the existence of a mesoscale circulation associated with the R-S line is found from

(a) surface analysis of operational and PAM-II data

(b) satellite imagery

(c) time-averaged divergence fields.

ii) Cooling due to melting/sublimation was found coincident in time with the development of a R-S line and stationary front.

iii) The passage of R-S lines does have some impact on surface variables.

iv) The GALE enhanced sounding network, together with an appropriately-tuned Barnes analysis scheme, is capable or resolving meso-ß scale structure in divergence and vertical velocity patterns. In a comparison of vertical velocity computations with the operational rawindsonde network, the GALE network was able to provide evidence of vertical velocities of twice the magnitude as those found by the conventional network.

The 22-year climatology of R-S lines in North Carolina leads to the following conclusions:

v) There is no one preferred R-S line location within North Carolina.

vi) A limited correlation exists between the positions of the parent surface cyclone and R-S line.

vii) The freezing temperature (0°C ± 2°) was the dominant surface dry-bulb, wet-bulb, and dew-point temperature range for frozen, freezing, and mixed precipitation.

viii) The three precipitation types occur most frequently with winds from NNE through ENE.

7. FUTURE RESEARCH

In this research, several observational indications of mesoscale circulations have been shown to exist. However, time limitations have precluded further investigation. The spatially and temporally dense GALE data set should be used to further confirm the existence of a mesoscale circulation associated with the R-S line and its interaction with the developing front. Specifically, depicting the ageostrophic wind components may be helpful in revealing a mesoscale circulation.

Time limitations precluded a detailed investigation into the interaction between the R-S line and developing stationary front. A analysis of the thermal field should be undertaken. A goal should be to calculate the terms of the frontogenesis equation.

Nielsen (1988) found that a gravity wave propagated through the Inner GALE Area during the period 2000 GMT 14 February to 0200 GMT 15 February 1986. An attempt should be made to further document the effects of the gravity wave passage on the R-S line and stationary front.

The concept of conveyor belts in mid-latitude cyclones introduced at the beginning of this thesis could be illustrated further using the GALE data set. The interaction between the developing surface front/R-S line and the location/orientation of conveyor belts are areas that could shed light on the mechanisms of precipitation production during this winter event.

The computation of vertical velocities was of high importance for this case study since motion in the the vicinity of the R-S line and front could be used to infer a mesoscale circulation. The kinematic method was used due to time limitations and its simplicity. However, the kinematic method requires knowledge of the horizontal (isobaric) divergence as a function of height (pressure), which can be calculated from a local network of simultaneous wind soundings. In addition, the surface vertical motion must be specified when the terrain is not level. A new approach, a quasi-geostrophic method for estimating lower tropospheric vertical motion (Zwack and Kabil, 1988), might be more useful since, in theory, it would require only standard surface pressure and pressure tendency data.

An analysis of errors introduced by the kinematic method of computing the vertical velocity should be completed. This would give researchers a quantitative estimate on how good results would be be using the kinematic approach.

The climatology presented here should be expanded. The relationship of R-S lines to

surface anticyclones and to 500 mb troughs, for example, may provide a forecaster with synoptic-scale clues typically accompanying the R-S line, thus improving forecasts. Penn's (1957) method of categorizong synoptic patterns according to a central reporting location (i.e. RDU or GSO) could possibly be used. In addition, the upper-air thicknesses (e.g. 1000-700 mb) associated with R-S line events at key stations should be compiled and stratified in some way, possibly according to precipitation type.

APPENDIX A

The following numbered dates (GMT) correspond to the numbers displayed in Fig. 4.3:

1. 1500 15 January 1966
2. 0900 22 January 1966
3. 2100 25 January 1966
4. 1800 29 January 1966
5. 0000 24 February 1966
6. 0900 24 February 1966
7. 1800 9 February 1967
8. 0300 13 January 1968
9. 0900 24 January 1968
10. 0900 24 February 1968
11. 0600 29 February 1968
12. 1200 9 November 1968
13. 2100 11 November 1968
14. 0300 16 February 1969
15. 1500 22 February 1969
16. 0000 1 March 1969
17. 1500 6 March 1969
18. 0000 22 December 1969
19. 1800 25 December 1969
20. 1200 6 January 1970
21. 0000 30 December 1970
22. 1200 31 December 1970
23. 0300 26 March 1971
24. 1500 3 December 1971
25. 0000 2 February 1972
26. 1800 18 February 1972
27. 1800 25 March 1972
28. 0900 31 March 1972
29. 0000 8 January 1973
30. 0900 10 February 1973
31. 1500 8 December 1973
32. 1500 16 December 1973
33. 0300 1 December 1974
34. 1500 3 February 1975
35. 0900 10 March 1975
36. 1800 23 November 1975
37. 2100 1 February 1976
38. 1500 3 January 1977
39. 2100 9 January 1977
40. 1800 24 January 1977
41. 0900 20 January 1978
42. 0900 2 February 1978
43. 0000 22 February 1978
44. 1800 28 February 1978
45. 0000 7 February 1979
46. 1800 18 February 1979
47. 0600 31 January 1980
48. 1500 6 February 1980
49. 1800 9 February 1980
50. 1500 1 March 1980
51. 1200 27 December 1980
52. 0900 22 March 1981
53. 1500 25 December 1981
54. 1200 13 January 1982
55. 0000 27 February 1982
56. 1200 13 January 1982
57. 0900 21 January 1983
58. 0900 6 February 1983
59. 1500 10 February 1983
60. 1500 24 March 1983
61. 1800 18 April 1983
62. 1200 6 February 1984
63. 0900 28 January 1985
64. 0900 12 February 1985
65. 0300 15 February 1986
66. 0900 1 January 1987
67. 0600 22 January 1987
68. 2100 25 January 1987
69. 1800 16 February 1987
70. 0900 3 April 1987

REFERENCES

Barnes, S. L., 1964: A technique for maximizing details in numerical weather map analysis. J. Appl. Meteor., 3, 396-409.

____, 1973: Mesoscale objective analysis using weighted time-series observations. NOAA Technical Memorandum ERL NSSL-62, Norman, OK., 60 pp.

Blevins, R. D., 1985: On the evolution of precipitation associated with a wintertime east coast cyclone- A GALE preliminary study. M.S. thesis, North Carolina State Univ.- Raleigh, 104 pp.

Bocchieri, J. R., and H. R. Glahn, 1976: Verification and further development of an operational model for forecasting the probability of frozen precipitation. Mon. Wea. Rev., 104, 691-701.

____, 1979: A new operational system for forecasting precipitation type. Mon. Wea. Rev., 107, 637-649.

____, 1980: The objective use of upper air soundings to specify precipitation type. Mon. Wea. Rev., 108, 596-603.

——, and G. J. Maglaras, 1983: An improved operational system for forecasting precipitation type. Mon. Wea. Rev., 111, 405-419.

Booth, 1973: A simplified snow predictor. Meteor. Mag., 102, 332-340.

Bosart, L. F., 1981: The president's day snowstorm of 18-19 February 1979: A subsynoptic-scale event. Mon. Wea Rev., 109, 1542-1566.

Browning, K. A. and C. W. Pardoe, 1973: Structure of low-level jet streams ahead of mid-latitude cold fronts. Quart. J. Roy. Meteor. Soc., 99, 619-638.

——, 1986: Conceptual models of precipitation systems. Wea. and Forecasting, 1, 23-41.

Carlson, T. N., 1980: Airflow through mid-latitude cyclones and the comma cloud pattern. Mon. Wea. Rev., 108, 1498-1509.

Dirks, R. A., J. P. Kuettner, and J. A. Moore, 1988: Genesis of Atlantic Lows Experiment (GALE): An overview. Bull. Amer. Meteor. Soc., 69, 148-160.

Emanuel, K. A., 1979: Inertial instability and mesoscale convective systems. Part I: Linear theory of inertial instability in rotating viscous fluids. J. Atmos. Sci., 36, 2425-2449.

Findeisen, W., 1940: The formation of the 0°C isothermal layer and fractocumulus under nimbostratus. Meteor. Z., 57, 49-54.

Forbes, G. S., R. A. Anthes, and D. W. Thomson, 1987: Synoptic and mesoscale aspects of an Appalachian ice storm associated with cold-air damming. Mon. Wea. Rev., 115, 564-591.

Glahn, H. R., and J. R. Bocchieri, 1975: Objective estimation of the conditional probability of frozen precipitation. Mon. Wea. Rev., 103, 3-15.

Hanks, H. H., D. R. Harpporte, and E. C. Grueber, 1967: Snow forecasting in the Central United States, Contract No. Cwb 11353, Final Report for ESSA Weather Bureau Techniques Development Laboratory, Kansas City, MO, Atmospheric Research & Development Corporation.

Harrold, T. W., 1973: Mechanisms influencing the distribution of precipitation within baroclinic disturbances. Quart. J. Roy. Meteor. Soc., 99, 232-251.

Holton, J. R., 1979: An Introduction to Dynamic Meteorology. International Geophysics Series, Vol. 23, Academi Press, New York, 391 pp.

Homan, J., and L. W. Uccellini, 1987: Winter forecast problems associated with light to moderate snow events in the mid-Atlantic states on 14 and 22 February 1986. Wea. and Forecasting, 2, 206-228.

Kocin, P. J., and L. W. Uccellini, 1985a: A survey of major East Coast snowstorms, 1960-83. Part 1: Summary of surface and upper-level characteristics. 101 pp. [NTIS N85-27471.]

——, and ——, 1985b: A survey of major East Coast snowstorms, 1960-83. Part 2: Case studies of eighteen storms. 214 pp. [NTIS N85-27472.]

Koolwine, T., 1975: Freezing rain. M.S. thesis, University of Toronto, 92 pp.

Lamb, H. H., 1955: Two-way relationship between the snow or ice limit and 1000-500 mb thickness in the overlying atmosphere. Quart. J. Roy. Meteor. Soc., 81, 172-189.

Lin, C. A., and R. E. Stewart, 1986: Mesoscale circulations initiated by melting snow. J. Geophys. Res., 91, 13299-13302.

Lumb, F. E., 1960: Cotswold snowfall of 1 November 1942. Meteor. Mag., 89, 11-16.

——, 1961: The problem of forecasting the downward penetration of snow. Meteor. Mag., 90, 310-319.

——, 1963: Downward penetration of snow in relation to the intensity of precipitation. Meteor. Mag., 90, 310-319.

Matsuo, T., Y. Sasyo, and Y. Sato, 1981: Relationship between types of precipitation on the ground and surface meteorological elements. J. Meteor. Soc. Japan, 59, 462-476.

Nielsen, J. W., 1988: Gravity wave-convection interaction during GALE IOP 6. GALE/CASP Workshop Preliminary Reports, Virginia Beach, VA, November 1987, 454 pp.[Available from GALE Project Office, P.O. Box 3000, Boulder, CO 80807]

Penn, S., 1957: The prediction of snow vs. rain. Forecasting guide No. 2, U.S. Weather Bureau, 299 pp. [Available from NOAA Library and Information Services Div., User Services Branch, D822, Rockville, MD 20852].

Petterssen, S., 1956: Weather Analysis and Forecasting (Vol. I), 428 pp. New York: McGraw-Hill Book Co.

Richwein, B. A., 1980: The damming effect of the southern Applachians. Nat. Wea. Dig., 5, 2-12.

Stewart, R. E., 1984: Deep 0°C isothermal layers within precipitation bands over southern Ontario. J. Geophys. Res., 89, 2567-2572.

——, 1985: Precipitation types in winter storms. Pure Appl. Geophys., 123, 597-609.

——, and P. King, 1987: Rain/snow boundaries over southern Ontario. Mon. Wea. Rev., 115, 1894-1907.

——, and G. M. McFarquhar, 1987: On the width and motion of a rain/snow boundary. Water Resources Res., 23, 343-350.

Szeto, K. K., C. A. Lin, and R. E. Stewart, 1988: Mesoscale circulations forced by melting snow. Part I: Basic simulations and dynamics. J. Atmos. Sci., (in press).

Wexler, R., R. J. Reed, and J. Honig, 1954: Atmospheric cooling by melting snow. Bull. Amer. Meteor. Soc., 35, 48-51.

Young, W. R., 1978: Freezing precipitation in the southeastern United States. M.S. thesis, Texas A&M University, 123 pp. [Available from Dept. of Meteorology, Texas A&M University, College Station, TX 77843.]

Zwack, P., and M. Kabil, 1988: Estimating lower tropospheric vertical motion from surface pressure and pressure tendency data alone. Mon. Wea. Rev., 116, 795-803.